BIOPROTA

**Key Issues in Biosphere Aspects of Assessment of the Long-term Impact of Contaminant Releases Associated with Radioactive Waste Management**

# C-14 Terrestrial Model-Data Comparisons

## Final Report

**Laura Limer, Masakazu Ota, Taku Tanaka, Mike Thorne, Russell Walke**

**Version 1.0, 10 July 2017**

## PREFACE

BIOPROTA is an international collaboration forum which seeks to address key uncertainties in the assessment of environmental and human health impacts in the long term arising from release of radionuclides and other contaminants as a result of radioactive waste management practices. It is understood that there are radio-ecological and other data and information issues that are common to specific assessments required in many countries. The mutual support within a commonly focused project is intended to make more efficient use of skills and resources, and to provide a transparent and traceable basis for the choices of parameter values, as well as for the wider interpretation of information used in assessments. A list of sponsors of BIOPROTA and other information is available at www.bioprota.org.

The general objectives of BIOPROTA are to make available the best sources of information to justify modelling assumptions made within radiological and related assessments of radioactive waste management. Particular emphasis is placed on key data required for the assessment of long-lived radionuclide migration and accumulation in the biosphere, and the associated radiological impact, following discharge to the environment or release from solid waste disposal facilities. The programme of activities is driven by assessment needs identified from previous and on-going assessment projects. Where common needs are identified within different assessment projects in different countries, a common effort can be applied to finding solutions.

This report describes collaborative C-14 terrestrial model-data comparisons undertaken by the BIOPROTA C-14 working group, based on 'real world' data sets. It provides background and data for three real scenarios: (i) short-term modelling of atmospheric deposition to pasture, (ii) short-term modelling of a methane source-term to the sub-soil in an agricultural context, and (iii) long-term modelling of C-14 release in groundwater from near-surface disposal and contamination of an adjacent wetland. The models applied to each scenario are summarised, and the results compared both to each other (model-model) and also to the observational data (model data).

The financial support provided for the project by Posiva Oy (Finland), Radioactive Waste Management Limited (RWM, UK), Nuclear Waste Management Organization (NWMO, Canada), Electricité de France (EDF), Swedish Nuclear Fuel and Waste Management Company (SKB), National Cooperative for the Disposal of Radioactive Waste (Nagra, Switzerland), French National Radioactive Waste Management Agency (ANDRA), Korea Radioactive Waste Agency (KORAD), Swedish Radiation Safety Authority (SSM), and Nuclear Waste Management Organization of Japan (NUMO) is gratefully acknowledged.

### Version History

Version 1.0 (Draft): First full draft compiled by Laura Limer and reviewed by Russell Walke and Mike Thorne. Distributed to participants and BIOPROTA project sponsor organisations on 2 June 2017.

Version 1.0: Final report. Updates Version 1.0 (Draft) to take account of review comments from Graham Smith and Taku Tanaka. Distributed to BIOPROTA members on 10 July 2017.

## EXECUTIVE SUMMARY

In many countries, C-14 is an important radionuclide in safety assessments associated with a wide range of contexts, including operational discharges from nuclear facilities and potential long-term releases from radioactive waste repositories. Over the past decade or so, the BIOPROTA forum has undertaken several projects concerning the behaviour C-14 in the biosphere. The BIOPROTA forum has also hosted a series of workshops focussing on the behaviour of C-14 in the biosphere and associated assessments of safety.

To date, the C-14 model comparison studies undertaken in BIOPROTA have used hypothetical release scenarios, with no data to compare with the results reported. The study documented in this report has provided an opportunity to test and support validation of models of C-14 dynamics in terrestrial ecosystems using 'real world' data.

Three experimental/observational datasets were used, with each offering a particular aspect against which models could be validated:

- high temporal resolution atmospheric C-14 concentrations with associated pasture concentrations at a field study site close to the La Hague facility, France;
- methane ($CH_4$) and carbon dioxide ($CO_2$) measurements through agricultural soil profiles following sub-surface $CH_4$ injection in field and laboratory studies at the University of Nottingham, UK; and
- measurements of C-14 in groundwater, soil gas and vegetation down-gradient of an historical near-surface disposal facility adjacent to Duke Swamp, Canada.

Organisations from Belgium, France, Japan, Sweden and the UK have participated in model-data and model-model comparison exercises based on these data sets, including a two-day workshop hosted by EDF in Paris in November 2016.

The study has helped to build understanding and confidence in several aspects of biosphere modelling for C-14.

- The La Hague case study has shown that the models for plant uptake from a well-defined above-canopy source term can be considered validated.
- The Nottingham case study has improved understanding of C-14 transport through soils from a sub-surface gaseous source term and has shown that the models applied typically overestimate the oxidation of $CH_4$ (which cannot be taken-up by plants) to $CO_2$ (which is taken up by plants).
- The Duke Swamp case is shown to be a direct analogue for near-surface waste disposal and radionuclide releases from which further understanding and confidence could be drawn in assessment models.

The study also highlights data sets where further understanding and confidence may be drawn from similar model-data and model-model comparisons. These include further study and modelling of the observational data for the Duke Swamp site, notably extending consideration to swamp sediments and vegetation, as well as making use of high temporal resolution data on C-14 in the atmosphere (with high vertical resolution) and carbon pools within a Finnish boreal forest.

# CONTENTS

# 1 INTRODUCTION

In many countries, C-14 is an important radionuclide in safety assessments associated with a wide range of contexts, including operational discharges from nuclear facilities and potential long-term releases from radioactive waste repositories. Over the past decade or so, the BIOPROTA forum has undertaken several projects concerning the behaviour C-14 in the biosphere, including a review of the assessment models used [Sheppard and Thorne, 2005] and modelling of C-14 uptake in agricultural crops [Limer et al., 2012; Norris et al., 2011; Mobbs et al., 2013]. The BIOPROTA forum has also hosted a series of workshops focussing on the behaviour of C-14 in the biosphere and associated assessments of safety [BIOPROTA, 2014; Smith and Smith, 2014; Smith, 2015].

To date, the C-14 model comparison studies undertaken in BIOPROTA have used hypothetical release scenarios, with no data to compare with the results reported. Independently of BIOPROTA studies, several waste management and research organisations have been further developing their C-14 modelling capabilities, and testing their conceptual models against real world datasets, e.g. Aulagnier et al., [2012; 2013], Le Dizès et al. [2012], and Limer et al. [2013a; 2015]. These have all focussed on modelling the uptake of C-14 into plants, and have used both laboratory (e.g. Tucker and Shaw [1997]) and field data (e.g. Le Dizès et al. [2012]). The French Institute for Radioprotection and Nuclear Safety (IRSN), in particular, has used the application of their TOCATTA model to the La Hague field data [Le Dizès et al., 2012] to further develop their modelling capability for C-14, which is now referred to as TOCATTA-χ [Aulagnier et al., 2013].

Opportunities for further model-data comparisons within BIOPROTA were discussed in light of the work that has been undertaken outside of BIOPROTA at a BIOPROTA C-14 workshop in 2015 and identified a being useful [Smith, 2015]. The work described herein was undertaken taking into account the discussions at that workshop.

## 1.1 AIM AND OBJECTIVES

The aim of this project has been to provide participants with an opportunity to test and support validation of their models of C-14 dynamics in terrestrial ecosystems using ‘real world’ data. Even where full validation is not possible, the process builds confidence in the practical application of the models. Three datasets had been identified as being potentially useful in this regard, with each offering a particular aspect against which models could be validated:

- the La Hague field study site, France – relating to plant uptake from the atmosphere;
- the University of Nottingham laboratory and field experiment data, UK – relating to gas migration through a soil profile and oxidation of methane in soil; and
- Duke Swamp area, Canada – relating to spatial dispersion of C-14 labelled groundwater and uptake into vegetation.

The specific objective of this project has been, based upon the interests of the participating organisations, to facilitate the validation of aspects of existing terrestrial biosphere models for C-14 using ‘real world’ data. Participating organisations were also able to develop and/or enhance their modelling capabilities to reflect the cases being simulated. The first two datasets relate to short-term modelling (minutes to months), whereas the last one relates to a long-term discharge (years to decades). As part of the project, an international two-day workshop was held on 22-23 November 2016, hosted by EDF in Paris, France. This gave participants in the project an opportunity to discuss the data

sets, and describe their models and results from the model-data comparisons, the details of which are available in Limer [2017]. The outputs of that workshop have fed into this project final report.

Details of project participants and the models that they applied to each dataset are given in Table 1. The project was coordinated by a Technical Support Team (TST) comprising Quintessa Limited, Mike Thorne and Associates Limited and RadEcol Limited.

***Table 1: Summary of Models Applied to the Datasets***

| Dataset | Organisation | Model |
|---|---|---|
| La Hague | French National Radioactive Waste Management Agency (ANDRA) | Aqua_C14 |
| | Federal Agency for Nuclear Control (FANC, Belgium) | PRISM † |
| | Institute de Radioprotection et de Sûreté Nucléaire (IRSN, France) | TOCATTA-$\chi$ |
| | Swedish Nuclear Fuel and Waste Management Company (SKB) | SVAT |
| | Swedish Radiation Safety Authority (SSM) | SSPAM$^{14}$C |
| Nottingham | Electricité de France (EDF) | EDF C-14 |
| | Japan Atomic Energy Agency (JAEA) | SOLVEG II |
| | Radioactive Waste Management Limited (RWM, UK) | T2Plants |
| | Project Technical Support Team (TST) | - |
| Duke Swamp | Project Technical Support Team (TST) | Transect Model |

Notes:

† FANC were give permission to apply the PRISM model for C-14 to the La Hague case by the United Kingdom (UK) Food Standards Agency (FSA).

## 1.2 REPORT STRUCTURE

The report describes each of the three modelling scenarios in turn, covering the following aspects:

- an overview system description;
- a summary of the models applied to that dataset;
- the dataset itself;
- a description of the calculation scenarios;
- results of the calculations; and
- discussion of the results for that particular system.

The La Hague system is considered in Section 2, the Nottingham Experimental Studies in Section 3, and the Duke Swamp system in Section 4. A discussion of the wider conclusions that can be drawn from the application of models to these real-world datasets is given in Section 5.

References are provided in Section 6.

Further details of some of the models used in the study are provided in an Appendix.

# 2 LA HAGUE FIELD MONITORING

The context for the La Hague data is described in Section 2.1, the models applied to the scenario are described in Section 2.2, the data set used in the study is presented in Section 2.3, the modelling scenario is described in Section 2.4, the results of the model-data comparisons are presented in Section 2.5 and the findings are discussed in Section 2.6.

## 2.1 SYSTEM DESCRIPTION

AREVA-NC La Hague (North France) is a nuclear fuel reprocessing plant that releases about 15 TBq of C-14 into the atmosphere per year [Aulagnier et al., 2012]. From September 2006 to July 2008, C-14 activity concentrations in samples from the terrestrial environment (air, grass and soil) were monitored monthly by IRSN on a grass field (Hameau Vaultier) located 2 km downwind of the AREVA-NC La Hague reprocessing plant with respect to the prevailing wind direction (Figure 1). Meteorological data at the site were collected on a half-hourly basis. In addition, C-14 activity concentrations in the atmosphere above the pasture was determined hourly over that period, derived from observational data[a]. Consequently, this dataset offers an opportunity to validate radioecology models used to assess C-14 transfer to grassland ecosystems independent of atmospheric dispersion modelling errors [Aulagnier et al., 2012, 2013].

*Figure 1: La Hague field sampling site*

Since 2009, IRSN has been developing its own C-14 model, TOCATTA (Transfer Of Carbon-14 And Tritium in Terrestrial and Aquatic environments [Le Dizès et al., 2012]), and has previously tested it against this dataset [Le Dizès et al., 2012; Aulagnier et al., 2012]. The main conclusion drawn from these comparisons highlighted the need to develop an hourly time-step model of C-14 transfer based more thoroughly on knowledge arising from plant physiology, soil science and meteorology. This led to the development of the TOCATTA-χ model [Aulagnier et al., 2013], which used studies such as Farquhar and von Caemmerer [1982] to inform model development.

[a] These observational data comprised Kr-85 activity concentration measurements taken above the plot, based on concurrent releases of C-14 and Kr-85 from the stacks of AREVA-NC La Hague and the observed ratio between the two radionuclides [Maro et al., 2008].

Independently, in 2011, the model SSPAM$^{14}$C (the Swedish Soil-Plant-Atmosphere Model for C 14) was developed on behalf of the Swedish Radiation Safety Authority (SSM), with the intention to use it in both long-term and short-term atmospheric and sub-soil release assessments [Limer et al., 2013a, 2013b; Limer and Klos, 2014].

In 2013-14 a collaborative model-model-data comparison was undertaken by IRSN and SSM against the La Hague data, using the TOCATTA-χ and SSPAM$^{14}$C models, respectively [Limer et al., 2015].

## 2.2 MODELS APPLIED TO THE LA HAGUE SCENARIO

In this section, an overview of models applied to the La Hague scenario is given in turn, before the key features are summarised in Table 2.

### 1.1.1 ANDRA (Aqua_C14)

The Andra C-14 model was originally developed by Penfold and Watkins [1998] and transcribed into the general radionuclide biosphere transfer model, Aquabios[b], jointly with equations describing transfer of "classical" radionuclides. During transcription, minor changes were carried out to allow parallel treatment of C-14 and classical radionuclides [van Hecke, 2001]. However, due to difficulties associated with parallel transcription, the C-14 model was later extracted from Aquabios, without changing the model equations given by van Hecke [2001]. The current version of the model is standalone and known as AquaC_14, and is mostly based on the original equations given in Penfold and Watkins [1998].

AquaC_14 is a simple compartment model which simulates:

- deposition of C-14 onto soil via precipitation or irrigation;
- atmospheric concentration modelled as arising from soil degassing and/or by atmospheric transport modelling; and
- transfer through the food chain based on an isotopic ratio approach.

A written description of the model is available in form of an Andra report [Albrecht, 2016; in French]. The usual time-step for ANDRA's biosphere long-term assessment models is 1 year. Therefore, for application to the La Hague scenario, it was adapted to one day making sure that all parameters with time-related units had been modified accordingly. The key features of the model are summarised in Table 2.

### 2.2.1 FANC

The model used by FANC as part of this study is a stripped-down version of the C-14 model found in the PRISM software [Walke et al., 2016]. The model was implemented in the AMBER compartment modelling software[c].

The PRISM model was developed by the FSA to consider the transport of contaminants in terrestrial food chains, to assess potential impacts on food quality of routine or accidental releases of contaminants to the atmosphere.

[b] For details on the Aquabios model see Albrecht and Miquel [2010].

[c] www.quintessa.org/amber/

External parts of the plant are disregarded, because it is assumed that contamination is dominated by photosynthetic uptake. The structure of the model employed is illustrated in Figure 2, and further details are given in Section A.1 of the Appendix.

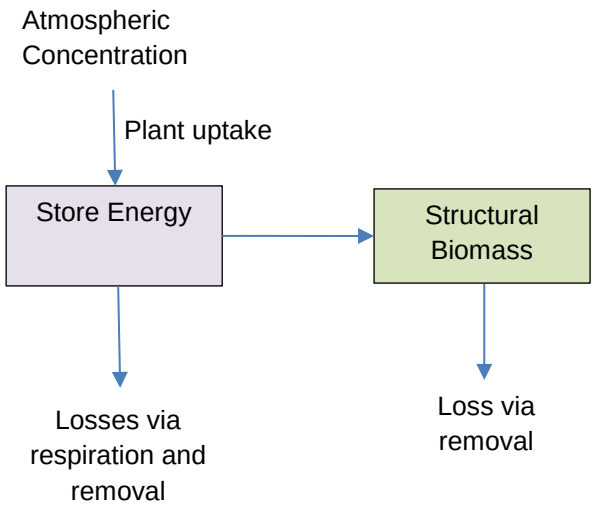


*Figure 2: Structure of the PRISM C-14 Model Employed to the La Hague Scenario*

### 2.2.2 IRSN (TOCATTA-χ)

Electricité de France (EDF) requires a reference tool for assessing doses resulting from radioactive releases from nuclear facilities under accidental, decommissioning or normal operating conditions, as well as from waste disposal facilities. Together with IRSN they co-funded the development of the SYMBIOSE modelling and simulation platform that aims to assess the fate and transport of a wide range of radionuclides in various environmental systems, and their impact on humans [Gonze et al., 2011; Mourlon et al., 2011]. Within this platform, IRSN has developed the dynamic compartment model TOCATTA, and the new version TOCATTA-χ, to estimate C-14 (and H-3) behaviour in agricultural soils and plants exposed to spray irrigation with contaminated water and/or airborne $^{14}CO_2$ releases from nuclear facilities under normal operating or accidental conditions [Aulagnier et al., 2013; Le Dizès et al., 2012].

### 2.2.3 SKB (C14-SVAT)

As part of the biosphere modelling studies carried out within the SR-PSU project, dedicated to the safety assessment of the Forsmark repository for LILW (SFR), SKB developed a new C-14 model for soil-vegetation-atmosphere (C14-SVAT) and also water-atmosphere transport [Avila and Kovalets, 2016, Saetre et al., 2013]. In previous safety assessments of Swedish radioactive waste disposal facilities (SAR-08 and SR-Site), doses from releases of C-14 to terrestrial and aquatic environments were calculated using the models described in Avila and Pröhl [2008].

### 2.2.4 SSM (SSPAM$^{14}$C)

To enable in-depth review of license applications submitted by operators, SSM needs to have independent modelling capacities for assessing the implications both for human and environmental safety associated with releases of radionuclides to the surface environment following the disposal of radioactive waste, operational releases of radionuclides, and incidents or accidents leading to short-term releases of radionuclides. For this reason, SSPAM$^{14}$C has been developed so that, in principle, it can be applied to the assessment of all these release scenarios, accepting a variety of source terms

(i.e. gaseous and liquid discharges from above and below ground), and considering processes within the ecosystem on a range of timescales [Limer et al., 2013a, 2013b].

## 2.3 LA HAGUE DATASET

A ryegrass field plot was used. Samples were taken from a fixed 1 $m^2$ area on an approximate monthly basis, with the pasture within this area being cut to a height of 1 cm. Typical soils of the Normandy coast have a 70-80 % silt fraction [Aulagnier et al., 2012].

The following data were made available.

- Hourly C-14 specific activity (Bq $kgC^{-1}$) in the atmosphere at a height of 1.5 m at the field site between 1 October 2006 and 31 December 2008 (Figure 3).
- 30-minute temperature (°C), humidity (%), global radiation (J $cm^{-2}$), wind speed (m $s^{-1}$) and precipitation (mm) at the field site 1 August 2006 to 18 December 2008. The meteorological data also include atmospheric pressure (HPa) and 30-minute average wind speeds (m $s^{-1}$) from 1 September 2006, plus some more intermittent data on wind direction.
- Mass of fresh and dry weight pasture harvested on an approximate monthly basis between 1 August 2006 and 4 December 2008, together with an estimate of total dry weight standing biomass immediately prior to harvest.
- Specific activity in the soil surface measured on an approximately monthly basis, and deeper soil measured on a less frequent basis, between 29 June 2006 and 31 August 2007.
- Specific activity in grass measured on an approximate monthly basis between 1 August 2006 and 25 July 2008.

## 2.4 CALCULATION SCENARIO DESCRIPTION

Using the monthly atmospheric concentration of C-14 data provided by IRSN (Figure 3), the aim of these calculations was to estimate the specific activity of C-14 in soil and in harvested pasture (Bq $kgC^{-1}$) between 1 August 2006 and 31 July 2008. The measured specific activity in the soil is shown in Figure 4, and that in plants is shown in Figure 5.

*Table 2: Summary of Key Model Features for those Models Applied to the La Hague Scenario*

| Model aspect | ANDRA (Aqua_C14) | FANC | IRSN (TOCATTA-χ) | SKB (SVAT) | SSM (SSPAM$^{14}$C) |
|---|---|---|---|---|---|
| Sub-models (if appropriate) | Soil-plant-atmosphere sub-model of AquaC_14 | None | Plant (S1), Soil (S2) | | Plant (S1), Soil (S2), Atmosphere (S3) |
| No. of soil compartments | 1 prairie soil compartment | 0 | 1 | 1 (soil rooting zone) | 5 |
| No. atmosphere compartments | 1 canopy compartment | 1 | 1 | 2 (Canopy, above canopy – only the canopy layer considered in this exercise) | 1 |
| No. of plant compartments | 1 grass compartment | 2 (Stored Energy, Structural Biomass) | 3 (Shoot structural dry matter pool; Root structural dry matter pool; Substrate (sap) pool) | 1 (Grass) | 3 (Aboveground plant; Belowground plant; Fruit) |
| Full list of processes in the model | (1) atmosphere to soil deposition modelled based on gas – water drop equilibrium using ideal gas and Henry's law as well as precipitation<br>(2) soil accumulation based on Kd concept plus degassing rate<br>(3) atmosphere - plant transfer based on isotopic ratios with a minor soil to plant root contribution | (1) Gaseous uptake (photosynthesis)<br>(2) transfer to structural biomass<br>(3) respiration<br>(4) removal of pasture | Biological growth<br>Photosynthesis<br>Growth and maintenance respiration<br>Senescence<br>Wet inputs of C to the soil<br>Soil decomposition and respiration<br>Volatilisation | Photosynthesis, respiration, root exudation, senescence are the processes considered for this exercise. Other processes were not necessary to consider, but can be considered in other contexts | Biological growth<br>Photosynthesis<br>Growth and maintenance respiration<br>Senescence<br>Soil decomposition and respiration<br>Volatilisation |

| Model aspect | ANDRA (Aqua_C14) | FANC | IRSN (TOCATTA-χ) | SKB (SVAT) | SSM (SSPAM$^{14}$C) |
|---|---|---|---|---|---|
| Water balance in soil layers | Data set chosen such that water balance (precipitation - evapotranspiration) = 0 | Not applicable | - | - | - |
| Modelling of $CH_4$ oxidation | Yes, available in the model but not applicable for the La Hague case (all C-14 considered present as carbonates ($CO_2$ or $CO_3^{2-}$) | Not applicable | - | - | - |
| Calculation of atmospheric concentration of $^{14}CO_2$ | Comparable to IRSN input data; losses via deposition in the form of rain and gain via degassing of soil do not significantly change the atmospheric C-14 concentration | Given input | Given input | Given input | Given input |
| Where does the plant obtain carbon (and C-14) from? | For stable C: 98% atmosphere, 2% root uptake, traces via interception of rain | Atmospheric intake | Atmospheric intake | From the canopy air by photosynthesis | Atmospheric intake (98%)<br>Root uptake (2%) |
| Is root uptake of C included? | Yes, 2% | Yes | No | Not in this study, but it can be considered | Yes |
| Between what compartments is isotopic equilibrium assumed? | Canopy atmosphere and grass | C-14 is taken to behave as stable carbon throughout the model | Between air and input to sap compartment via photosynthesis<br>Between sap compartment and loss from sap due to biological growth<br>Between sap compartment and losses from sap due to growth and maintenance respiration | Between air and newly created biomass | Between lower atmosphere and above-ground plant |

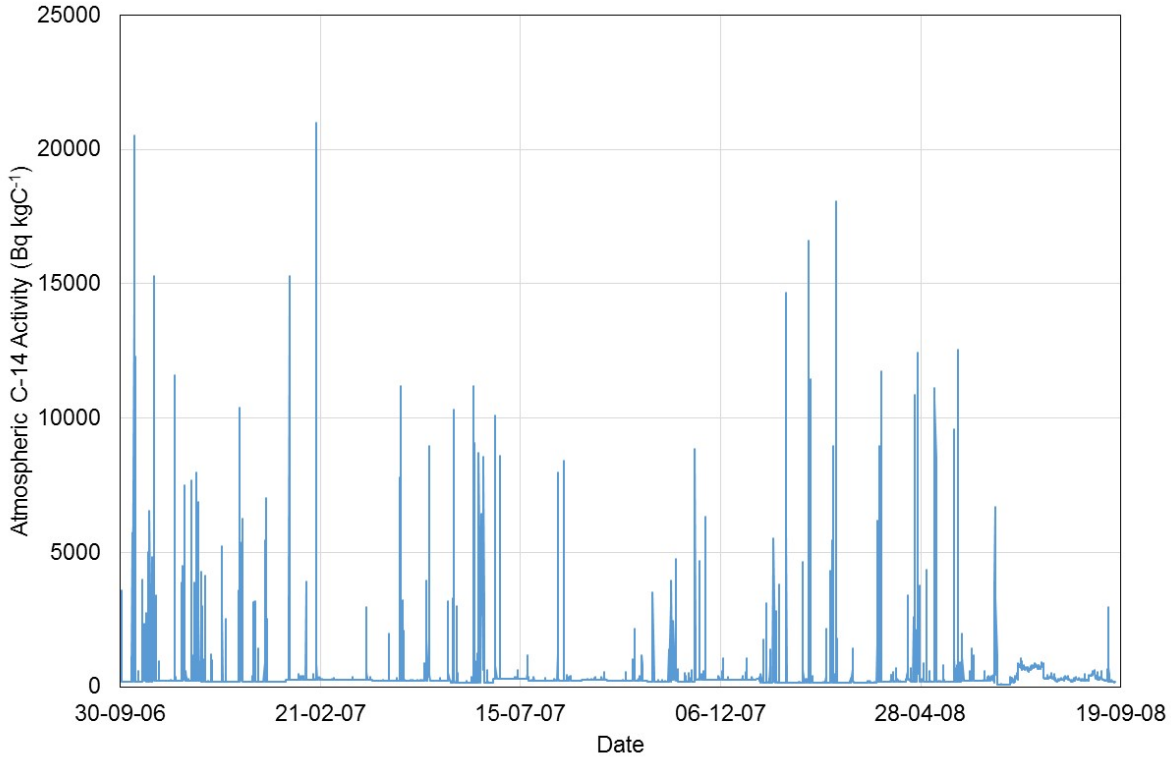


***Figure 3:*** ***Derived hourly specific activity of C-14 in the atmosphere at the site (Bq $kgC^{-1}$), based on hourly measurements of the Kr-85 concentration in the atmosphere at the site and an inferred ratio of Kr-85 to C-14 in the atmosphere based on monthly measurements at the site***

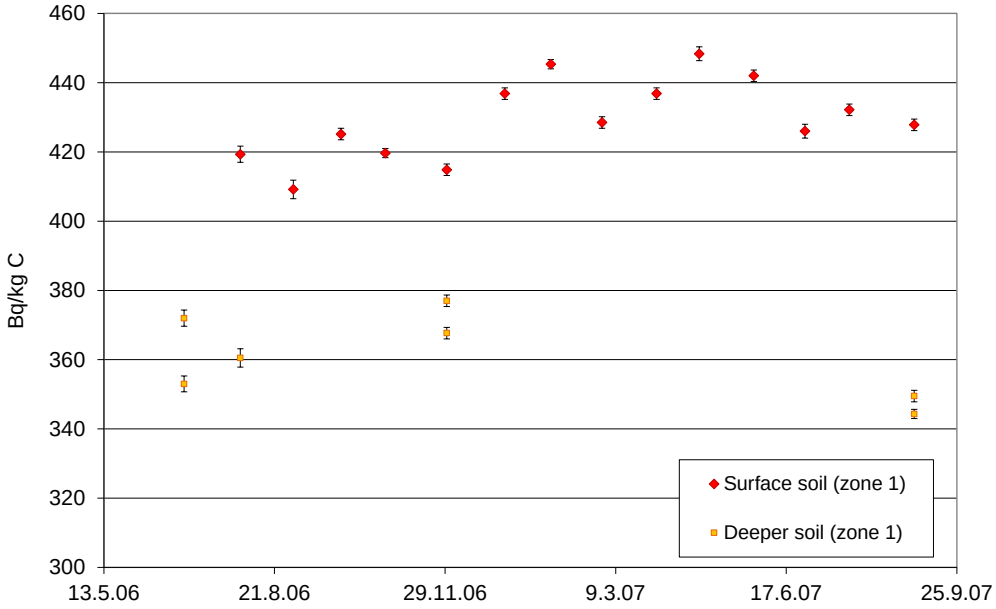


***Figure 4:*** ***Measured specific activity of C-14 in the soil surface (0-3 cm) and deeper soil (0-20 or 3-20 cm) at the field study site near La Hague. Standard deviations of the measurements are indicated with error bars.***

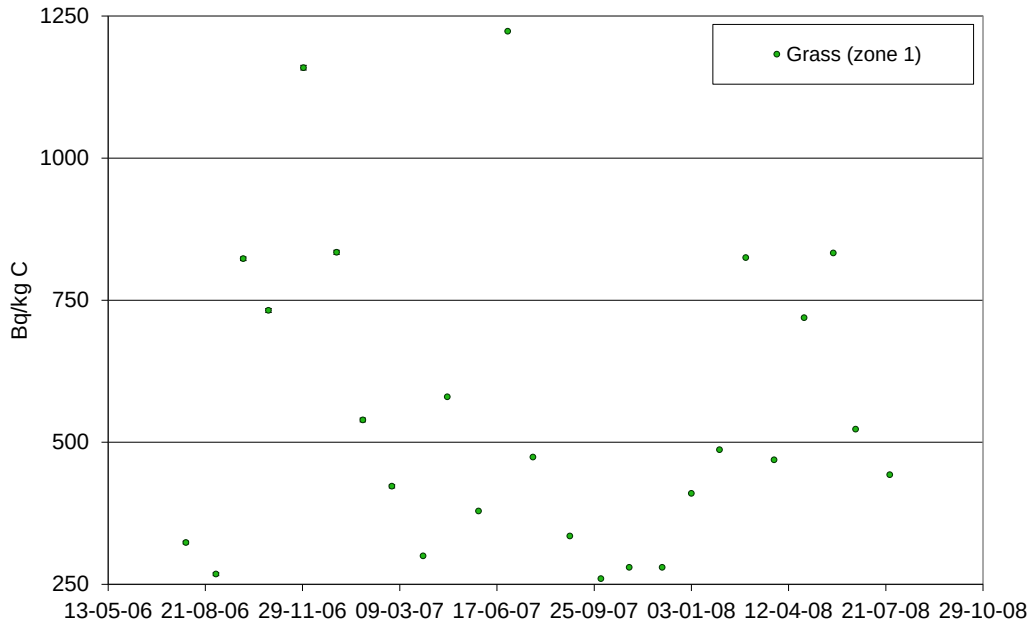


***Figure 5:*** ***Measured specific activity of C-14 in the grass at the field study site near La Hague***

## 2.5 RESULTS

Results for pasture concentrations are presented in Section 2.5.1, whilst those for soil are given in Section 2.5.2.

### 2.5.1 Calculated Activity of C-14 in Pasture

The calculated and observed concentrations of C-14 in the pasture are shown in Figure 6. The models generally represent the observed dynamics, with a high degree of correlation at the sampling points (Table 3).

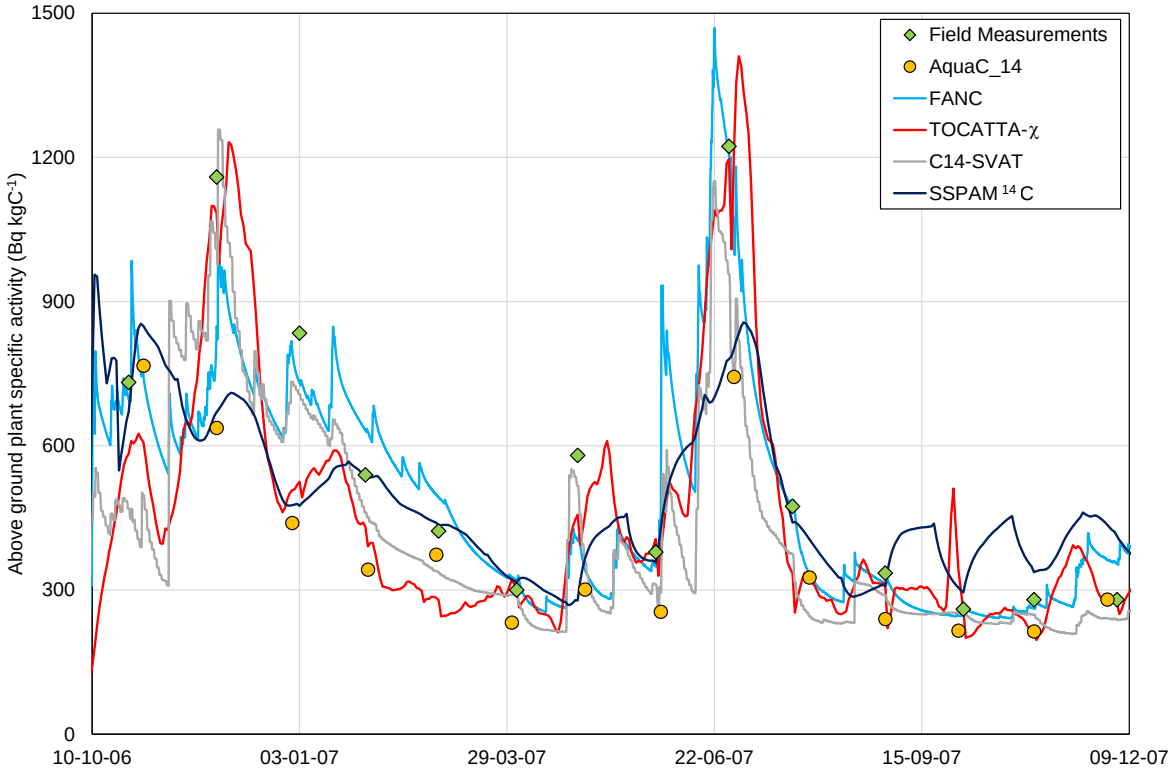


***Figure 6: Calculated and field measurements of C-14 specific activity in pasture at La Hague (Bq kgC$^{-1}$)***

*Table 3: Comparison of Calculated Concentration of C-14 in Pasture (Bq kgC$^{-1}$) at times of Field Sampling for the La Hague Scenario*

| Date | Concentration of C-14 in pasture (Bq kgC$^{-1}$) | | | | | |
|---|---|---|---|---|---|---|
| | Field obs. | Aqua_C14 * | FANC | TOCATTA-χ | SSPAM$^{14}$C | SVAT |
| 25-10-06 | 732 | *767* | 701 | 583 | 722 | 457 |
| 30-11-06 | 1159 | 637 | 903 | 1084 | 677 | 1124 |
| 03-01-07 | 834 | *440* | 731 | 525 | 475 | 701 |
| 30-01-07 | 539 | 342 | 631 | 431 | 538 | 457 |
| 01-03-07 | 423 | *374* | 490 | 279 | 435 | 335 |
| 02-04-07 | 300 | *232* | 322 | 301 | 316 | 280 |
| 27-04-07 | 580 | *301* | 404 | 457 | 278 | 488 |
| 29-05-07 | 379 | *255* | 353 | 406 | 389 | 291 |
| 28-06-07 | 1223 | *743* | 1185 | 1196 | 780 | 869 |
| 24-07-07 | 474 | *326* | 475 | 335 | 440 | 347 |
| 31-08-07 | 335 | 240 | 318 | 312 | 308 | 282 |
| 02-10-07 | 260 | *215* | 253 | 258 | 295 | 251 |
| 31-10-07 | 280 | 214 | 267 | 214 | 339 | 245 |
| 04-12-07 | 280 | *280* | 359 | 271 | 412 | 238 |
| | | | | | | |
| Correlation coefficient with field measurements | | 0.87 | 0.96 | 0.96 | 0.84 | 0.96 |
| $r^2$ | | 0.76 | 0.92 | 0.92 | 0.70 | 0.92 |

* The outputs in the cells highlighted in grey are for time points close to, but not identical to those of the field observations.

### 2.5.2 Calculated Activity of C-14 in Soil

Setting an initial activity of 420 Bk kgC$^{-1}$, both TOCATTA-χ and C14-SVAT calculated soil activities stay close to the observed values, which vary around that level [Aulagnier et al., 2012]. The results from Aqua_C14, however, are substantially lower than the observed values, in part because a zero initial concentration in the soil is not assumed.

## 2.6 DISCUSSION

In C-14 model comparison exercises that were carried out within a previous BIOPROTA study [Limer et al., 2011, 2012; Mobbs et al., 2013; Norris et al., 2011], large discrepancies between the predictions made with models. The discrepancies could largely be explained by differences in approaches to modelling the C-14 transport in the canopy atmosphere. It was concluded from that study that there was a need for a more rigorous modelling of these processes. This lead to SKB developing the C14-SVAT model described in Avila and Kovalets [2016] that has been used in this current study, as a replacement to the Avila and Pröhl [2008] model used in the previous BIOPOTA study.

The application of the five models here has shown that, for a well-defined atmospheric concentration, the isotopic ratio model for simulation of atmosphere – plant transport and the associated parameter values can be considered to be validated.

Over the time period of the field measurements, there is very little change in the soil concentration with time, but it diminishes somewhat with depth. The soil concentration comprises natural background (about 240 Bq $kgC^{-1}$) plus the contribution from the reprocessing plant from the 1950s to the present day. The diminished effect at depth is likely because the organic matter at depth is older, probably by several decades, so it has been less influenced by the history of C-14 discharges from La Hague.

To better validate the soil components of the models, a longer-term soil data set would be required beginning during the initial period of operations of La Hague, to observe the build-up of C-14 from natural background concentrations in chemically and physically stabilised organic matter. A longer-term historical data set of this nature would permit the following issues regarding C-14 accumulation and dynamics in soil to be examined:

- C-14 deposition via rain or solid organic matter;
- temporary storage in the soil in living or dead organic matter;
- recycling between the soil available and unavailable pools; and
- recycling between the plant and the soil (death and decay of plants, root exudation).

# 3 NOTTINGHAM EXPERIMENTAL STUDIES

The context for the Nottingham experimental data is described in Section 3.1, the models applied to the scenario are described in Section 3.2, the data set used in the study is presented in Section 3.3, the modelling scenarios are described in Section 3.4, the results of the model-data comparisons are presented in Section 3.5 and the findings are discussed in Section 3.6.

## 3.1 SYSTEMS DESCRIPTION

Potential impacts associated with release of C-14 bearing gaseous species from radioactive waste disposal facilities are of interest in many programmes. The gas most likely to reach the biosphere from a geological disposal facility containing substantial amounts of cementitious material (particularly cementitious grout) is $^{14}CH_4$, since $^{14}CO_2$, which is also expected to form, is likely to react with those cementitious materials (e.g. Heyes et al. [2015]).

There has been much recent work on the behaviour of both methane and carbon dioxide in soils, which has principally been focused on climate change. However, prior to the University of Nottingham studies, there remained considerable uncertainty over (a) the interaction of a sub-soil C-14 source term (gaseous or in solution) with soil microorganisms and organic matter, and (b) the degree of potential plant uptake of C-14 following a sub-soil source. Incorporation, either via root uptake or photosynthesis, will result in C-14 exposures to grazing animals and human consumers of plant and animal products.

In view of these uncertainties, Radioactive Waste Management Limited (RWM[d]) commissioned a combined experimental and modelling project with the following objectives.

1. To obtain experimental data on the behaviour of $^{14}CH_4$ and $^{14}CO_2$ from a sub-soil source term in the soil zone, and subsequent uptake of C-14 by plants.

2. To interpret the results of the experiments using appropriate techniques and models.

3. To develop an assessment model that can be used to calculate the activity concentrations of C-14 in plant material that arises from a below-ground flux of C-14 bearing gas.

Scientists working at the University of Nottingham undertook a series of three field and four laboratory experiments, considering the behaviour of these gases in disturbed and undisturbed agricultural soils, subject to differing vegetation cover; in the laboratory studies consideration was also given to the soil wetting profiles (see Figure 7 and Table 4). The results from these experiments have been published in a series of reports [Atkinson et al., 2011, 2012 and 2014]. Note that the majority of these experiments used C-13 labelled methane as a non-radioactive, but traceable, surrogate for C-14 labelled methane. However, a laboratory soil column study confirmed that C-14 and C-13 behaved similarly in this experimental system [Atkinson et al., 2014].

Only small pulses of methane were injected at depth in the soil (to avoid stimulating the population of methanotrophic microbes), so it was not possible to detect the subsequent uptake of any oxidised labelled carbon dioxide by the plants (either by their leaves, due to photosynthesis, or by their roots, in the transpiration stream). Hoch et al. [2014] outline the following possible reasons for this.

[d] Previously the Radioactive Waste Management Directorate (RWMD) of the UK Nuclear Decommissioning Authority (NDA).

1. Injection of the pulse of $^{13}C$-labelled methane induced a small shift (at most 20‰) in the isotopic signature of carbon dioxide in the soil.
2. The shift lasted for only a day or two (i.e. for about 1% of the growing season).
3. There was a lag between consumption of methane and production of carbon dioxide, which meant that the peak $^{13}CO_2$ release probably happened during the night, when photosynthesis would not have been occurring.


*Figure 7: Photographs show gas sampling from unvegetated (a) and vegetated (b) plots and the use of a closed headspace chamber for efflux analysis with the 50 cm high chamber used in unvegetated treatments (c) with chambers of differing heights through time in the vegetated plots (d and e), due to the height change of the spring wheat crop. (Reproduced from Atkinson et al. [2014])*

*Table 4: Summary of RWM $^{14}C$ experiments undertaken by the University of Nottingham*

| Expt. | Summary of setup | Antecedent measurements | Post-injection measurements |
|---|---|---|---|
| LE 1 | Homogenised unvegetated 50 cm high soil columns, with a maintained (fixed) water content of 20%.<br>$^{13}C$-labelled methane used. | Bulk gas concentrations throughout soil profile and in headspace two months prior to injection.<br>Specific activities of $^{13}CO_2$ and $^{13}CH_4$ throughout soil profile and in headspace two months and 24 hours prior to injection. | Bulk gas concentrations and specific activities of $^{13}CO_2$ and $^{13}CH_4$ throughout soil profile and in headspace for 15 days. |
| LE 2 | Intact (undisturbed) unvegetated 50 cm high soil columns, maintained water content of field conditions.<br>$^{13}C$-labelled methane used. | Bulk gas concentrations of $CO_2$ and $CH_4$ throughout soil profile and in headspace 4 days and 1 day prior to injection.<br>Specific activities of $^{13}CO_2$ and $^{13}CH_4$ throughout soil profile and in headspace two months prior to injection.<br>Soil organic matter content. | Bulk gas concentrations and specific activities of $^{13}CO_2$ and $^{13}CH_4$ throughout soil profile and in headspace for 15 days. |
| LE 3 | Intact (undisturbed) 50 cm high soil columns, either planted with ryegrass or unvegetated. Variable soil moisture.<br>$^{13}C$-labelled methane used. | Bulk gas concentrations of $CO_2$ and $CH_4$ throughout soil profile and in headspace 2 weeks and 1 day prior to injection.<br>Specific activity in vegetation. | Bulk gas concentrations and specific activities of $^{13}CO_2$ and $^{13}CH_4$ throughout soil profile and in headspace for 48 hours.<br>Specific activities in vegetation and soil upon completion. |
| LE 4 | Homogenised unvegetated 50 cm high soil columns. Variable soil moisture.<br>The first injection comprised $^{13}C$-labelled methane, whereas the second comprised $^{14}C$-labelled methane. | Bulk gas concentrations of $CO_2$ and $CH_4$ throughout soil profile and in headspace 1 day prior to injection. | Bulk gas concentrations and specific activities of $^{13/14}CO_2$ and $^{13/14}CH_4$ throughout soil profile and in headspace for 7 days following each of the injections. |
| FE 1 | 12 randomised plots either fully vegetated with ryegrass orl with the central 0.5 m diameter unvegetated.<br>$^{13}C$-labelled methane used. | Bulk gas concentrations of $CO_2$ and $CH_4$ throughout soil profile and in headspace 1 week prior to injection. | Bulk gas concentrations and specific activities of $^{13}CO_2$ and $^{13}CH_4$ throughout soil profile and headspace for 7 days following each of the three injections.<br>Specific activities in vegetation and soil upon completion. |

| Expt. | Summary of setup | Antecedent measurements | Post-injection measurements |
|---|---|---|---|
| FE 2 | 12 randomised plots either fully vegetated with spring wheat or with the central 0.5 m diameter unvegetated. $^{13}C$-labelled methane used. | Bulk gas concentrations of $CO_2$ and $CH_4$ throughout soil profile and in headspace 2 weeks prior to injection. Soil organic matter content. | Bulk gas concentrations and specific activities of $^{13}CO_2$ and $^{13}CH_4$ throughout soil profile and in headspace for 7 days following each of the three injections. |
| FE 3 | 12 randomised plots either fully vegetated with spring wheat or with the central 0.5 m diameter unvegetated. Experiments run in parallel to FE 2, but in additional plots set up some distance away and injected with $^{13}C$-labelled carbon dioxide. | Bulk gas concentrations of $CO_2$ and $CH_4$ throughout soil profile and in headspace 2 weeks prior to injection. | Bulk gas concentrations and specific activities throughout soil profile and in headspace for 7 days following each of the three injections. |

Notes: LE = Laboratory Experiment; FE = Field Experiment

## 3.2 MODELS APPLIED TO THE NOTTINGHAM SCENARIOS

In this section, an overview of each model is given in turn, before the key features are summarised in Table 5.

### 3.2.1 EDF

EDF R&D developed a new C-14 terrestrial model using the Ecolego platform[e]. The EDF C-14 terrestrial model contains several compartments, between which differential equations are solved to give time-dependent contents. The model comprises four sub-models: soil, root, shoot, and canopy air. The soil sub-model consists of *n* layers of compartments, whereas the others include only a single compartment for each. The model is used to simulate the transfers of $^{14}CO_2$ and $^{14}CH_4$ in the soil-plant-air system. The radioactive decay of C-14 is taken into account in each differential equation. Figure 8 shows the schematic representation of the model. The main processes considered in the model are numbered in Figure 8:

1. Oxidation;
2. Diffusion between soil layers;
3. Downward advection over soil layers;
4. Diffusion through the soil-canopy air interface;
5. Root uptake by the transpiration stream;
6. Xylem outflow;
7. Gas exchange between shoot and canopy air; and
8. Dilution by external air.

Further details about this model can be found in Section A.2 of the Appendix.

[e] http://ecolego.facilia.se

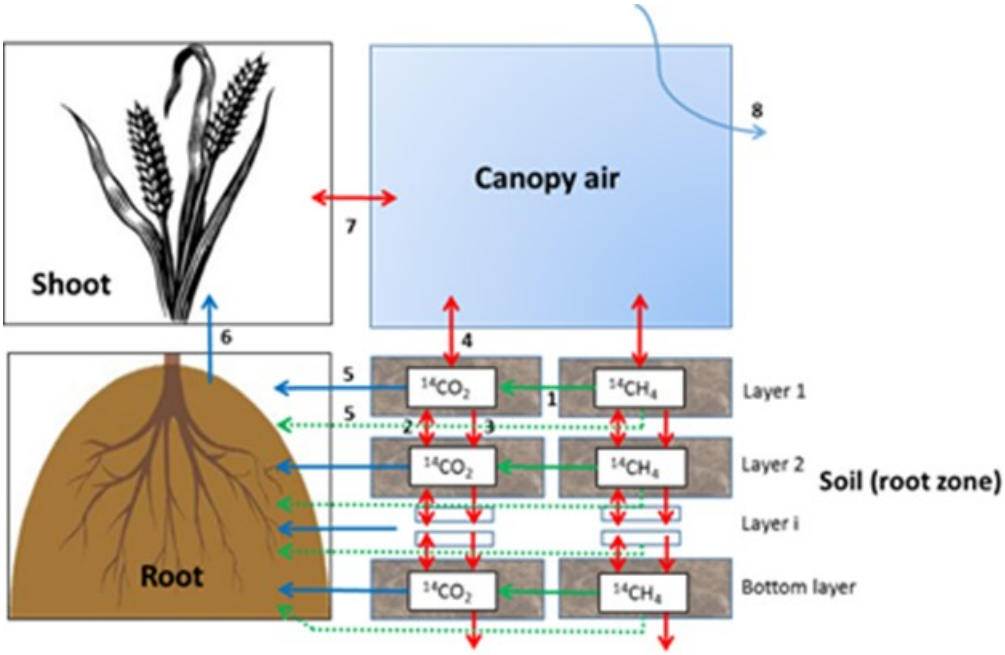


*Figure 8: Schematic representation of the EDF C-14 terrestrial model*

### 3.2.2 JAEA (Solveg II)

SOLVEG-II is a one-dimensional model for predictions of heat, water and $CO_2$ transfers in a multi-layered atmosphere-vegetation-soil system [Yamazawa, 2001; Nagai, 2002, 2005]. The model is driven by meteorological input to the upper boundary of the modelled atmosphere, below which the vegetation canopy and soil exist. The atmospheric model calculates turbulent diffusion of heat, vapour and $CO_2$, and the vegetation model predicts leaf transpiration and photosynthesis in the canopy by using the Farquhar's photochemistry [Farquhar et al., 1980] and the Ball-Berry and Leuning's stomata-photosynthesis interdependent model [Collatz et al., 1991]. In soil, unsaturated-zone transports of heat, water and $CO_2$ are calculated, in which the water transport is expressed by Richard's equation. Modelled processes for the exchange of heat, water, $CO_2$ and other trace gases have been validated for many land use types, such as grassland and wheat crops [Nagai, 2002, 2005; Katata et al., 2011; Ota et al., 2007, 2013, 2016a, 2016b].

The $^{14}CO_2$ model of SOLVEG-II (Figure 9) is run with input of concentrations of $^{14}CO_2$ in the atmosphere as the upper boundary condition [Ota et al., 2012, 2016b]. The atmospheric model calculates transport of $^{14}CO_2$ by turbulent diffusion. In the soil, diffusion of $^{14}CO_2$ in the soil air, and diffusion, advection and dispersion of $^{14}CO_2$ in the soil water are predicted, with an assumption that $^{14}CO_2$ in the soil air and water are in an equilibrium expressed by Henry's law. The vegetation model predicts concentrations of $^{14}CO_2$ in leaf cellular water and $^{14}C$ in leaf organic matter by considering the $^{14}C$ budget in the leaf cellular water as determined by a number of processes (Figure 9): atmosphere-leaf exchange of $^{14}CO_2$ via stomata, soil-to-leaf transfer of $^{14}CO_2$ by root-water uptake, assimilation of $^{14}C$ from the leaf cellular water to the leaf organic matter by photosynthesis, and production of $^{14}CO_2$ during decomposition of the leaf organic matter by respiration. Model calculations of foliar deposition of $^{14}CO_2$ have been validated [Ota et al., 2012; 2016b] with data from a $^{14}CO_2$ exposure experiment using grape plants [Guenot and Belot, 1984] and observations of $^{14}C$ accumulation in rice grain cropped around a $^{14}CO_2$-releasing facility [Aomori Prefecture, 2008; Akata et al., 2013].

Processes related to $^{14}CO_2$ transfer are from Ota et al. [2012, 2016b]. Full details of the $^{14}CH_4$ model of SOLVEG-II are given in Section A.3 of the Appendix.

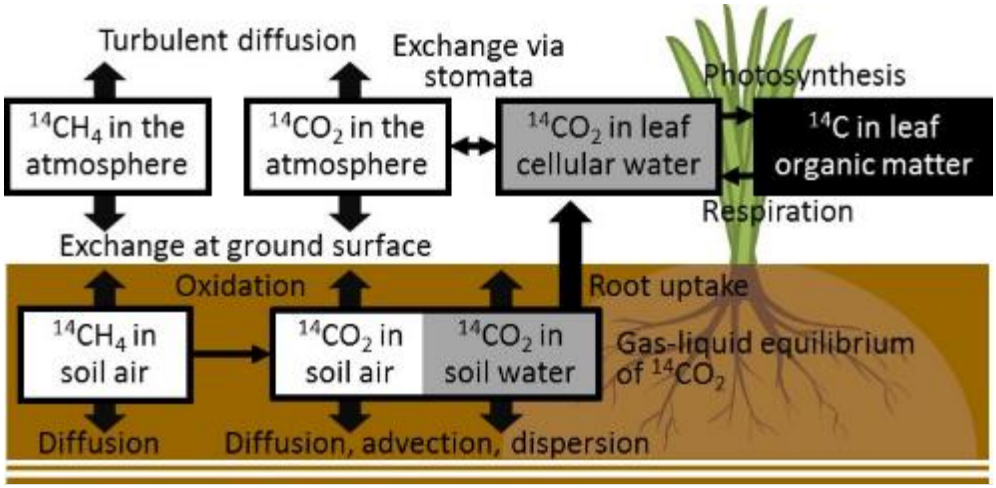


*Figure 9: Processes of transfer of $^{14}CO_2$ and $^{14}CH_4$ considered in SOLVEG-II*

### 3.2.3 RWM (T2Plants)

In addition to the experimental work at Nottingham University, RWM supported a programme of modelling to help interpret the observational data. As such, a conceptual model of the system was developed and applied to some of the data [Hoch, 2014; Hoch et al., 2014]; both a process-based and an assessment-level model were developed. It is the results from calculations using the process-based model that are presented as part of this current study. It is therefore the process-based model that is summarized here, with full details given in Hoch et al., [2014].

The model includes the following processes:

- diffusion of component gases through the gas-occupied porosity of the soil;
- soil respiration, forming carbon dioxide;
- methane oxidation by methanotrophic microbes, converting methane into carbon dioxide; and
- coupled flows of water and gas through a partially saturated soil.

The last process has to be accounted for because it determines the volumetric water content of the soil, which in turn will affect the effective diffusion coefficients of the component gases. To simulate these processes, a computer program called T2Plants [Webb, 2013] has been developed. T2Plants was based on TOUGH2v2 [Pruess, 1987, 1991; Pruess et al., 1999][f], which is a computer program for simulating non-isothermal flows of multi-component, multiphase fluids in porous media.

Further details of the model are given in Section A.4 of the Appendix.

For the laboratory experiments, because both the geometry and the boundary conditions (e.g. the injection of $^{13}C$-labelled methane) are symmetrical about the axis of each soil column, it is possible to

[f] For details on the TOUGH series of codes, see http://esd1.lbl.gov/research/projects/tough/.

simulate gas transport through the soil using a two-dimensional, cylindrically-symmetric model (Figure 10). For the field experiments, the geometry and the boundary conditions (e.g. the injection of $^{13}C$-labelled methane) also were symmetrical, in this case about a vertical axis passing through the point of methane injection in the soil. Therefore, it was also possible to simulate gas transport through the soil using a two-dimensional, cylindrically-symmetric model.

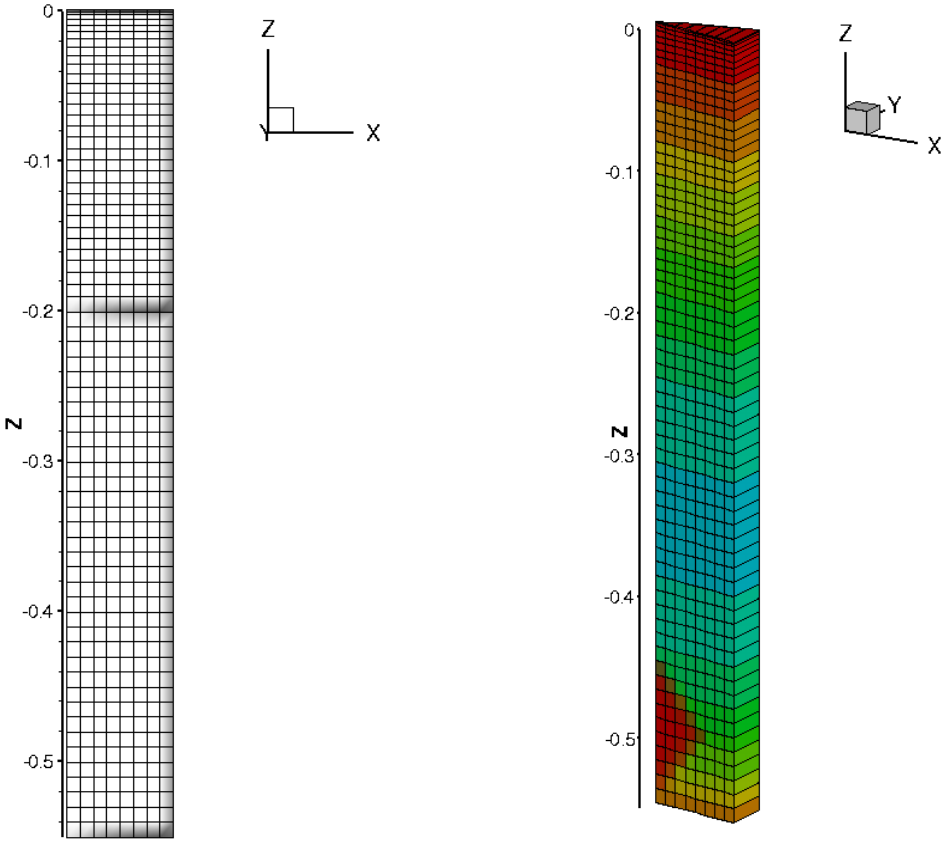


***Figure 10: The numerical grid (left-hand figure) representing a sector through a soil column (right-hand figure) in T2Plants. In the right-hand figure, the contours shown are of the concentration of $^{12}CH_4$ in the soil column. The injection of methane at a depth of 50 cm can be seen.***

### 3.2.4 BIOPROTA Technical Support Team

A 1D model was developed by the BIOPROTA Technical Support Team for this project, to illustrate how the pulse injection studies undertaken at the University of Nottingham can be interpreted for assessment purposes using the minimum in special assumptions. Specifically, the reciprocal theorem was used to relate pulse-injection results to those that would be obtained if the pulse injection was to be replaced by a continuous constant flux (which is the situation of interest for assessment purposes). The details of that model are given in Section A.4 of the Appendix.

*Table 5: Summary of Key Model Features for those Models Applied to the Nottingham Scenarios*

| Model aspect | EDF | JAEA (SOLVEG II) | RWM | TST |
|---|---|---|---|---|
| Calculation time-step | Minute order | Seconds (freely definable) | Seconds (freely definable) | Use of the reciprocal theorem to define an equivalent equilibrium system |
| Sub-models (if appropriate) | Canopy air, shoot, root, and soil | Sub-models to calculating transport of heat, water, and $CO_2$ are included. | Not applicable | Not applicable |
| No. of soil compartments | The number of layers can be freely determined. In this exercise, it was fixed to 10 layers. | Number of soil layers are freely definable | Laboratory experiments: 529 blocks<br>Field experiments: 1667 blocks | Exponential interpolation between measurement depths |
| No. atmosphere compartments | One layer | Number of atmospheric layers are freely definable | 0 | 0 |
| No. of plant compartments | One layer | Number of canopy layer are freely definable | 0 | 0 |
| Full list of processes in the model | See Figure 1 | Available from literature | Multi-phase transport of fluids in soil, exchanges between the fluid phases, plant uptake from soil | Advection-diffusion with oxidation of methane and minimal process assumptions |
| Water balance in soil layers | Tipping bucket water balance model | Calculated with Richard's equation | Multi-phase modelling with Richard's equation | Specified from observations |
| Modelling of $CH_4$ oxidation | First-order rate constant ($T^{-1}$) represents the oxidation process. A constant value was set for this exercise. | Modelled as a function of temperature, water content and depth in soil | First-order rate coefficient via intermediate forms | First-order rate coefficient |
| Calculation of atmospheric concentration of $^{14}CO_2$ | The canopy air concentration is calculated by exchange processes between soil – air and between plant – air, and an empirically derived dilution factor that considers mixing with external air. | Calculated by considering turbulent diffusion of $^{14}CO_2$ | Coupled to surface atmosphere boundary layer behaviour | Specified boundary conditions at the soil surface |
| Where does the plant obtain carbon (and C-14) from? | Soil and canopy air compartments | $^{12}C$: from atmosphere<br>$^{14}C$: from atmosphere and soil | Plant uptake was observed experimentally to be very limited, so this was not simulated | Not applicable |

| Model aspect | EDF | JAEA (SOLVEG II) | RWM | TST |
|---|---|---|---|---|
| Is root uptake of C included? | Yes. Root uptake of C-14 dissolved in soil water is included. | Yes. | No. | Not applicable |
| Between what compartments is isotopic equilibrium assumed? | Not assumed. | None. | Not assumed | Not applicable |

### 3.3 NOTTINGHAM DATASET

This study has focussed on two of experiments, specifically laboratory experiment 3 (LE3) and the complimentary field experiment 2 (FE2). Both experiments involved injection of $^{13}C$-labelled pulses of methane to the subsoil, and therefore included the effects of the metabolism of methane to carbon dioxide within the soil column. Full details of these two experiments are given in Atkinson et al. [2014], including the exact timings and nature of the source term used in each experiment; this information was provided to the modelling groups on request. Here, a summary is given of the types of dataset that are available.

#### 3.3.1 Laboratory Experiment 3 (LE3)

The setup of this experiment is described in Section 5.1 of Atkinson et al. [2014]. It involved six undisturbed soil cores of which three were seeded with ryegrass and three remained non-vegetated. The experiment was conducted in a controlled growth room with a 16-hour day, with 75% sunlight, and a six hour night. The day temperature was 18°C and the night temperature was 10°C. Humidity was 75%. Samplers were installed at depths of 10, 20, 30, 40 and 50 cm, with that at 50 cm also being used for gas injection. A 20 cm high PVC head chamber was used to capture gas above the soil. Details of gas, preparation injection and sampling are given in Sections 5.1 and 5.2 of Atkinson et al. [2014].

Soil porosity was estimated from soil bulk density using a particle density of 2.85 g $cm^{-3}$. Soil volumetric water content, bulk density and porosity are shown in Figures 6.1 to 6.3 of Atkinson et al. [2014]. Prior to the injection of labelled methane, antecedent concentrations of methane and carbon dioxide were measured at different depths in the soil (see Figure 11 and Figure 12), and both concentrations in and effluxes to the air in a headspace chamber were also measured (see Tables 6.1 to 6.4 of Atkinson et al. [2014]).

The antecedent ratio of $^{13}CH_4$:$^{12}CH_4$ (referred to as $\delta^{13}CH_4$) in the soil was below the limit of detection of the experiment. The antecedent $\delta^{13}CO_2$ (ratio of $^{13}CO_2$:$^{12}CO_2$) in the soil was in the range -24‰ to -22‰.

The results that are available are summarised below; detailed discussion of the experimental results can be found in Sections 6.2 and 6.3 of Atkinson et al. [2014].

- Bulk methane concentrations just prior to and for 48 hours following injection of isotopically enriched methane in the soil show a clear signal of the enriched methane moving through the soil column and were useful for model testing. In contrast, the corresponding data for carbon dioxide show little effect on concentrations, except possibly at the 50 cm sampler level. The $\delta^{13}C$ signature of both gases were considered useful in testing the performance of the models in respect of the competition between methane transport in soils and metabolism to carbon dioxide, including the delay between the initial and final steps of metabolic conversion.

- The methane efflux from the soil columns is clearly enhanced following injection, with a more limited effect seen for the carbon dioxide efflux. The efflux is also somewhat different in vegetated and non-vegetated columns. Enhancement is again observed in the $\delta^{13}C$ of both gases in the soil efflux data.
- Values of $\delta^{13}C$ in the ryegrass and soil from the experiment showed no significant changes, and are not useful for model testing.

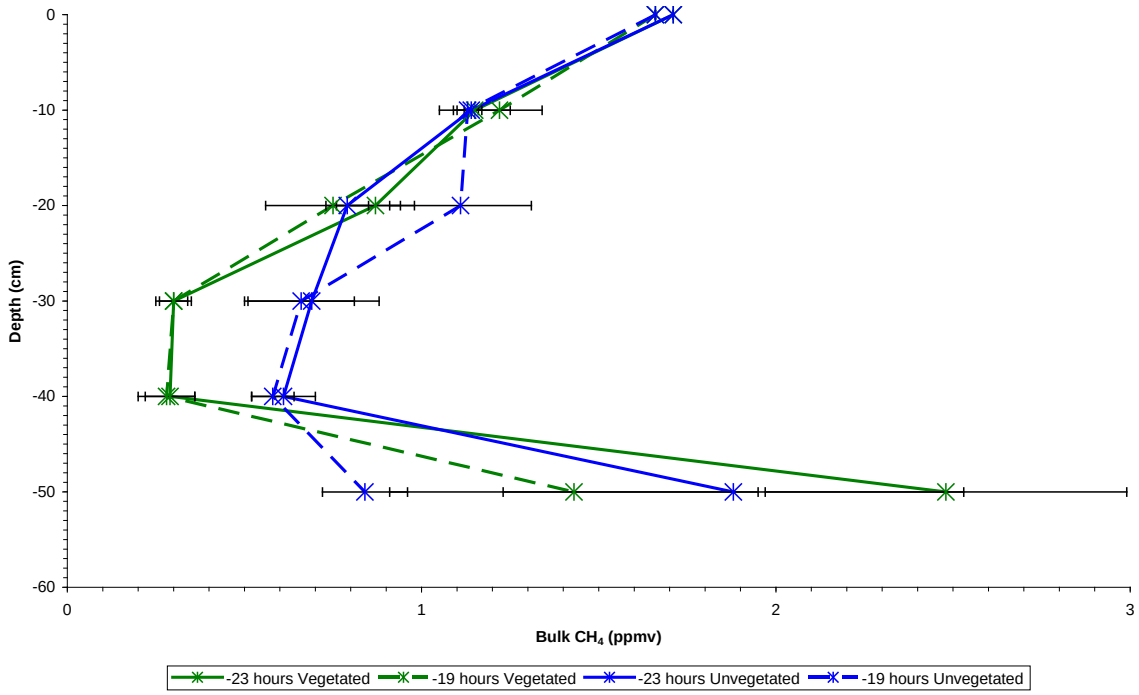


*Figure 11: Antecedent bulk $CH_4$ concentrations at different depths within the vegetated (blue) and unvegetated (green) soil columns (LE3). (Reproduced from Hoch et al. [2014])*

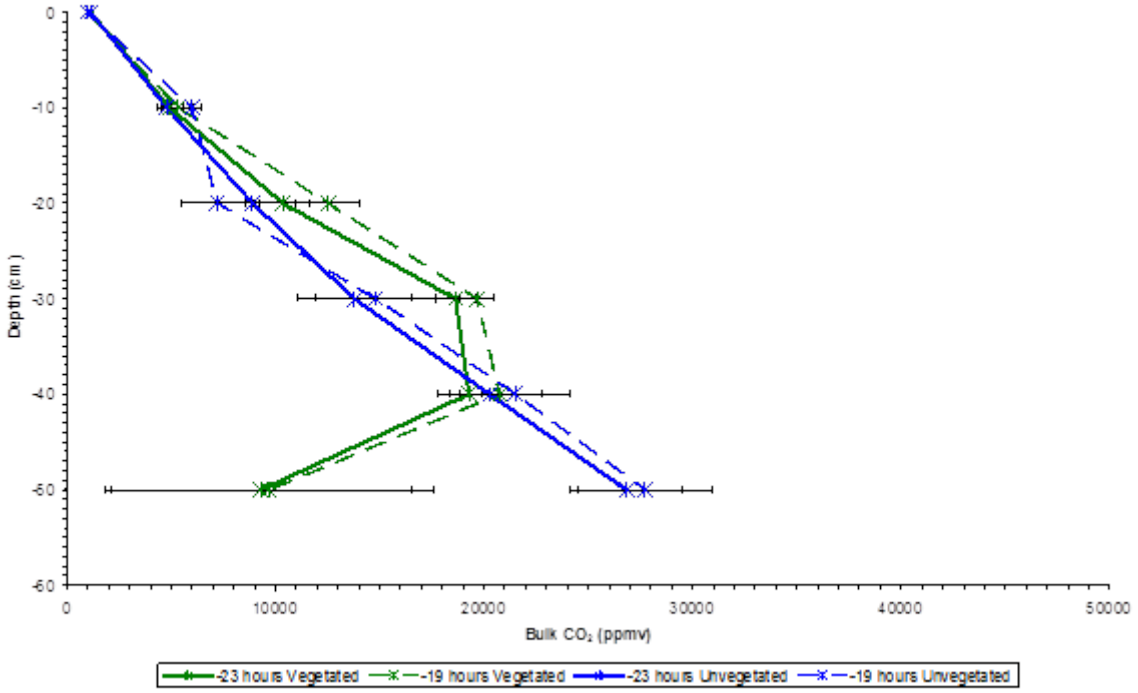


*Figure 12: Antecedent bulk $CO_2$ concentrations at different depths within the vegetated (blue) and unvegetated (green) soil columns (LE3) (Reproduced from Hoch et al. [2014])*

### 3.3.2 Field Experiment 2 (FE2)

The experimental set up is described in Section 3.1 of Atkinson et al. [2014]. Twelve randomised plots were used (4 control – with two vegetated and two non-vegetated, 4 non-vegetated and 4 vegetated). Gas was injected at a depth of 50 cm and was free to diffuse in all directions. Samplers were installed at depths of 10, 20, 30, 40 and 50 cm, with that at 50 cm also used for gas injection. A 10 cm high PVC collar was installed to a depth of 5 cm at the soil surface for the purpose of mounting the head chamber. Vegetated plots had been sown with spring wheat prior to sampler installation. Details of gas preparation injection and sampling are given in Section 3.3 of Atkinson et al. [2014].

Environmental measurements were made throughout the experimental period. These related to soil moisture, soil temperature and standard weather station parameters (rainfall, temperature, humidity, barometric pressure, wind speed and wind direction). These data are plotted in Figures 4.1 to 4.5 of Atkinson et al. [2014]. Soil samples were collected from each plot to determine vertical profiles of bulk density and porosity, organic matter content, volumetric water content and pH at the end of the experimental period. These data are plotted in Figures 4.6 to 4.10 of Atkinson et al. [2014].

The antecedent concentrations of $CH_4$ and $CO_2$ in the soil at all the sampler depths (10, 20, 30 40 and 50 cm) and at the soil surface are shown in Figure 13 and Figure 14 respectively. Similar measurements were also taken up to 168 hours after injection. Measurements of $\delta^{13}C$ for both methane and carbon dioxide were also available.

A detailed discussion of the experimental results can be found in Sections 4.2, 4.3 and 4.4 of Atkinson et al. [2014].

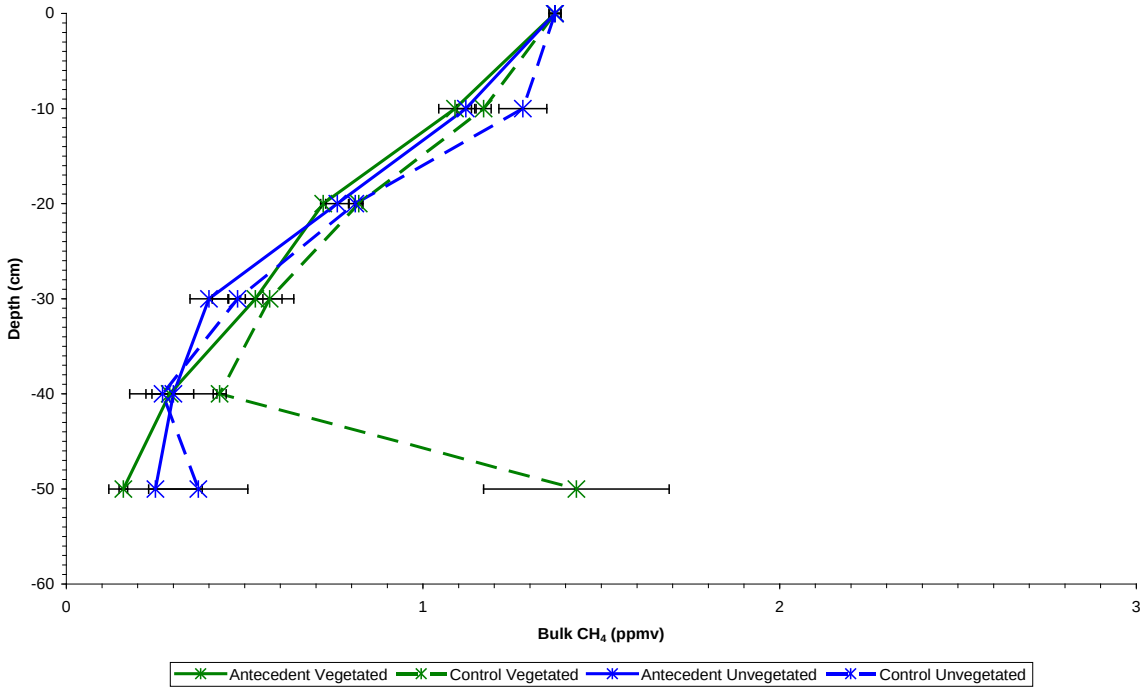


*Figure 13: Antecedent bulk $CH_4$ concentrations at different depths within the vegetated (blue) and unvegetated (green) soil (FE2). (Reproduced from Hoch et al. [2014])*

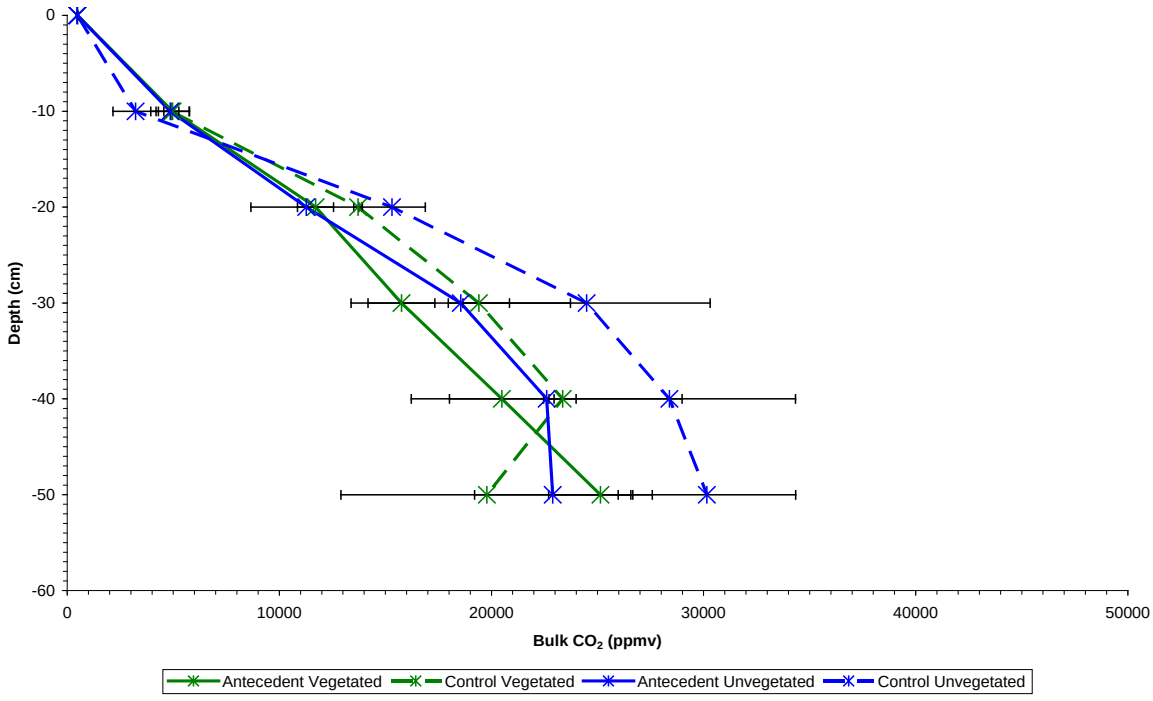


*Figure 14: Antecedent bulk $CO_2$ concentrations at different depths within the vegetated (blue) and unvegetated (green) soil (FE2). (Reproduced from Hoch et al. [2014])*

### 3.4 CALCULATION SCENARIO DESCRIPTIONS

The two experiments described in the preceding section provide the opportunity to test the following aspects of models for a sub-soil gaseous source term:

- LE3: 1-D diffusion-reaction calculation in soil; and
- FE2: conversion of $CH_4$ to $CO_2$, migration of $CH_4$ and $CO_2$ in soil, and plant uptake.

The model scenario for each experiment is described in the subsections below.

#### 3.4.1 Laboratory Experiment 3 (LE3)

The main issues to be investigated were the transport of methane and carbon dioxide in the gas phase in the soil zone, and the degree and kinetics of conversion of methane to carbon dioxide during that transport. Modelling was proposed to be conducted in two steps. In the first step, the model was to be used to simulate the following quantities (the tables in Atkinson et al. [2014] that provide the data are given in brackets).

1. Bulk methane concentrations at all soil-sampler levels to 48 hours after injection (Table 6.5).
2. Bulk methane efflux from the soil surface to 48 hours after injection (Table 6.7).
3. Bulk carbon dioxide concentrations at all soil-sampler levels to 48 hours after injection (Table 6.6).
4. Bulk carbon dioxide efflux from the soil surface to 48 hours after injection (Table 6.8).

Item 1 is the primary dataset of interest, since the data are clear and comprehensive. Item 2 largely provides a consistency check, since the concentration profile and its time-development fully determines the resultant efflux. Items 3 and 4 are secondary and investigate whether the models give limited perturbations in bulk carbon dioxide concentrations and effluxes comparable in magnitude with those observed.

In the second step, it was proposed that the models should be used to simulate the following quantities (again with the associated tables in Atkinson et al. [2014] given in brackets).

1. The isotopic signature of methane at all soil-sampler levels to 48 hours after injection (Table 6.9).
2. The isotopic signature of methane in the efflux from the soil surface to 48 hours after injection (Table 6.11).
3. The isotopic signature of carbon dioxide at all soil-sampler levels to 48 hours after injection (Table 6.10).
4. The isotopic signature of carbon dioxide in the efflux from the soil surface to 48 hours after injection (Table 6.12).

In this second step, both Item 1 and Item 3 were of primary interest, since these datasets exhibit clear signals. It was proposed that as items 2 and 4 should yield results consistent with Items 1 and 3, respectively, and that this consistency should be checked.

### 3.4.2 Field Experiment 2 (FE2)

For FE2, the modelling was required to be conducted in two steps, relating to bulk gas and isotopic measurements, respectively. In the first step, it was proposed that the model should be used to simulate the following quantities (tables in Atkinson et al. [2014] that provide the data are given in brackets):

1. Bulk methane concentrations at all soil-sampler levels to 168 hours after injection (Table 4.6).
2. Bulk methane efflux from the soil surface to 169 hours after injection (Table 4.8).
3. Bulk carbon dioxide concentrations at all soil-sampler levels to 168 hours after injection (Table 4.7).
4. Bulk carbon dioxide efflux from the soil surface to 48 hours after injection (Table 4.9).

As for LE3, Item 1 is the primary dataset of interest, since the data are clear and comprehensive. Item 2 largely provides a consistency check, since the concentration profile and its time-development fully determines the resultant efflux. Items 3 and 4 are secondary and investigate whether the models give limited perturbations in bulk carbon dioxide concentrations and effluxes comparable in magnitude with those observed.

In the second step, the model was required to be used to simulate the following quantities (again with the associated tables in Atkinson et al. [2014] given in brackets).

1. The isotopic signature of methane at all soil-sampler levels to 168 hours after injection (Table 4.10).
2. The isotopic signature of methane in the efflux from the soil surface to 168 hours after injection (Table 4.12).
3. The isotopic signature of carbon dioxide at all soil-sampler levels to 168 hours after injection (Table 4.11).
4. The isotopic signature of carbon dioxide in the efflux from the soil surface to 169 hours after injection (Table 4.13).

In this case, although the carbon dioxide signal is limited, it is reasonably clear, so all four items are of primary interest. In addition, it was proposed that it would be useful to provide a model estimate of the change in $\delta^{13}C$ in plants to compare with the limited shift shown in Figures 4.35 and 4.36 of Atkinson et al. [2014], and to enable model-model comparisons.

## 3.5 RESULTS

In this section, the results from the four groups who simulated the RWM Nottingham studies are presented separately.

- Section 3.5.1 – Laboratory Experiment 3: RWM
- Section 3.5.2 – Laboratory Experiment 3: Project Technical Support Team
- Section 3.5.3 – Field Experiment 2: EDF
- Section 3.5.4 – Field Experiment 2: JAEA
- Section 3.5.5 – Field Experiment 2: RWM
- Section 3.5.6 – Field Experiment 2: Project Technical Support Team

In the modelling of EDF and JAEA, the models report C-14 activities. The method used to convert the field measurements of C-13 to C-14 activity is given in Section A.7of the Appendix.

### 3.5.1 Laboratory Experiment 3: RWM T2Plants

Figure 15[g] shows the calculated and the laboratory measurements of bulk $CH_4$ at different depths of the intact soil columns. It is clear that the measured and modelled levels of $CH_4$ are elevated above the antecedent levels (cf. Figure 11). The calculated and laboratory measurements of bulk $CO_2$ at different depths of the intact soil columns are shown in Figure 16. These show a similar depth profile of $CO_2$ concentrations to the antecedent measurements (cf. Figure 12).

Methane with a $^{13}C$:$^{12}C$ ratio of 3:7, for which $\delta^{13}C$ = 37,139‰, was injected. Therefore, $\delta^{13}CH_4$ increases to approximately this value. Because the microbial process of methane oxidation discriminates very slightly (i.e. by a few percent) against $^{13}C$, the numerical model predicts that $\delta^{13}CH_4$ (i.e. the $^{13}C$:$^{12}C$ ratio) increases slightly with time until the point at which most of the methane either has been consumed or has left the system (see Figure 17). The data, however, show a significant decrease in $\delta^{13}CH_4$ with time. The data seem to suggest that $^{13}CH_4$ is consumed more rapidly than $^{12}CH_4$ as the pulse of methane diffuses up the column.

Figure 18 compares the prediction of $\delta^{13}CO_2$ at different depths within the soil with the data. The rate constant of the uptake of methane has been calibrated to ensure that the peak $\delta^{13}CO_2$ is at the right time, but the magnitude of the peak is too large (see Section 6.2 of Hoch et al. [2014] for more details). The simplest explanation is that the assumed branching fraction for formation of carbon dioxide from the “intermediate” is too high.

[g] The small kinks in the modelled curves are due to the extraction of 15 ml of soil gas from depths of 40 cm, 30 cm, 20 cm and 10 cm at each of the experimental sampling times.

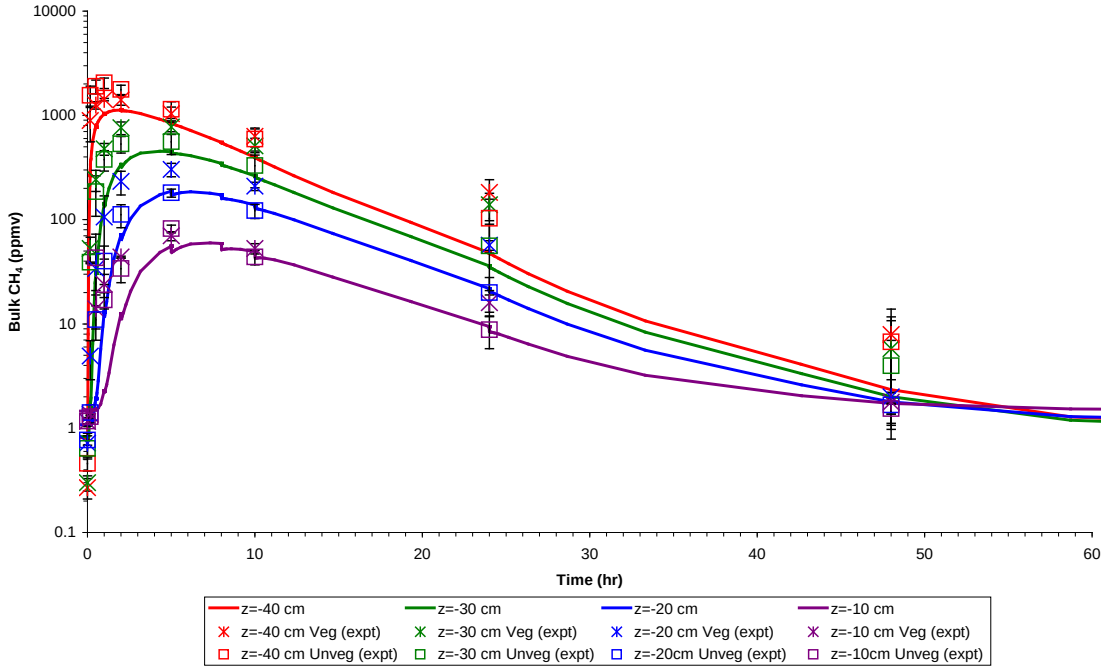


*Figure 15: Prediction of average bulk methane concentrations at different depths within the soil columns. Data are shown separately for vegetated ("Veg") and unvegetated ("Unveg") columns. (Reproduced from Hoch et al. [2014])*

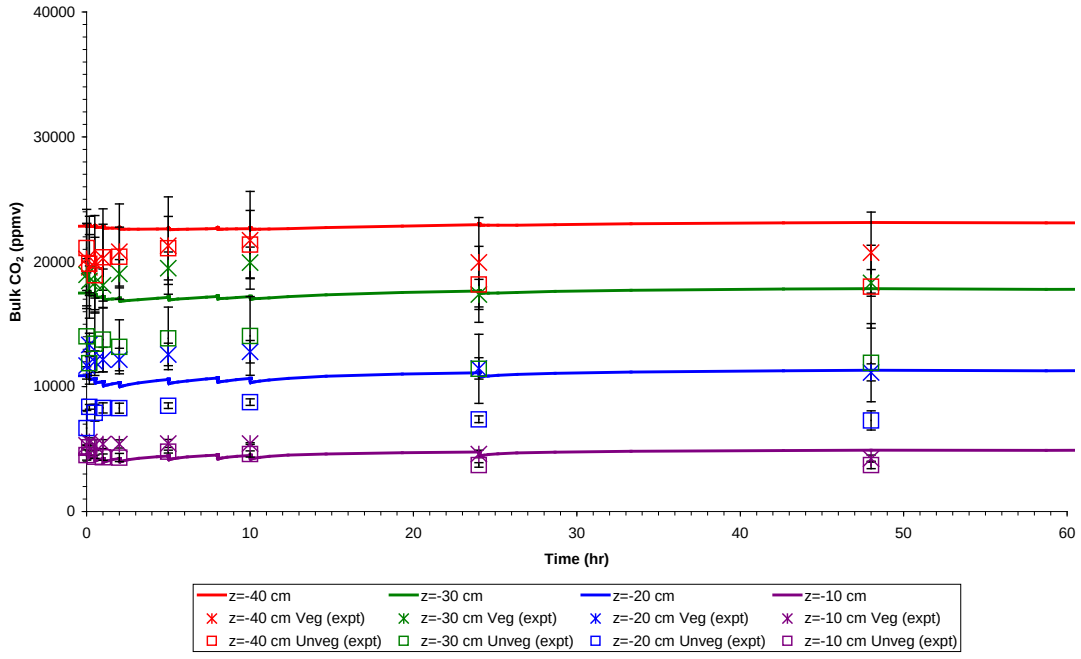


*Figure 16: Prediction of average bulk carbon dioxide concentrations at different depths within the soil columns. Data are shown separately for vegetated ("Veg") and unvegetated ("Unveg") columns. (Reproduced from Hoch et al. [2014])*

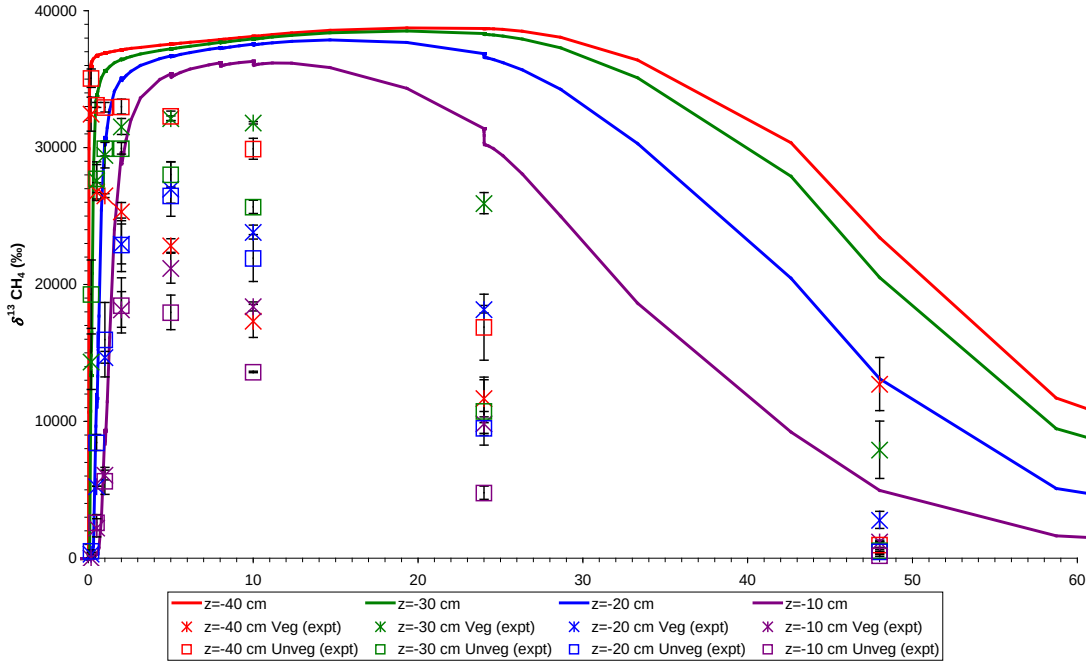


*Figure 17: Prediction of average $\delta^{13}CH_4$ (‰) at different depths within the soil columns. Data are shown separately for vegetated ("Veg") and unvegetated ("Unveg") columns. (Reproduced from Hoch et al. [2014])*

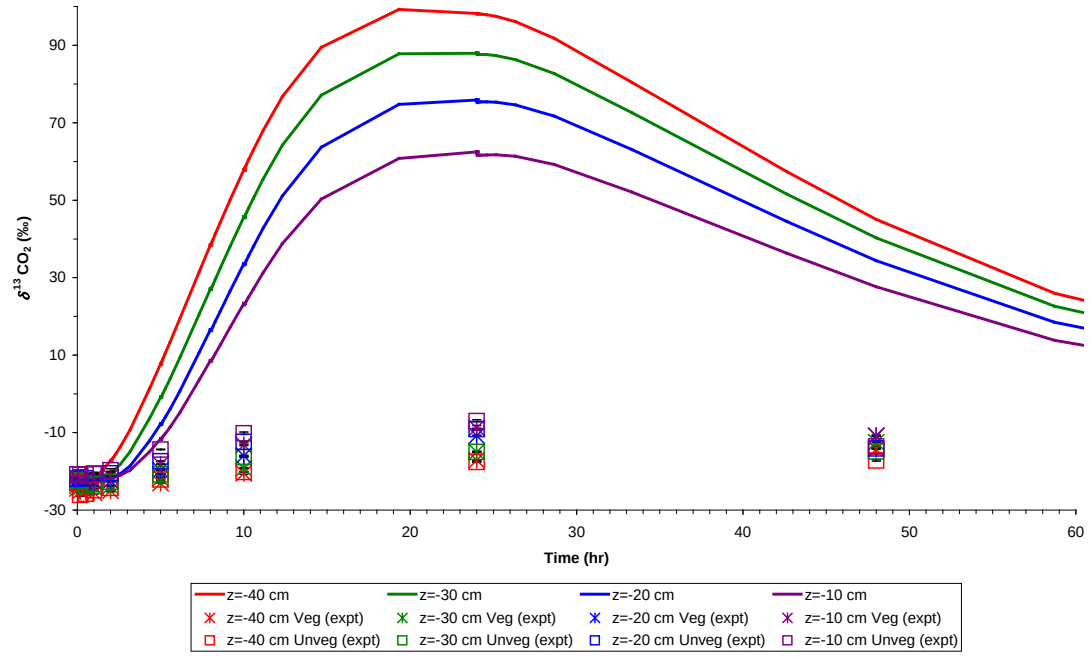


*Figure 18: Prediction of average $\delta^{13}CO_2$ (‰) at different depths within the soil columns. Data are shown separately for vegetated ("Veg") and unvegetated ("Unveg") columns. (Reproduced from Hoch et al. [2014])*

### 3.5.2 Laboratory Experiment 3: Technical Support Team Model

In the modelling undertaken by the TST, it was assumed that the response of the system to any input is linear, and that for a continuous uniform input, the system would reach equilibrium after some period. The reciprocal theorem (see Section A.5 of the Appendix) was then used to derive a 1D advection-dispersion equation, which also had a term for losses of methane as a result of depth-independent oxidation to carbon dioxide. As the model is 1D it can strictly only be applied to the soil column experiments undertaken in the laboratory, where non-trivial lateral dispersion was not possible.

Figure 19 shows the observed concentrations of $CH_4$ in the soil column for laboratory experiment 3. It is possible to estimate a time integral of $CH_4$ concentration in a given layer, with units of ppm-h. That can then be converted to a concentration per unit length (ml-h $CH_4$ $cm^{-1}$), which can then be compared to results from the 1D model for a continuous input of 1 ml $CH_4$ $h^{-1}$ (Table 6).

These results indicate that both for the vegetated and unvegetated soil columns, the decrease in concentration of $CH_4$ can be explained by a single exponential fall-off with distance above the point of $CH_4$ injection. For the unvegetated soil that calculated attenuation rate is 0.1 $cm^{-1}$, whereas for the vegetated case that decline is 0.08 $cm^{-1}$. For an initial input of 1.5 ml of $CH_4$, at equilibrium the expected recovery of $CH_4$ at the surface (50 cm from the injection) would be 0.01 ml for the unvegetated soil and 0.027 ml for the vegetated soil column. However, the laboratory experimental results indicate a release of more like 0.2 ml for the same input, i.e. an effective attenuation coefficient of 0.04 $cm^{-1}$. That the observed degree of attenuation is lower than the model predictions may be due to the presence of fast transport pathways in the column, possibly at the boundary between the soil and the column wall.

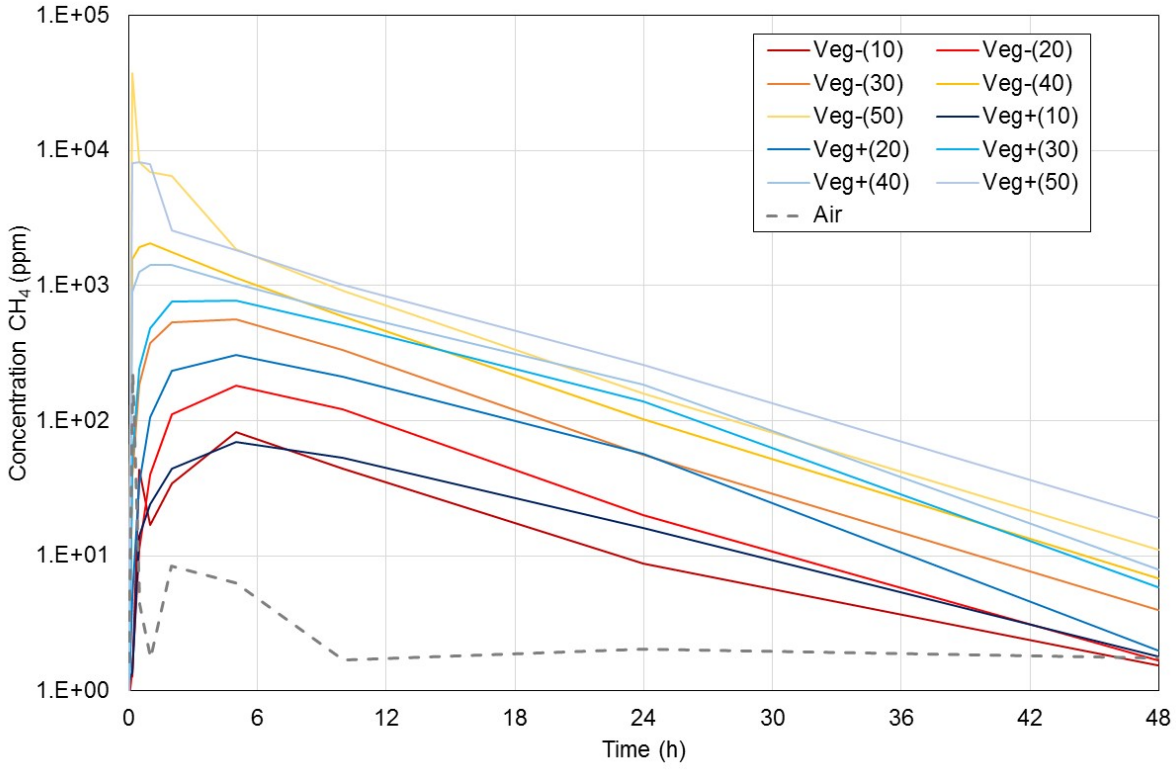


*Figure 19: Observed concentration of $CH_4$ (ppm) in the soil column in Laboratory Experiment 3.*

*Table 6: Time integrated $CH_4$ concentrations in soil gas*

| | Time Integral (ppm-h) | EXPERIMENT RESULTS Time-Integrated Concentration per Unit Length (ml-h methane $cm^{-1}$) | MODEL RESULTS Concentration for an Input Rate of 1 ml methane $h^{-1}$ (ml methane $cm^{-1}$) |
|---|---|---|---|
| **Air** | 155 | 0.01 | 0.00 |
| **Veg-(10)** | 928 | 0.04 | 0.02 |
| **Veg-(20)** | 2261 | 0.09 | 0.06 |
| **Veg-(30)** | 7159 | 0.28 | 0.19 |
| **Veg-(40)** | 17016 | 0.67 | 0.45 |
| **Veg-(50)** | 45429 | 1.80 | 1.20 |
| **Veg+(10)** | 1115 | 0.04 | 0.03 |
| **Veg+(20)** | 4356 | 0.17 | 0.11 |
| **Veg+(30)** | 11428 | 0.45 | 0.30 |
| **Veg+(40)** | 16760 | 0.66 | 0.44 |
| **Veg+(50)** | 35834 | 1.42 | 0.95 |

### 3.5.3 Field Experiment 2: EDF C-14 Model

Figure 20 presents time evolutions of the calculated (shown by line) and measured (shown by dot) volumetric water contents ($\theta_{w\_soil}$) in each soil layer (at depths of 10, 20, 30, and 40 cm). The data show a dry top layer grading to much wetter conditions at 30 cm or more. The upper part of the soil shows limited time variation, but there is almost no time variation at depth. The modelled soil water contents are in closer agreement with the upper soil (depths of 10 and 20 cm), than the deeper soil.

As noted in at the start of Section 3.5, in undertaking this model-data comparison EDF converted the C-13 field measurements to C-14 activities using the method described in Section A.6 of the Appendix.

In Figure 21 calculated activity concentrations of $^{14}CH_4$ in soil air at different soil depths (10, 20, 30, 40, and 50 cm) are compared with the measurements. The model was able to reproduce a general trend of observations which shows rapid falls within one day after each injection and after that, relatively moderate declines. When considering the first 48 hours following an injection (see Figure 22 for the calculated $^{14}CH_4$ concentration in soil after the third injection), the model shows a transition from the lower soil having a higher activity than the upper soil, to the upper soil having the greater $^{14}CH_4$ activity occurring around 12 hours post-injection. This behaviour is also seen the calculated bulk $CH_4$ concentrations in soil obtained using the RWM model, T2Plants, for this experiment (see Figure 25).

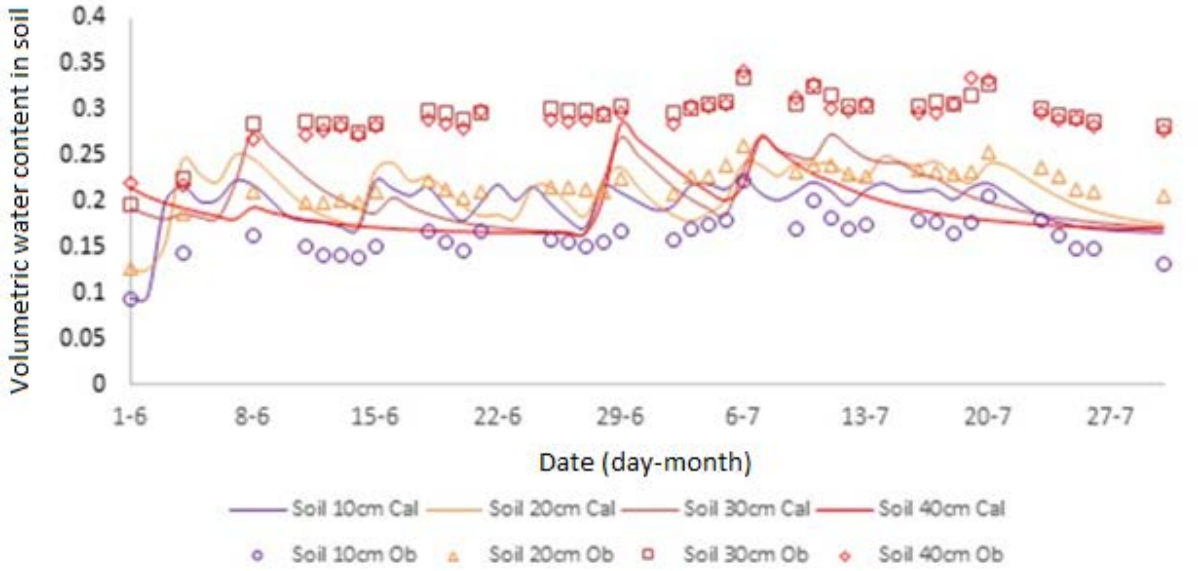


*Figure 20: Comparison between calculated and measured volumetric water contents in soil*

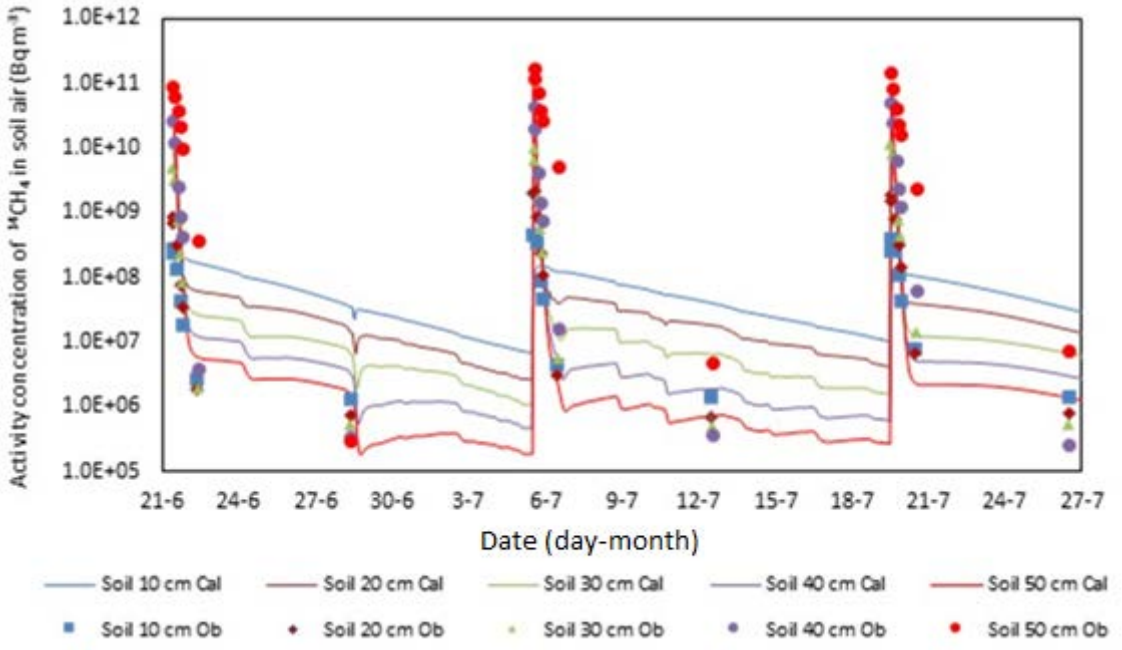


*Figure 21: Comparison between calculated and measured activity concentrations of $^{14}CH_4$ in soil air*

Table 7 presents the contribution of each process to the change in $^{14}CH_4$ activity in total soil ($A_{14CH4\_soil}$) at 20 and 50 cm depths. A positive value means that a process contributes to the increase of $A_{14CH4\_soil}$, while a negative value indicates that a process contributes to the decrease of $A_{14CH4\_soil}$. A contribution value is expressed by the unit of Bq $h^{-1}$. Average contributions of each process were calculated over two time phases, the first time phase being the 24h after the first injection and the second being from

one day after the first injection until the second injection[h]. Table 7 shows only the contributions of diffusion and oxidation processes as those from other processes (root uptake and advection) turned out to be relatively insignificant.

***Table 7: Contribution of each process to the change in $^{14}CH_4$ activity in soil air at different soil depths***

| Depth from soil surface | Average contribution during the first time phase (Bq $h^{-1}$) | | Average contribution during the second time phase (Bq $h^{-1}$) | |
|---|---|---|---|---|
| | Net diffusion | Oxidation | Net diffusion | Oxidation |
| 20 cm depth | 2.70E08 | -3.16E08 | 5.06E06 | -5.14E06 |
| 50 cm depth (injection point) | -1.29E09 | -1.70E09 | 4.51E05 | -4.59E05 |

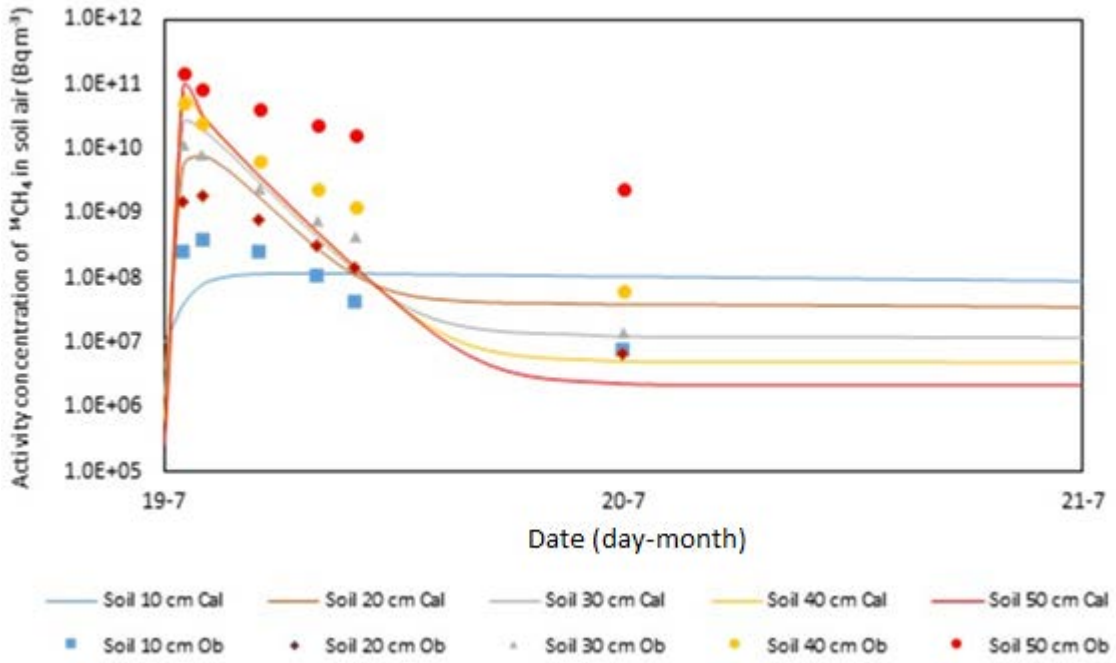


***Figure 22: Comparison between calculated and measured activity concentrations of $^{14}CH_4$ in soil for the 48 hours after the third injection***

During the first time phase, at 20 cm depth, there was a high gain by net diffusion but its positive contribution was offset by the more significant loss by oxidation (a factor of 1.17 greater than the gain), which gave rise to a sharp drop of the $^{14}CH_4$ activity concentration in soil air, as seen in Figure 21. At 50 cm depth, the methane concentrations were reduced by a combination of both loss by oxidation and net diffusion due to high concentration gradients between the injection point (50 cm depth) and the upper and lower soil layers. During the second time phase, losses by oxidation were slightly more than gains by net diffusion at both depths (by a factor of 1.02 this time); however, the rates of loss and gain were much lower during the second time phase which led to moderate declines of $^{14}CH_4$ activity concentrations (Figure 21).

[h] The equivalent contributions of each process for the second injection onwards were not calculated.

Figure 23 compares calculated and measured[i] activity concentrations of $^{14}CO_2$ in soil air at different soil depths (10, 20, 30, 40, and 50 cm). The model succeeded in capturing a general trend of observations, particularly, during 24h after each injection, but it underestimated the observations at one week after injections.

Table 8 presents the average contribution of each process to the variation of $^{14}CO_2$ activity in total soil ($A_{14CO2\_soil}$) at 20 and 50 cm depths. During the first phase, at 20 cm depth, there was high gain by net diffusion and also by oxidation, leading to a continuous increase of the $^{14}CO_2$ activity concentration in soil air, as seen in Figure 23. After that, a moderate decline was caused by a loss by net diffusion which exceeded a gain by oxidation. At 50 cm depth, a significant loss by net diffusion was driven by high concentration gradients during the first time phase as seen for $^{14}CH_4$, followed by a moderate decline during the second time phase.

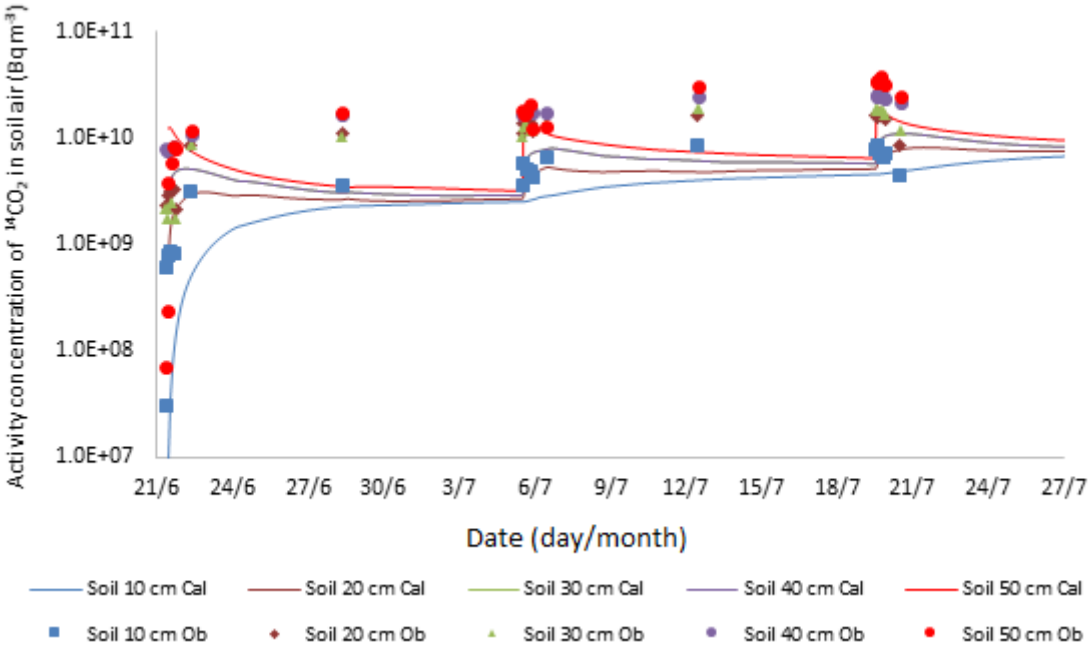


***Figure 23: Comparison between calculated and measured activity concentrations of $^{14}CO_2$ in soil air***

[i] Derived from C-13 measurements.

*Table 8: Contribution of each process to the variation of $^{14}CO_2$ activity in soil air at different soil depths*

| Depth from soil surface | Average contribution during the first time phase (Bq $h^{-1}$) | | Average contribution during the second time phase (Bq $h^{-1}$) | |
|---|---|---|---|---|
| | Net diffusion | Oxidation | Net diffusion | Oxidation |
| 20 cm depth | 3.13E08 | 3.16E08 | -8.73E06 | 5.14E06 |
| 50 cm depth (injection point) | -1.85E09 | 1.70E09 | -6.81E07 | 4.59E05 |

### 3.5.4 Field Experiment 2: JAEA SOLVEG-II Model

As noted in at the start of Section 3.5, in undertaking this model-data comparison JAEA converted the C-13 field measurements to C-14 activities using the method described in Section A.6 of the Appendix.

From results of the model calculation and the field observation, similar time-trends of dynamics of $^{14}C$ (concentrations of $^{14}CH_4$ and $^{14}CO_2$ in the soil and fluxes of $^{14}CH_4$ and $^{14}CO_2$ at the ground surface) were obtained at the three gas-injection trials. The modelling therefore focused on the results from the 3rd gas-injection trial, where the most complete experimental data were obtained. During the 3rd gas-injection trial, model calculations of temperature and water content in the soil at the depths of 10, 20, 30 and 40 cm approximately agreed with measured values (data not shown). This result indicated that the settings of the SOLVEG-II model used for the calculations of heat and water transport at the test site were reasonable.

Calculated and measured concentrations of $^{14}CH4$ in the soil during the 3rd gas-injection trial are shown in Figure 24a. At the depth of the gas injection (50 cm), the model-calculated $^{14}CH4$ concentration (grey solid curve) peaked at the time of the gas injection and decreased by three orders of magnitude during the following one-day period. The model calculated results also revealed a large vertical gradient of $^{14}CH4$ concentration across the soil horizon above the gas injection; e.g., the calculated $^{14}CH4$ concentrations differed by a factor of 30 between the depths of 10 cm and 50 cm. In the model calculation that hypothetically assumed no-oxidation of methane in the soil (grey doted curve in Figure 24a), predicted $^{14}CH4$ concentrations were different. The $^{14}CH4$ concentration decreased by two orders of magnitude during the one-day period after the injection, and the $^{14}CH4$ concentrations differed by a factor of four to five between the soil depths of 10 cm and 50 cm. The $^{14}CH4$ concentrations calculated with the default settings generally agreed with the measured values in terms of the time-trend and magnitude. However, the model calculation systematically overestimated the measured $^{14}CH4$ concentrations by about an order of magnitude at depths from 10 cm to 40 cm in the soil.

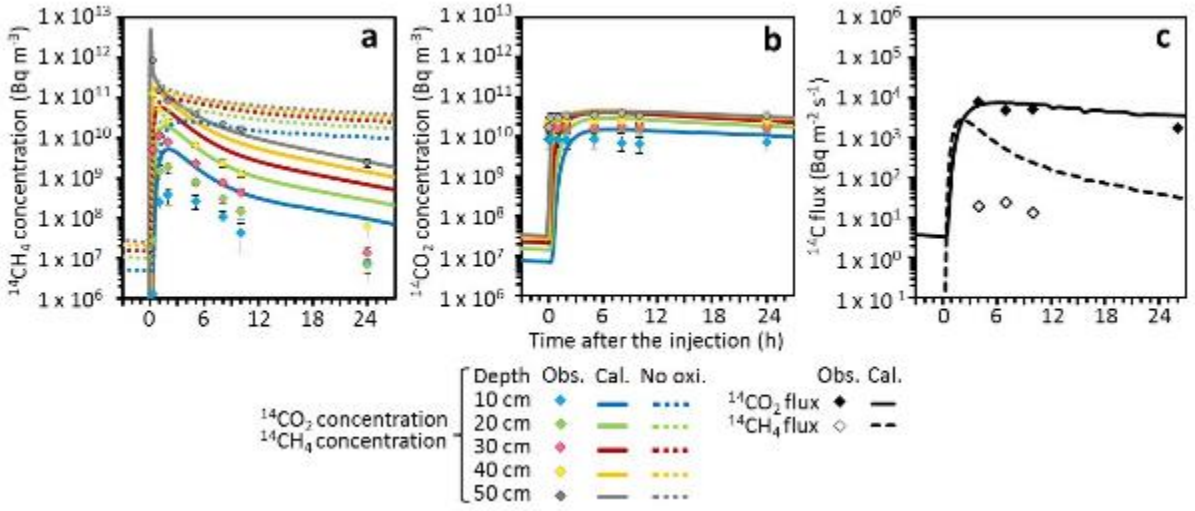


***Figure 24:*** ***Measured and calculated concentrations of (a) $^{14}CH_4$ and (b) $^{14}CO_2$ in the soil, and (c) fluxes of $^{14}CH_4$ and $^{14}CO_2$ at the ground surface during the experiment. Time of the start of the 3rd gas-injection trial (12:00 on 19 July, 2012) was defined as 0 h. Vertical bars attached to the measured data represent standard deviations of multiple measurements of concentrations (ppmv) and $\delta^{13}C$ values. Dotted curves in Figure 24a show the results from the additional calculation that hypothetically assumed no oxidation of methane in the soil***

Model predictions of $^{14}CO_2$ concentrations in the soil (Figure 24b) revealed different time-trends from the calculation of $^{14}CH_4$ concentrations in the soil. The calculated $^{14}CO_2$ concentrations increased during about six hours after the $^{14}CH_4$ injection. Thereafter the $^{14}CO_2$ concentrations decreased by a factor of two during the one day period. The vertical gradient of the model-calculated $^{14}CO_2$ concentration in the soil above the gas-injection depth was smaller than that calculated for the $^{14}CH_4$ concentration (Figure 24a). In general, the model predictions of $^{14}CO_2$ concentration were in good agreement with the measurements, although the model tended to overestimate the measured values by a factor of two to three.

Model calculations of fluxes of $^{14}CH_4$ and $^{14}CO_2$ from the soil to the atmosphere revealed different time trends (Figure 24c). Predicted $^{14}CH_4$ flux peaked soon (~2 h) after the $^{14}CH_4$ injection, and decreased by two orders of magnitude by one-day after the injection. For $^{14}CO_2$, the calculated flux peaked late (~6 h) after the $^{14}CH_4$ injection and decreased by a factor of two during the subsequent one-day period. The model calculated $^{14}CO_2$ flux agreed well with the measurements, whereas the calculated $^{14}CH_4$ flux systematically overestimated the measurements by an order of magnitude, or more.

The application of the model to the transfer of $^{14}CH_4$ and $^{14}CO_2$ observed at the field $^{14}CH_4$ injection experiment demonstrated that the processes regulating below-ground dynamics of $^{14}CH_4$ and $^{14}CO_2$ differ; the dynamics of the added $^{14}CH_4$ were mainly influenced by a 'fast' methane-oxidation process, whereas the dynamics of produced $^{14}CO_2$ were controlled by a relatively 'slow' diffusion process. From the two calculations with and without methane oxidation in the soil (Figure 24a), different time-trends were obtained for the soil $^{14}CH_4$ concentration at the depth of the gas-injection (50 cm). The difference indicates that the soil layer near the gas-injection depth acted as a strong sink for the added $^{14}CH_4$. The vertical gradients of soil $^{14}CH_4$ concentrations in the horizon above the gas-injection depth were also different in the two calculations; the vertical gradient was larger at the calculation with default settings (with methane oxidation in the soil). The result suggests that a large fraction of the injected $^{14}CH_4$ was

oxidized to $^{14}CO_2$ during the upward migration in this horizon. It is clear that the methane oxidation dominantly controlled the dynamics of $^{14}CH_4$ released in this soil.

In contrast, the predicted concentrations of $^{14}CO_2$ in the soil showed a smaller vertical gradient in the soil above the gas-injected depth, and decreased more moderately after the gas injection, compared with the model-calculated results of $^{14}CH_4$ concentrations. The small vertical gradient of the $^{14}CO_2$ concentrations was attributable to a fact that the vertical profile of $^{14}CO_2$ was influenced only by diffusion; whereas the profile of $^{14}CH_4$ was more influenced by the methane oxidation. The moderate decrease of $^{14}CO_2$ concentration in the soil was also because of the slow diffusion process. As a result of the below-ground dynamics of $^{14}CO_2$, where the diffusion was the dominant transport mechanism, the calculated fluxes of $^{14}CO_2$ outgassing from the soil revealed a moderate time trend after the $^{14}CH_4$ injection, whereas the flux of $^{14}CH_4$ outgassing from the soil rapidly decreased soon after the $^{14}CH_4$ injection due to the rapid oxidation of $^{14}CH_4$ in the soil (Figure 24c).

The above predictions of SOLVEG-II generally reproduced the migrations of $^{14}CH_4$ and $^{14}CO_2$ in the soil observed during the gas-injection trial. However, when the reference parameter values were used, the model overestimated the concentrations of $^{14}CH_4$ in the soil above the gas-injected depth (Figure 24a) and the flux of $^{14}CH_4$ from the soil (Figure 24c) by an order of magnitude, or more. For $^{14}CO_2$, the model was better able to reproduce the observed concentrations in the soil and flux from the soil (Figure 24b and c), but the model-calculated $^{14}CO_2$ concentrations tended to overestimate the observations by a factor of two to three. The following points were considered as possible reasons for the discrepancy between the model calculations and field observations of $^{14}CH_4$ and $^{14}CO_2$:

- effects from lateral diffusion of $^{14}CH_4$ and $^{14}CO_2$ in the soil at the experimental field,
- errors in the model calculation due to uncertainty in predicted effective diffusivity in the soil and modelled rate of methane oxidation in the soil, and
- effect from the model's overvaluation of $^{14}CO_2$ production during $^{14}CH_4$ consumption in the soil.

The effect from lateral diffusion of $^{14}CH_4$ in the field soil can be considered as a probable reason for the discrepancies between the calculations and observations of $^{14}CH_4$. At the experiment, $^{13}CH_4$ gas was released to the soil as a point source via the injection using the gas sampling/injection probe. The injected $^{13}CH_4$ was therefore expected to have diffused in the soil both vertically and horizontally. The SOLVEG-II model does not account for the horizontal transport of trace gases in the soil. Thus, the model calculation could have overestimated the vertical flux of the added $^{14}CH_4$ in the soil, which resulted in the overestimation of the concentrations of $^{14}CH_4$ in the horizon above the gas-injection depth and the flux of $^{14}CH_4$ exhaling from the soil surface. The effect from lateral diffusion would also be a possible reason for the discrepancy between the calculated and observed dynamics of $^{14}CO_2$, because the below-ground distribution of the source of $^{14}CO_2$ (i.e., the added $^{14}CH_4$) and transport of the produced $^{14}CO_2$ would have been influenced by the lateral diffusion process in the field.

Errors in the model calculation due to uncertainty in predicting the effective diffusivity in the soil can be ruled out as a common reason for the inconsistencies between the calculations and the observations of $^{14}CH_4$ and $^{14}CO_2$. The Penman's equation [Penman, 1940] tends to overestimate the effective diffusivity for trace-gas diffusion in soils [Bartelt-Hunt and Smith, 2002; Komatsu et al., 2007]. In the model application in this work, overestimation of effective diffusivity in the soil would facilitate the injected $^{14}CH_4$ to diffuse out from the soil to the atmosphere. Therefore, a lesser fraction of $^{14}CH_4$ would be oxidized in the soil, resulting in overestimation of $^{14}CH_4$ concentrations in the soil above the gas-injected depth and flux of $^{14}CH_4$ exhaling from the soil. Indeed, an additional model simulation which used a reduced effective diffusivity (one-third of the default value) predicted smaller concentrations of

$^{14}CH_4$ in the soil above the gas injection depth and decreased flux of $^{14}CH_4$ outgassing from the soil; e.g., the $^{14}CH_4$ concentration at the depth of 10 cm and $^{14}CH_4$ flux at the soil surface calculated with the reduced effective diffusivity were on the same order of magnitude as the measured values. However, the reduced effective diffusivity regulated the upward diffusion of the produced $^{14}CO_2$ in the soil. As a result, the flux of $^{14}CO_2$ at the ground surface calculated with the reduced effective diffusivity underestimated the measured values by one to two orders of magnitude. This result suggests that the uncertainty in the prediction of effective diffusivity is not the common reason for the discrepancy in the calculated and measured results of $^{14}CH_4$ and $^{14}CO_2$.

The model's overestimations of $^{14}CH_4$ concentration in the soil and $^{14}CH_4$ flux from the soil could have originated from uncertainty in the modelled rate of methane oxidation in the soil. In the model of methane oxidation, uncertainties exist for parameterization of the rate of oxidation for the surface soil and the depth-scale of methane oxidation in the subsurface soil. An increase in either would result in a more rapid rate of methane oxidation in the deeper parts in the soil, enabling more efficient loss of the added $^{14}CH_4$ in the deeper horizon. In additional calculations (results not shown here), increasing either of these parameters by a factor of three[j] led to the calculated $^{14}CH_4$ concentration at a depth of 10 cm and $^{14}CH_4$ flux at the soil being either on the same order of magnitude as, or less than, the measured values.

Overvaluation of $^{14}CO_2$ production in the soil by the model simulation can be considered as a possible explanation for the model's overestimations of $^{14}CO_2$ concentrations in the soil and $^{14}CO_2$ flux from the soil. The model assumed that all the $^{14}CH_4$ that consumed by methanoprophic bacteria was oxidized to $^{14}CO_2$ (see Section A.2 of the Appendix). However, a substantial fraction, from 19% to 69%, of $CH_4$-derived carbon can be assimilated to methanotrophic bacteria during the consumption of methane, and not immediately released to as $CO_2$ [Whalen and Reeburgh, 1990; Whalen et al., 1990, 1992]. Hence, the model calculation could have overestimated the production of $^{14}CO_2$ under a given concentration of $^{14}CH_4$ in the soil, resulted in overestimations of soil $^{14}CO_2$ concentrations and $^{14}CO_2$ flux outgassing from the soil.

### 3.5.5 Field Experiment 2: RWM T2Plants

A complication with interpreting the field data is that a larger volume of methane was injected into the soil than in the laboratory experiments (i.e. 15 ml as compared to 1.5 ml; a larger volume was used to compensate for migration of the methane being unconfined), and the moisture content of the soil was high. Therefore, when the methane spread out as a spherical "bubble" from the point of injection, the "bubble" expanded to a radius that was greater than 10 cm before diffusion became the dominant gas transport process over advection. The consequence was a rapid (almost instantaneous) change in the methane concentration at a depth of 40 cm. In other words, the model has to account for advection as well as for diffusion when interpreting the early rise of the bulk methane concentrations within the soil.

The calculated and measured concentrations of bulk $CH_4$ and $CO_2$ in the soil following the injection of $^{13}CH_4$ are shown in Figure 25 and Figure 26 respectively. For the $CH_4$ concentrations, the unvegetated and vegetated soils are shown separately. The model is able to broadly replicate the enhanced concentrations of $CH_4$ in the soil, and the stability of the $CO_2$ concentrations. The measured bulk methane concentrations show a faster response to injection than the numerical simulations at all depths.

[j] Higher reference oxidation rate taken from Ridgwell et al. [1999], and greater depth scale value taken from Koschorreck and Konrad [1993] and Kightley et al. [1995].

This is probably due to details in the way that the model represents transport of the pulse of methane through a partially-saturated soil.

The radii of the assumed spherical volumes of methane that formed soon after gas injection were expected to be larger in the case of the unvegetated treatments, which had lower porosity and were wetter. Although the models showed this effect, it was not as pronounced as for the experiments.

The modelled and measured levels of $^{13}CH_4$ and $^{13}CO_2$ (as ‰) for FE2 are shown in Figure 27 and Figure 28 respectively. As with LE3, the uptake of methane has been calibrated to get the peak in the calculated concentration of $^{13}CO_2$ to occur at the same time as the empirical data. However, once again the peak calculated $^{13}CO_2$ is higher than the empirical data. The same explanation, that the branching fraction for formation of carbon dioxide from the “intermediate” is too high, holds here also.

The modelled effluxes of bulk methane from the soil underestimate the early observations, but perform much better after 8 hours (Figure 29). In contrast, the model overestimates the flux of $^{13}CH_4$ from the soil (Figure 30) in the first 12 hours after the injection.

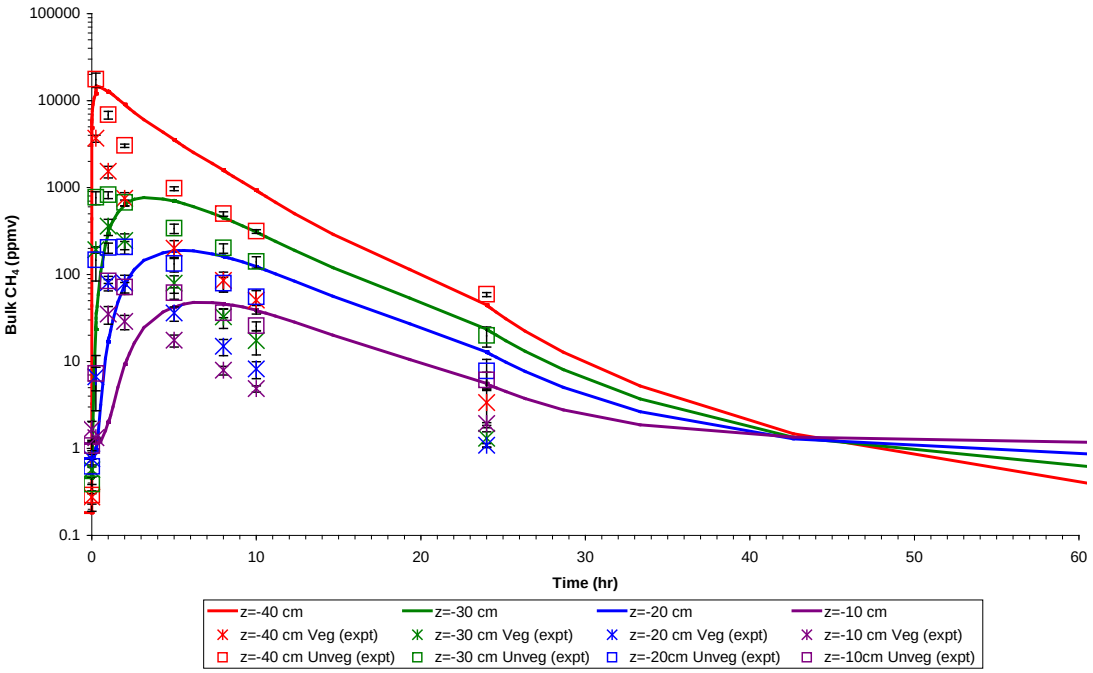


**(a)**

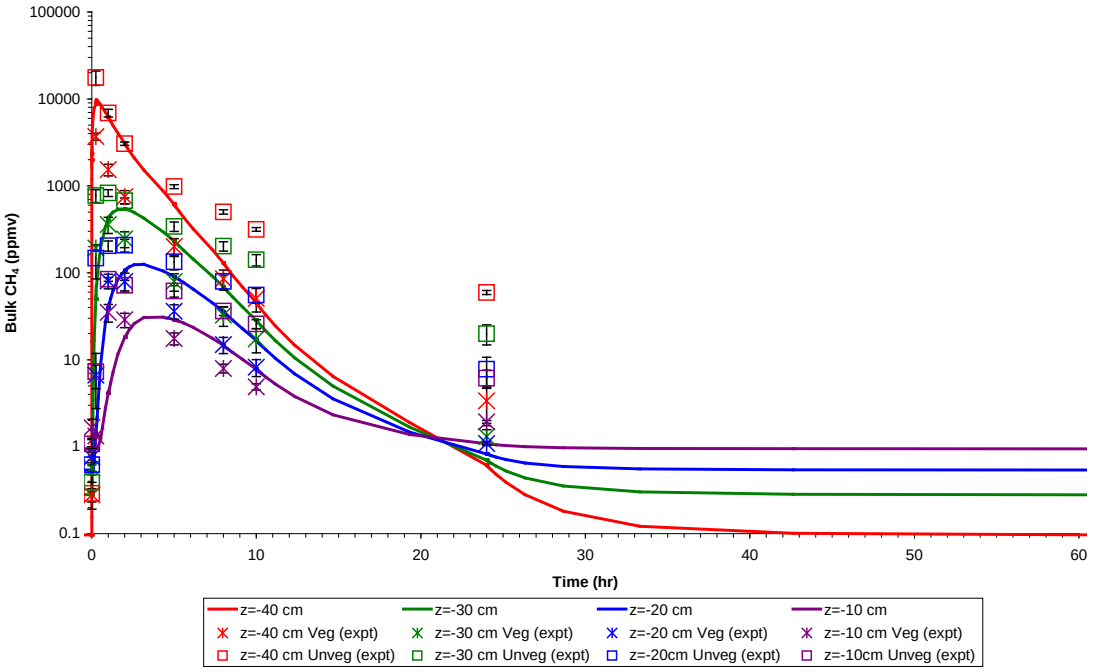


**(b)**

***Figure 25:*** ***Prediction of average bulk methane concentrations at different depths within the soil. Results are from models of (a) the unvegetated treatments (i.e. slightly lower porosity and wetter soil), and (b) the vegetated treatments (i.e. slightly higher porosity and drier soil). Experimental data are shown separately for vegetated ("Veg") and unvegetated ("Unveg") treatments. (Reproduced from Hoch et al. [2014])***

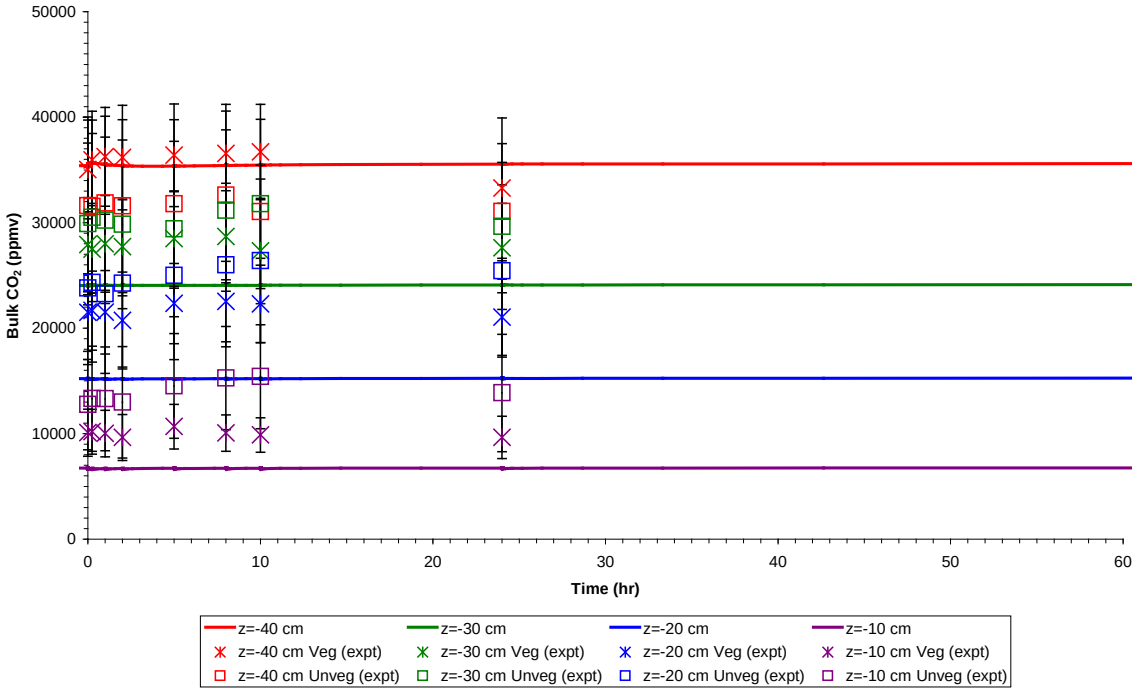


***Figure 26: Prediction of average bulk carbon dioxide concentrations at different depths within the soil. Results are from a model of the unvegetated treatments (i.e. slightly lower porosity and wetter soil). Experimental data are shown separately for vegetated ("Veg") and unvegetated ("Unveg") treatments. (Reproduced from Hoch et al. [2014])***

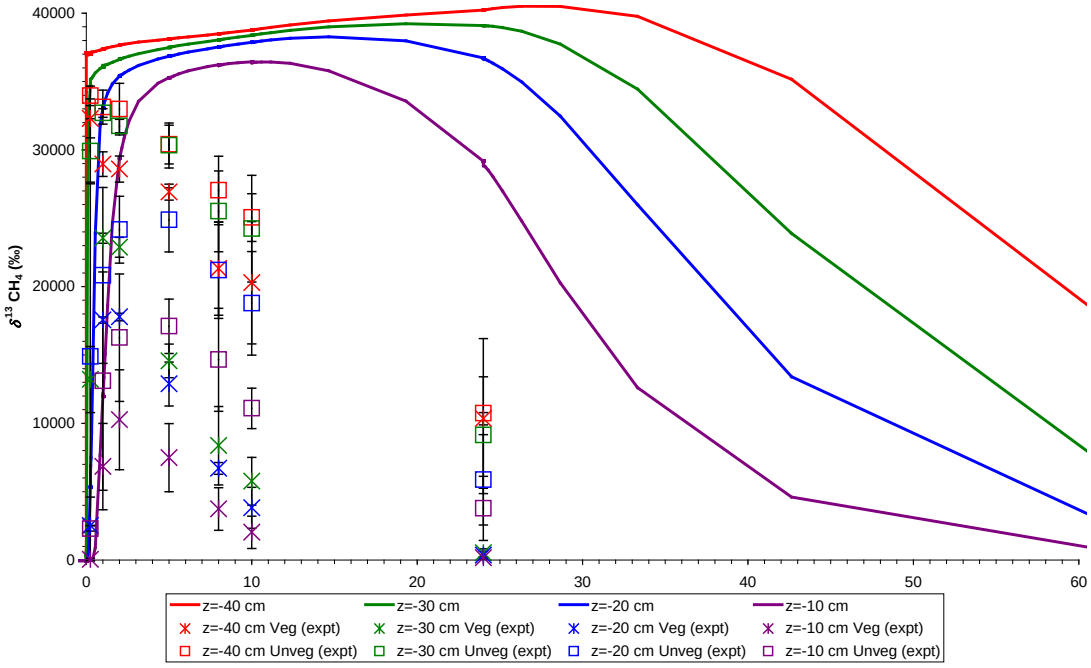


**(a)**

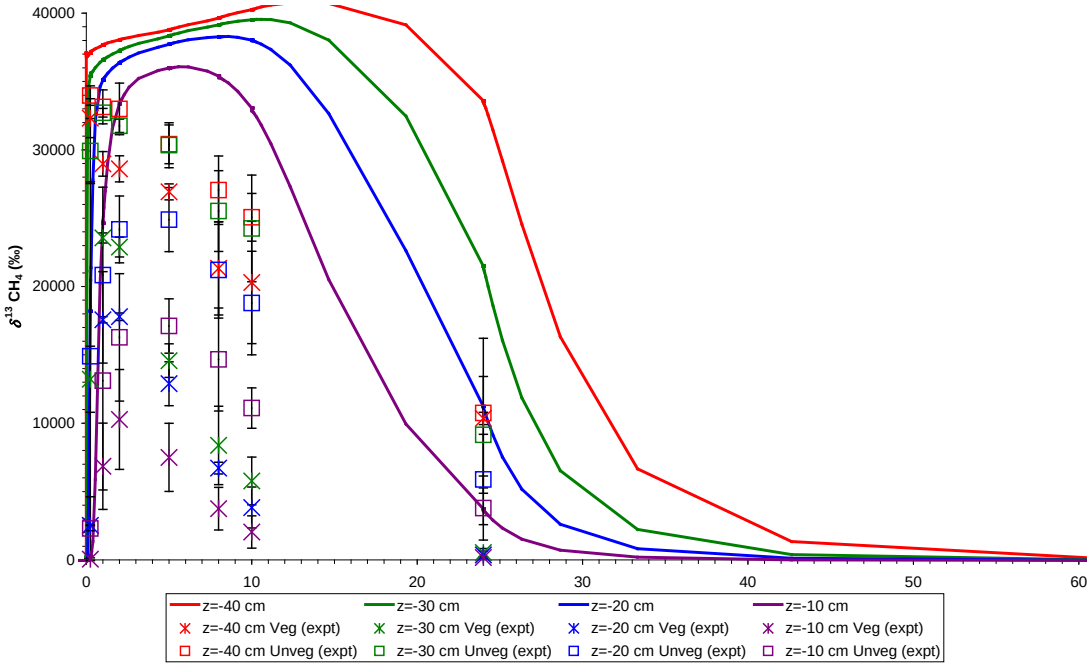


**(b)**

***Figure 27:*** ***Prediction of average $\delta^{13}CH_4$ (‰) at different depths within the soil. Results are from models of (a) the unvegetated treatments (i.e. slightly lower porosity and wetter soil), and (b) the vegetated treatments (i.e. slightly higher porosity and drier soil). Experimental data are shown separately for vegetated ("Veg") and unvegetated ("Unveg") treatments. (Reproduced from Hoch et al. [2014])***

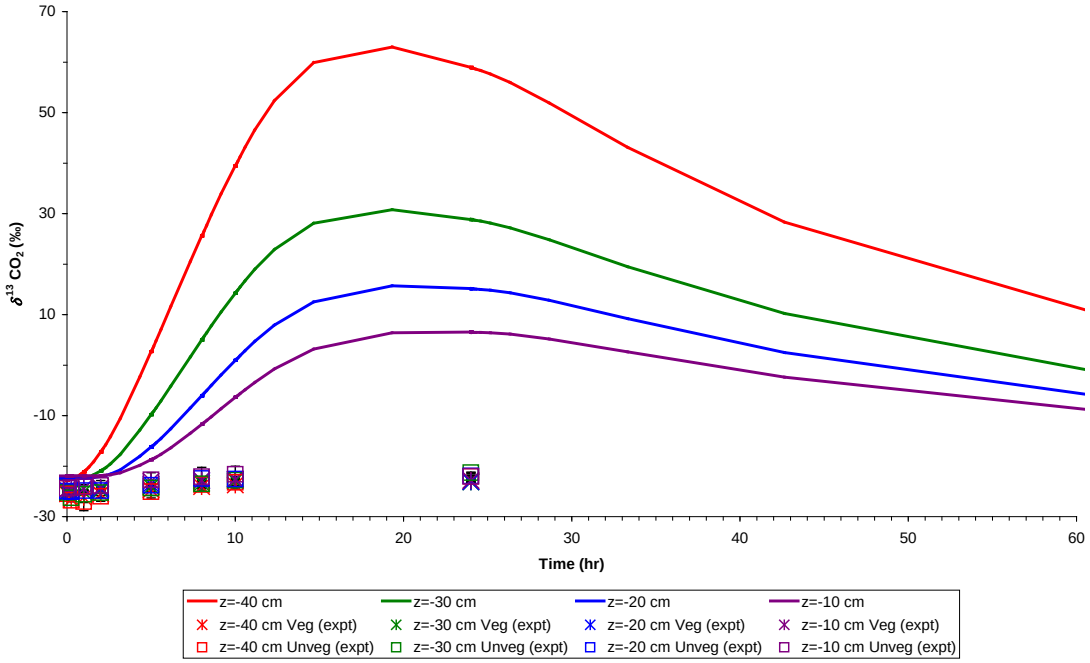


**(a)**

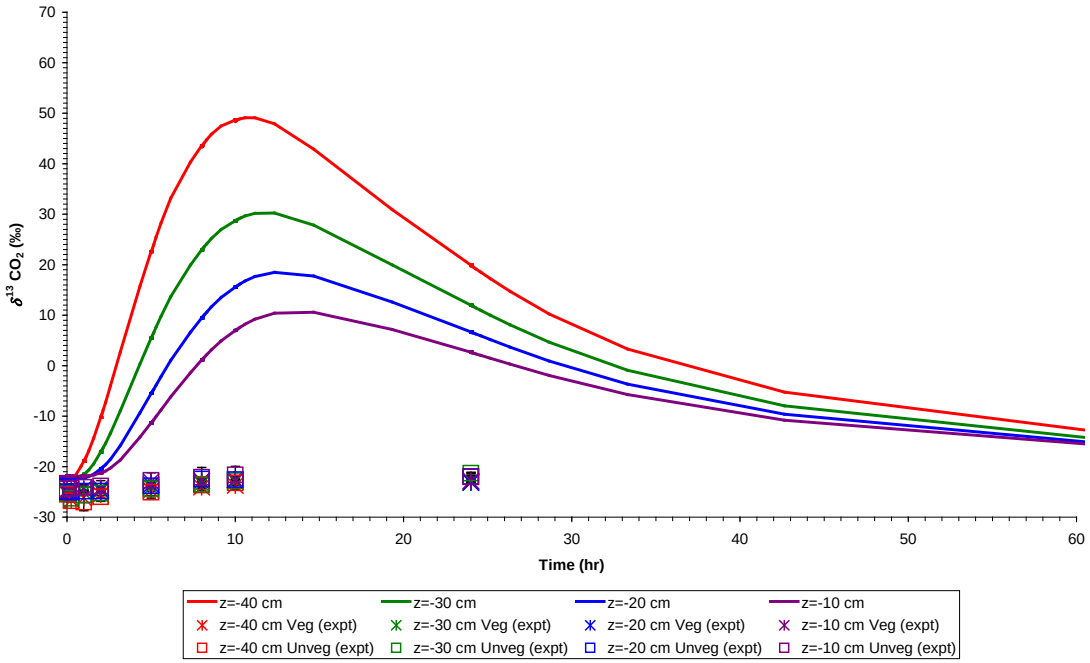


**(b)**

***Figure 28:*** ***Prediction of average $\delta^{13}$CO2 (‰) at different depths within the soil. Results are from models of (a) the unvegetated treatments (i.e. slightly lower porosity and wetter soil), and (b) the vegetated treatments (i.e. slightly higher porosity and drier soil). Experimental data are shown separately for vegetated ("Veg") and unvegetated ("Unveg") treatments. (Reproduced from Hoch et al. [2014])***

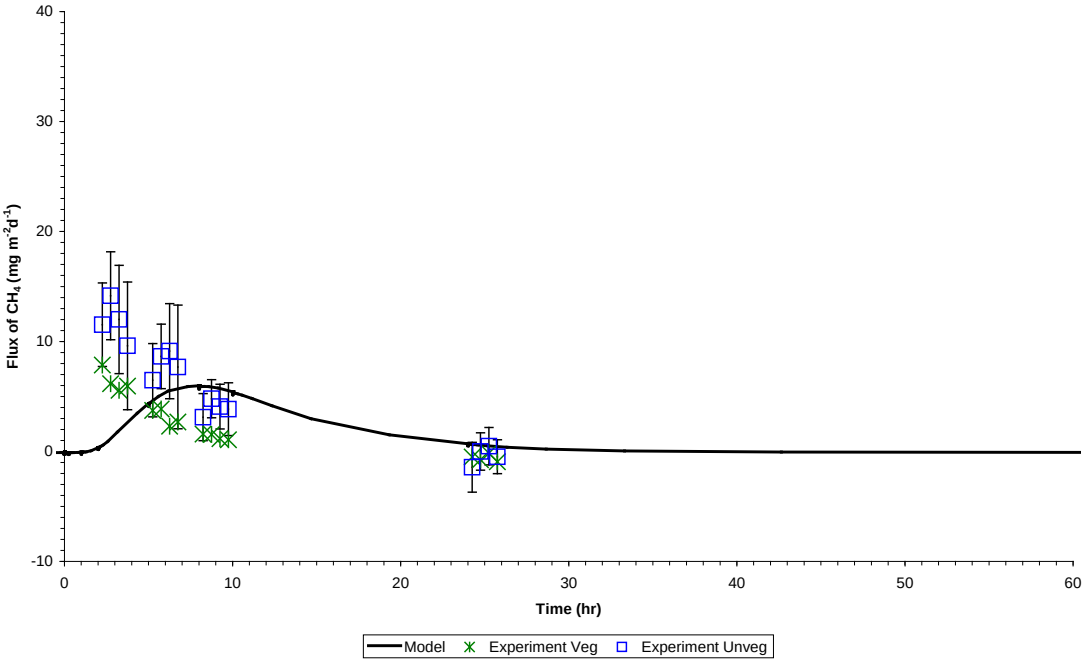


**(a)**

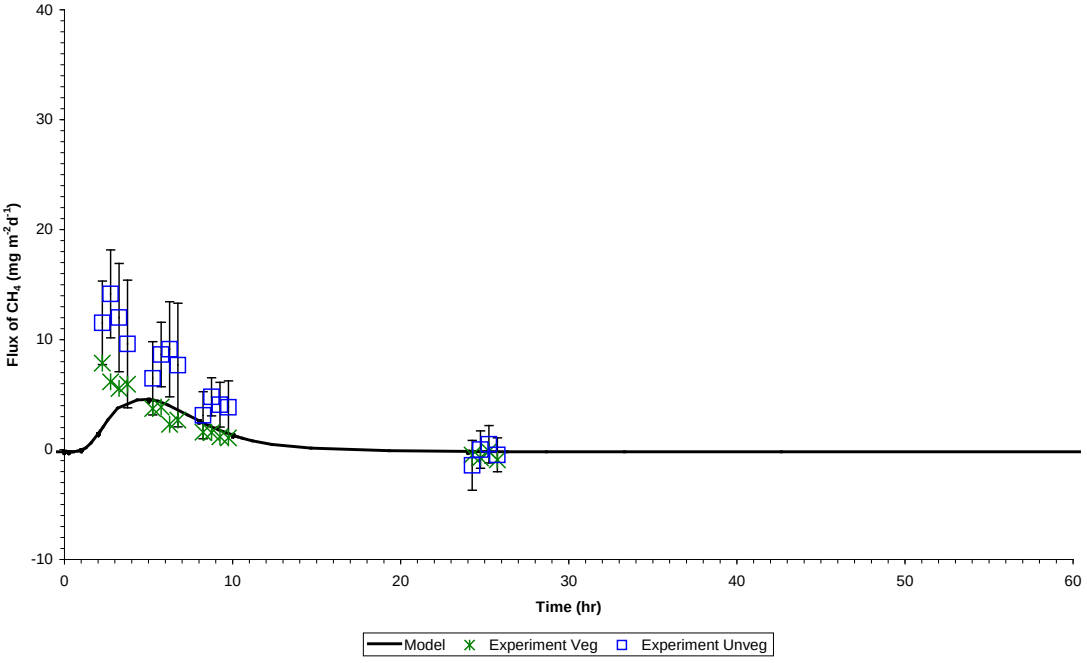


**(b)**

***Figure 29:*** ***Prediction of bulk methane efflux from the soil. Results are from models of (a) the unvegetated treatments (i.e. slightly lower porosity and wetter soil), and (b) the vegetated treatments (i.e. slightly higher porosity and drier soil). Experimental data are shown separately for vegetated ("Veg") and unvegetated ("Unveg") treatments. (Reproduced from Hoch et al. [2014])***

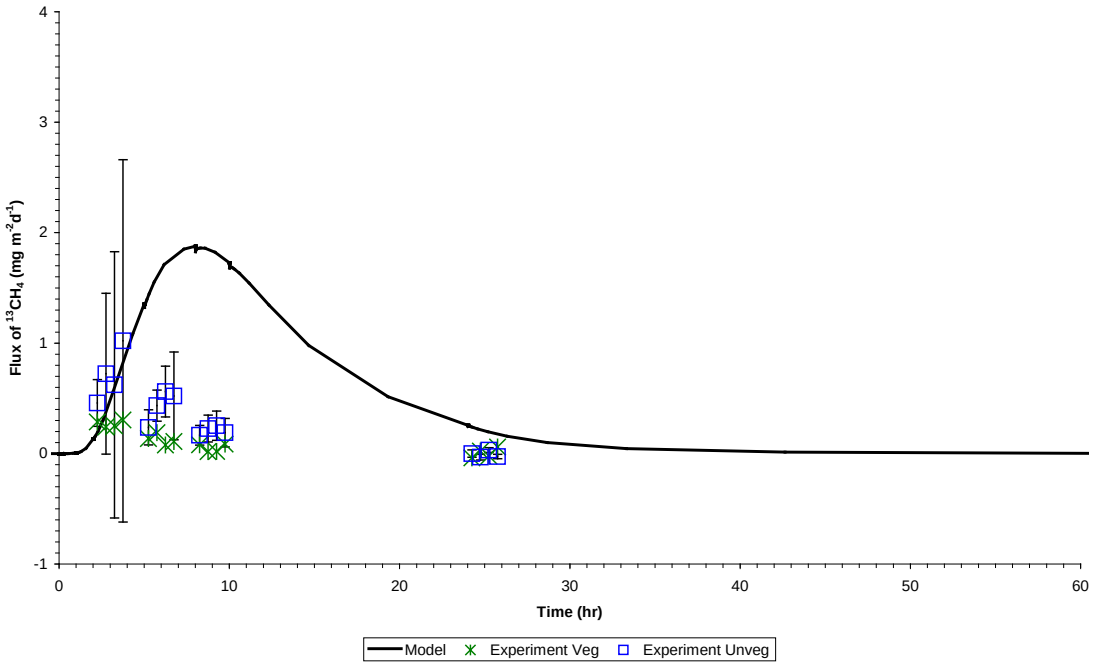


**(a)**

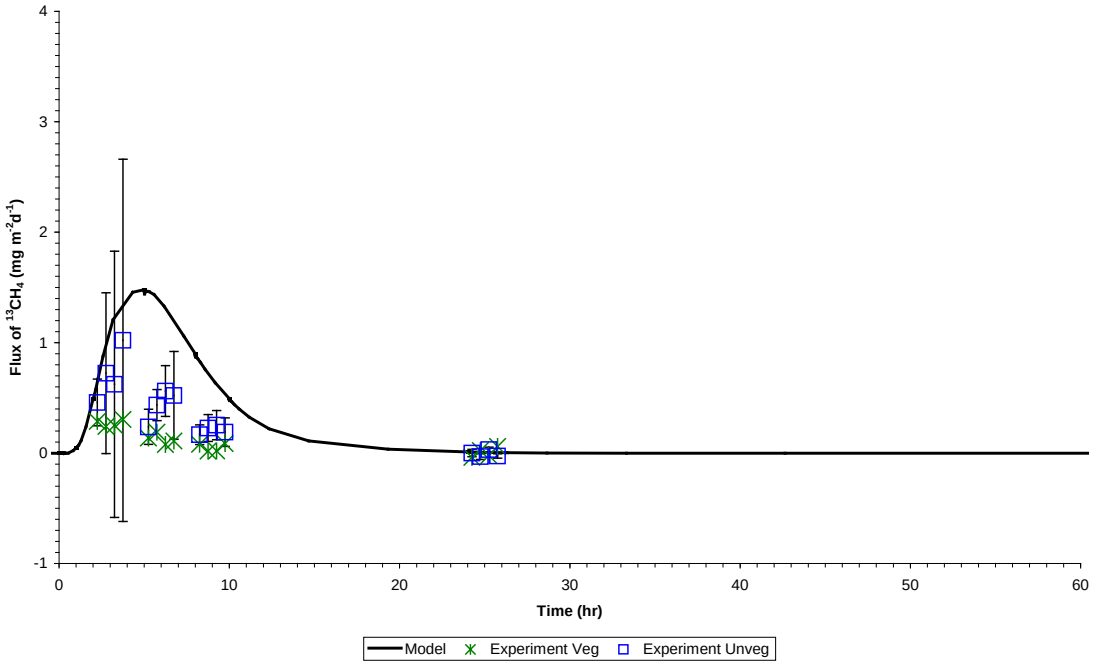


**(b)**

***Figure 30:*** ***Prediction of isotopic $^{13}CH_4$ efflux from the soil. Results are from models of (a) the unvegetated treatments (i.e. slightly lower porosity and wetter soil), and (b) the vegetated treatments (i.e. slightly higher porosity and drier soil). Experimental data are shown separately for vegetated ("Veg") and unvegetated ("Unveg") treatments. (Reproduced from Hoch et al. [2014])***

### 3.5.6 Field Experiment 2 Technical Support Team Model

The natural logarithm of the bulk $CH_4$ concentrations measured in FE2 are shown in Figure 31 (data taken from Table 4.6 of Atkinson et al. [2014]). As these natural logarithms vary smoothly with time, linear interpolation of the concentration is used to evaluate time integrals (Table 9). Unlike the case of the LE3, the time-integrated concentration per unit length cannot be computed, because the plume can disperse laterally as it moves upward, so the plume cross-section will increase as it moves upward, with the degree of that increase being undefined.

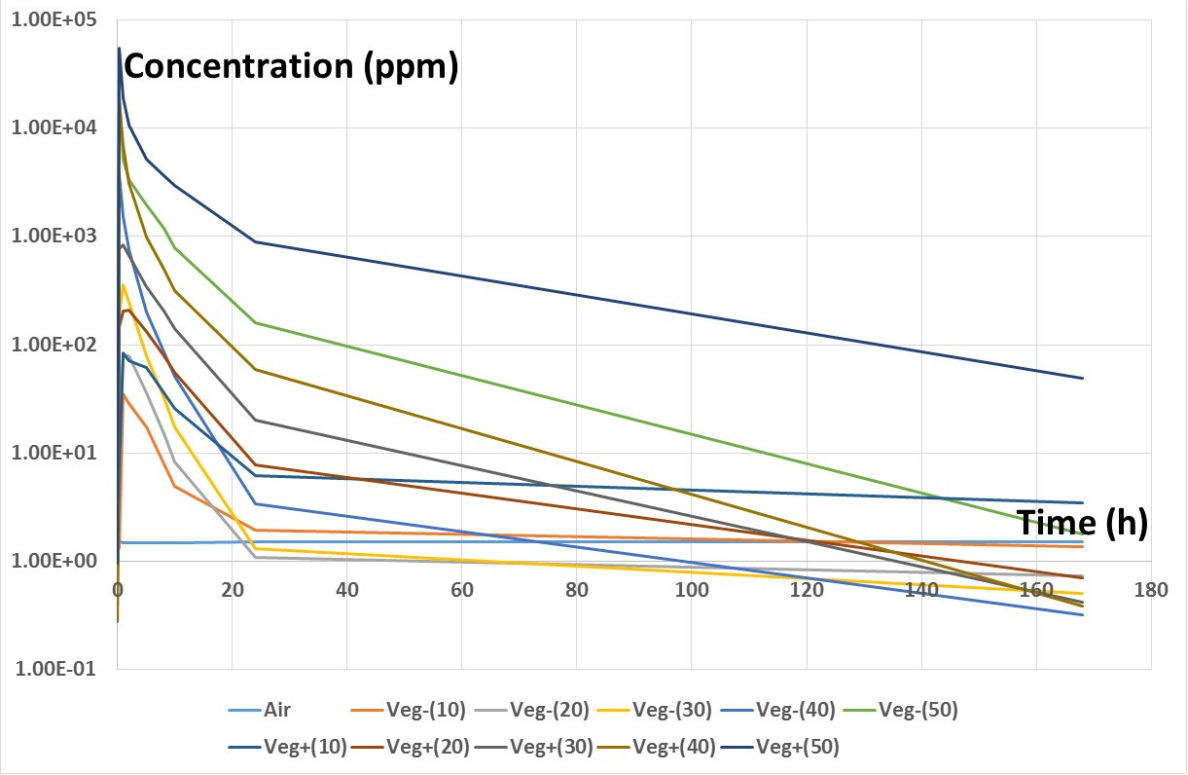


*Figure 31: Variations in Bulk Methane Concentrations in Soil over Time for FE3*

*Table 9: LE3: Time Integrals of the Methane Concentrations at Different Depths*

| | Time Integral (ppm-h) | | Time Integral (ppm-h) |
|---|---|---|---|
| Air | 255 | | |
| Veg-(10) | 437 | Veg+(10) | 1378 |
| Veg-(20) | 544 | Veg+(20) | 2083 |
| Veg-(30) | 1377 | Veg+(30) | 5650 |
| Veg-(40) | 5339 | Veg+(40) | 26418 |
| Veg-(50) | 38649 | Veg+(50) | 152204 |

As in the soil column experiment, the time-integrated concentration falls off approximately exponentially with upward distance from the point of injection (Figure 32), though the rate of change decreases upward. In this case, the coefficient of fall-off for the vegetated and non-vegetated cases is as listed in Table 10.

These rates are comparable in magnitude with the rates of 0.1 $cm^{-1}$ (non-vegetated) and 0.08 $cm^{-1}$ (vegetated) found for LE3. The larger values at distances of 0 to 10 and 10 to 20 cm from the source can probably be attributed to an increasing area of the plume as it moves upward in the soil column. However, the lower rate of decrease at 30 to 40 cm cannot be attributed to a change in lateral dimensions and may, more plausibly, be attributed to differences in soil structure between field and laboratory conditions, as these would alter the diffusion rate, or to distinctions in the microbial population present or its metabolic activity. However, the most likely cause is the advection of methane between 50 cm and above 40 cm depth due to the larger volume of gas injected in the field experiment. This would have occurred rapidly and given little opportunity for oxidation.

The other data set of relevance is that relating to the efflux of methane from the soil surface. These data are provided in Table 4.8 of Atkinson et al. [2014] and are summarised in Table 11, below.

The volumetric effluxes given in the rightmost two columns of Table 10 are calculated based on 1 mg of $CH_4$ corresponding to 1.4 ml at STP and assuming that the headspace chamber captured all the methane released. As these chambers had a diameter of 0.5 m, the appropriate area to assume is $\pi(0.25)^2 = 0.196\ m^2$. As in the case of LE3, these data should not be over-interpreted, but they indicate that the release occurs mainly over about the first 9 hours at an average release rate of about 0.05 ml $h^{-1}$. This implies a total release of about 0.45 ml, which can be compared with a total injection volume of 15 ml (Section 3.3.4.1 of Atkinson et al. [2014]). Thus, approximately 0.03 of the injected methane reached the surface, implying an average depletion rate of 0.07 $cm^{-1}$. This is consistent both with the soil column experiment (Section 3.5.2) and the results given in Table 10, once account is taken of the effects of lateral dispersion on concentrations in soil (lateral dispersion does not affect the estimate based on measured effluxes, provided that the headspace chamber captures the whole plume).

Finally, it is of interest to examine the specific activity data for the columns. This information is given in Table 4.10 of Atkinson et al. [2014] and is reproduced in Table 12. The injected methane had an isotopic ratio of 37139‰. Thus, Table 12 can be rewritten as the fraction of soil methane that derives from the injected gas. Results are shown in Table 13.

For un-vegetated conditions, the plume largely comprises injected methane, except that when the main phase of upward migration is complete (at 10 or more hours), there is some mixing with background methane. For vegetated conditions, the plume initially moves up to 40 cm during the first two hours, largely without dilution. However, as it moves up the soil, and at later times when the main phase of migration is over, there is significant dilution. This may arise because of exchange with the overlying atmosphere, but also because the plume expands laterally, mixing with an increased volume of the soil atmosphere.

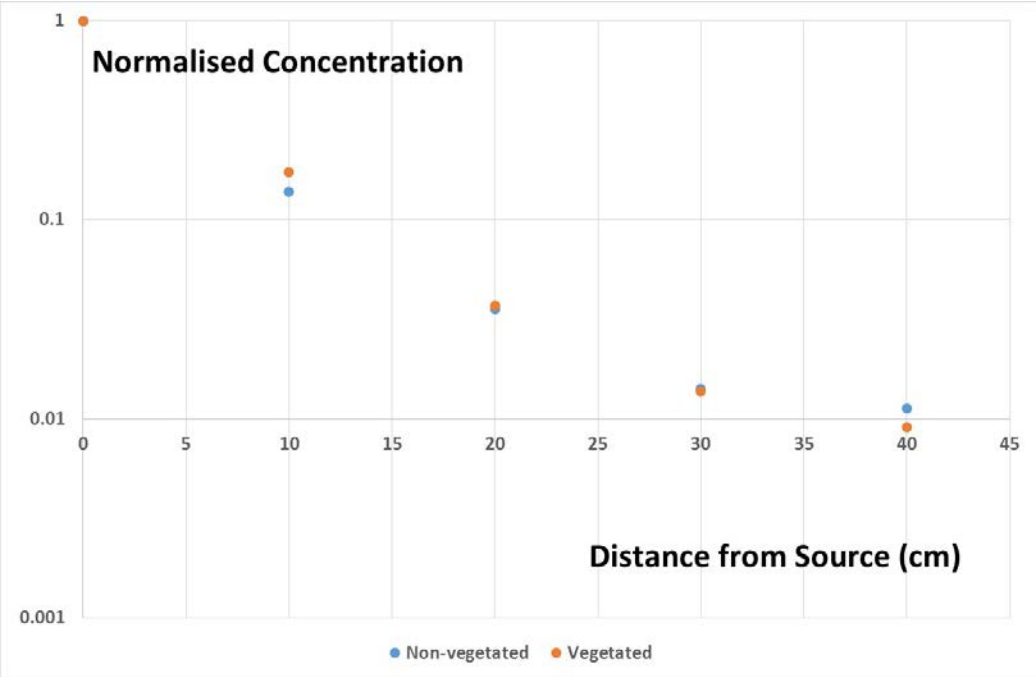


*Figure 32: Normalised Methane Concentration as a Function of Distance Upward from the Source for Field Experiment #3*

*Table 10: Rate of Fall-off in Time-integrated Concentration as a Function of Distance from the Source in Field Experiment #3*

| Distance from source (cm) | Rate of fall-off ($cm^{-1}$) | |
|---|---|---|
| | Non-vegetated | Vegetated |
| 30 to 40 | 0.022 | 0.041 |
| 20 to 30 | 0.093 | 0.100 |
| 10 to 20 | 0.136 | 0.154 |
| 0 to 10 | 0.198 | 0.175 |

*Table 11: Efflux of Methane from the Soil Surface in Field Experiment #3*

| Time (h) | Efflux (mg $m^{-2}$ $h^{-1}$) | | Efflux (ml $h^{-1}$) | |
|---|---|---|---|---|
| | Veg+ | Veg- | Veg+ | Veg- |
| Antecedent | -0.0220 | -0.0143 | -0.0060 | -0.0039 |
| 3 | 0.2300 | 0.3385 | 0.0631 | 0.0929 |
| 6 | 0.1354 | 0.2315 | 0.0372 | 0.0635 |
| 9 | 0.0582 | 0.1148 | 0.0160 | 0.0315 |
| 25 | -0.0148 | -0.0075 | -0.0041 | -0.0021 |
| 48 | 0.0007 | -0.0189 | 0.0002 | -0.0052 |

*Table 12: Isotopic Ratios from Field Experiment #3 (‰). Results are only shown for normal conditions, i.e. they exclude data collected at the time of the extreme rainfall event that affected this experiment.*

| Isotopic Ratio (‰) | | | | | | | |
|---|---|---|---|---|---|---|---|
| **Time (h)** | **0.25** | **1** | **2** | **5** | **8** | **10** | **24** |
| Veg-(10) | 2297 | 13103 | 16278 | 17112 | 14663 | 11103 | 3794 |
| Veg-(20) | 14897 | 20834 | 24175 | 24893 | 21207 | 18792 | 5879 |
| Veg-(30) | 29912 | 32712 | 31758 | 30340 | 25519 | 24246 | 9149 |
| Veg-(40) | 33966 | 33141 | 32995 | 30403 | 27048 | 25065 | 10742 |
| Veg-(50) | 35023 | 34283 | 35370 | 32675 | 30106 | 28344 | 22586 |
| Veg+(10) | 52 | 6853 | 10274 | 7501 | 3743 | 2042 | 179 |
| Veg+(20) | 2530 | 17569 | 17796 | 12888 | 6720 | 3832 | 368 |
| Veg+(30) | 13216 | 23556 | 22890 | 14580 | 8377 | 5781 | 531 |
| Veg+(40) | 32916 | 31489 | 29968 | 21434 | 13065 | 9716 | 1000 |
| Veg+(50) | 32320 | 28978 | 28608 | 26928 | 21328 | 20295 | 10353 |

*Table 13: Fraction of Methane from Injection at 50 cm (shaded entries signify total concentrations above 100 ppm)*

| Fraction from Injected Gas | | | | | | | |
|---|---|---|---|---|---|---|---|
| **Time (h)** | **0.25** | **1** | **2** | **5** | **8** | **10** | **24** |
| Veg-(10) | 0.06 | 0.35 | 0.44 | 0.46 | 0.39 | 0.30 | 0.10 |
| Veg-(20) | 0.40 | 0.56 | 0.65 | 0.67 | 0.57 | 0.51 | 0.16 |
| Veg-(30) | 0.81 | 0.88 | 0.86 | 0.82 | 0.69 | 0.65 | 0.25 |
| Veg-(40) | 0.91 | 0.89 | 0.89 | 0.82 | 0.73 | 0.67 | 0.29 |
| Veg-(50) | 0.94 | 0.92 | 0.95 | 0.88 | 0.81 | 0.76 | 0.61 |
| Veg+(10) | 0.00 | 0.18 | 0.28 | 0.20 | 0.10 | 0.05 | 0.00 |
| Veg+(20) | 0.07 | 0.47 | 0.48 | 0.35 | 0.18 | 0.10 | 0.01 |
| Veg+(30) | 0.36 | 0.63 | 0.62 | 0.39 | 0.23 | 0.16 | 0.01 |
| Veg+(40) | 0.89 | 0.85 | 0.81 | 0.58 | 0.35 | 0.26 | 0.03 |
| Veg+(50) | 0.87 | 0.78 | 0.77 | 0.73 | 0.57 | 0.55 | 0.28 |

### 3.6 DISCUSSION

With respect to the modelling of the migration and oxidation of methane through soil, the models, which are typically 1D in nature, tend to overestimate the bulk and isotopically enriched methane in the soil profile in the period following a pulse injection. In the laboratory systems, this could be attributable to the presence of "fast" pathways for soil gas to the surface along the inside of the soil column tubing, which the models do not represent. In the field systems, this could be attributable to lateral diffusion of methane outside of the region being sampled, which the models do not fully represent. The models presented above typically overestimated the activity in isotopically labelled carbon dioxide generated as a result of the methane oxidation, the one exception being the EDF C-14 model (see Section 3.5.3).

The main feature of the data that the numerical models cannot explain is more rapid consumption of $^{13}CH_4$ than $^{12}CH_4$ as the pulse of methane diffuses up the column (e.g. see Figure 27).

# 4 DUKE SWAMP MONITORING

The context for the Duke Swamp data is described in Section 4.1, the model applied to the scenario is described in Section 4.2, the data set used in the study is presented in Section 4.3, the modelling scenario is described in Section 4.4, the results of the model-data comparisons are presented in Section 4.5 and the findings are discussed in Section 4.6.

## 4.1 SYSTEM DESCRIPTION

Duke Swamp is a wetland ecosystem on Atomic Energy of Canada Limited (AECL)'s Chalk River Laboratories (CRL) site that receives C-14 through releases from the up-gradient Waste Management Area (WMA) "C", primarily through groundwater influx (Figure 33). Groundwater flow is from 'Lake 233' on one side of WMA-C towards the Duke Swamp, below WMA-C; a cross-section of the stratigraphy is given in Figure 34.

WMA-C consists of a series of unlined sand trenches that were constructed in 1963 and which received about 100,000 $m^3$ of low-level radioactive waste through to 2006. The facility is located on a large dune ridge above the highest recorded water table. The area is predominantly compacted sandy glacial till underlain by granitic gneiss bedrock [Donders et al., 1996]. Waste was initially covered with 1.5 m uncontaminated sand backfill from 1983 and subsequently provided with an engineered cover *c*. 2013-14 (see Figure 35); also, in 1983 a polyethylene cover was placed over about 1/6 of the southern end of the disposal area.

The uptake of C-14 in vegetation in Duke Swamp itself has been studied for over 20 years [e.g. Milton et al., 1998; King-Sharp et al., 2005], as has the quantification of C-14 levels in a wider range of environmental media, including air, groundwater, surface water and plants [e.g. Sheppard et al., 1994; Evenden et al., 1998].

Historical focus was limited to the area within the swamp where the highest radionuclide concentrations were expected to occur. In 2001, a sampling survey was carried out across a broader area within Duke Swamp, to quantify C-14 levels in surface vegetation and, to a lesser extent, in soils. A subset of the sites sampled was then selected for more detailed study to assess whether C-14 levels measured in sedentary species (e.g., plants and fungi) reflected those measured in mobile organisms (e.g., animals). There followed a series of reports that were not readily available [e.g. King-Sharp et al., 2005], though an analysis of those findings with regards C-14 concentrations in environmental media and uptake into biota was later published in the Journal of Environmental Radioactivity [Yankovich et al., 2013]. Subsequent to that publication, a study into the spatial distribution of C-14 concentrations in sphagnum moss (Figure 36) and the underlying sediment has been published [Yankovich et al., 2014]. All of this work has focussed on the Duke Swamp area itself.

Independent of the work described above, in recent years a PhD student from Oregon State University has undertaken two sampling campaigns in 2013 and 2014, looking at the area between the discharge zone, WMA-C, and Duke Swamp [Napier, 2015]. Groundwater, soil gas, and plant samples were collected to observe vertical profiles of stable and radioactive carbon at 22 sampling locations between the release zone and Duke Swamp (Figure 37).

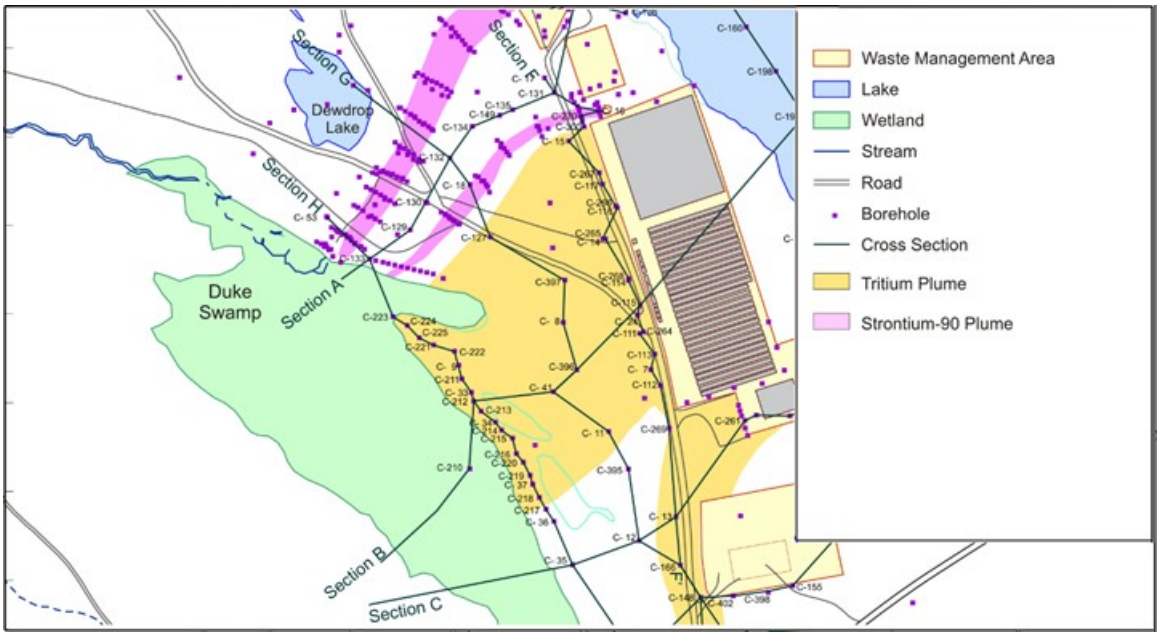


*Figure 33: Well map in the vicinity of WMA-C at Chalk River Laboratories. The C-14 plume is expected to be similar to the tritium plume highlighted in the figure; taken from a presentation to BIOPROTA given by J. Napier in 2015.*

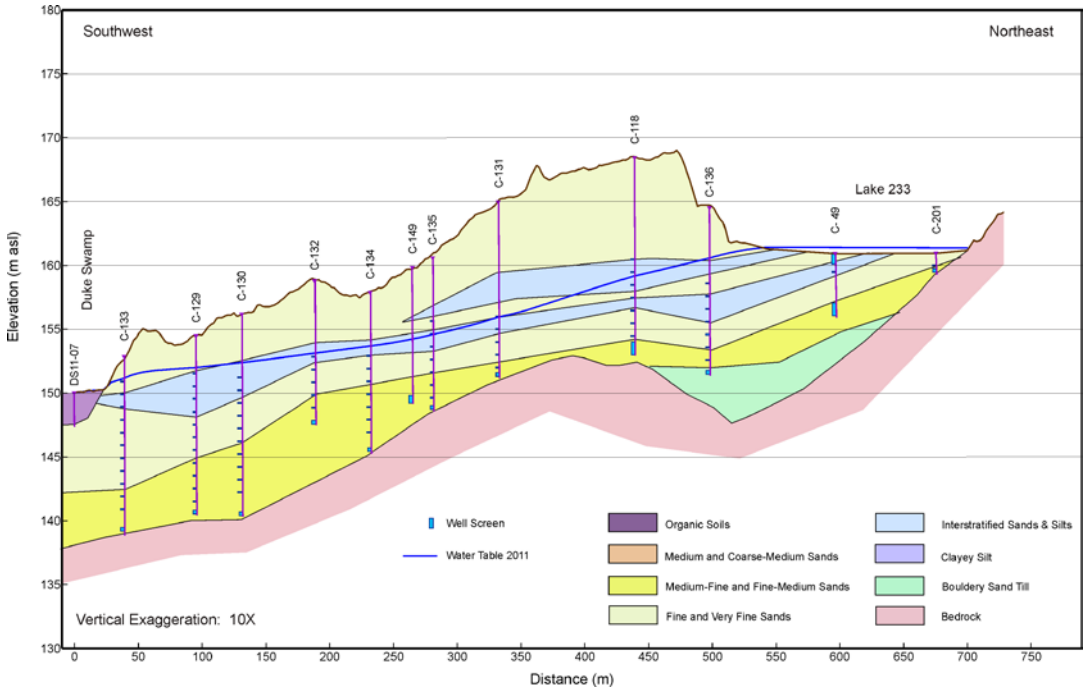


*Figure 34: Cross-section of the stratigraphy between WMA-C at Chalk River Laboratories and Duke Swamp (Section A from Figure 33); taken from presentation to BIOPROTA given by J. Napier in 2015.*

*Figure 35: Waste Management Area C before (top) and after (bottom) installation of engineered cover (from CNSC [2015])*


*Figure 36: Sphagnum moss and sediment sampling locations from Yankovich et al. [2014]*

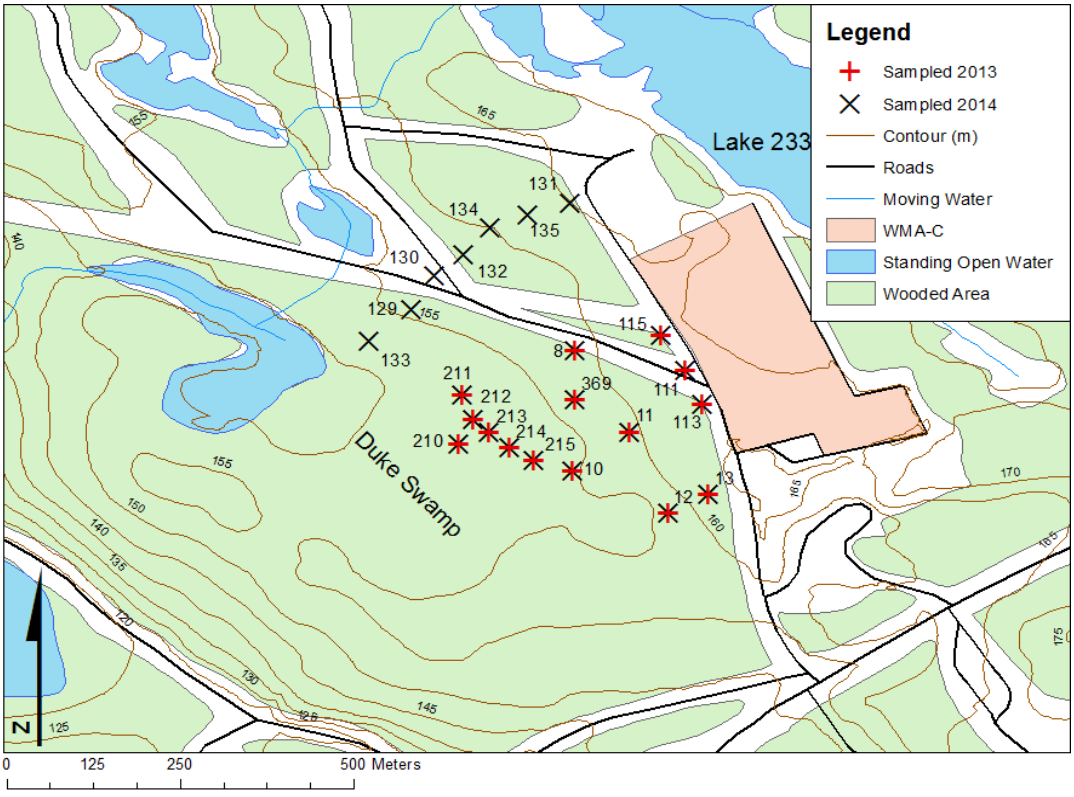


*Figure 37: Topography and sampling locations from Napier [2015]*

### 4.2 MODEL APPLIED TO THE DUKE SWAMP SCENARIO

A single model was applied to the Duke Swamp scenario, and that model was developed by the TST. The model considers a transect through the regions of interest (Figure 38), with the system discretised into the WMA-C, vadose zone, silty-clay lens, aquifer and Duke Swamp (cf. Figure 34). The geometry of the compartments was defined to follow those of the transect data and the model was implemented in AMBER (Figure 39).

A summary of the key model features is given in Table 14. It was assumed that the water table sits at the top of the silty-clay lens. The movement of C-14 contaminated water and gas throughout the soil is modelled considering lateral advection below the water table, and infiltration and vertical diffusion above the water table. The exchange of C-14 between the gaseous and dissolved form is modelled using Henry's Law.

Further details of the model are given in Section A.4 of the Appendix.

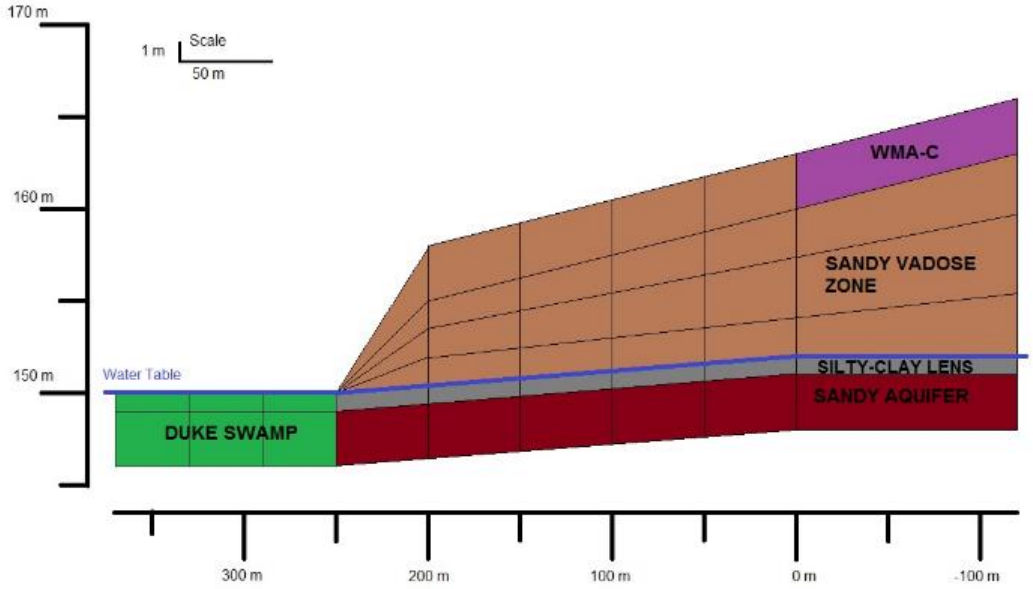


*Figure 38: Schematic of Duke Swamp Transect Model*

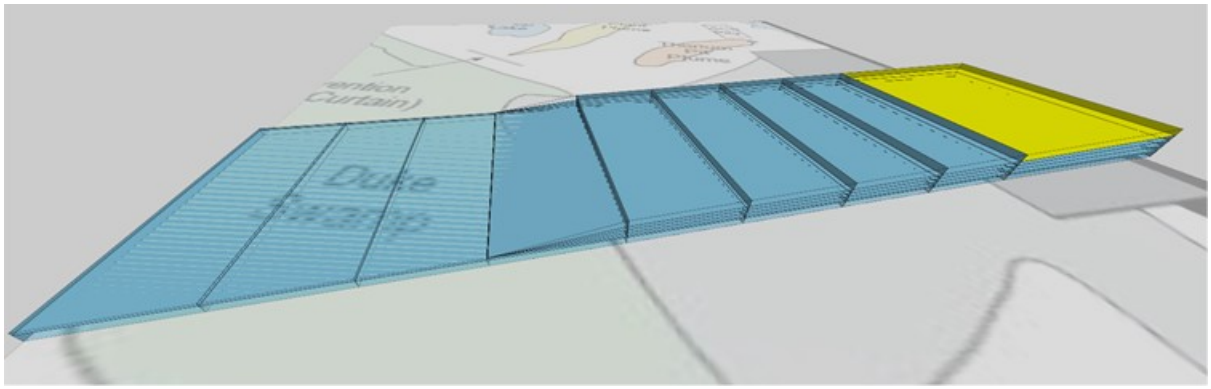

*Figure 39: Screenshot of the geometry of the Transect Model as implemented in AMBER, with WMA-C highlighted*

*Table 14: Summary of Key Model Features for the Model Applied to the Duke Swamp Scenario*

| Model aspect | TST (Transect Model) |
|---|---|
| Calculation time-step: | Determined by AMBER, dependent on the dynamics of the system |
| Sub-models: | WMA-C, Vadose zone, Clay lens, Aquifer, Duke Swamp |
| Number of compartments: | Vadose zone: 23<br>Silty-clay lens: 6<br>Aquifer: 6<br>Duke Swamp: 6 |
| Full list of modelled processes: | Advection, Diffusion, Infiltration, Gas-water exchange of carbon |

## 4.3 DUKE SWAMP DATASET

### 4.3.1 Hydrology

Annual precipitation is about 800 mm at Chalk River, of which about 190 mm falls as snow during winter months. Evapotranspiration is about 420 mm $y^{-1}$, which leaves a hydrologically effective rainfall of about 380 mm $y^{-1}$ [Napier, 2015].

Groundwater enters Duke Swamp from Lake 233, and from Duke Swamp ultimately drains into Maskinonge Lake (Figure 40). Water leaves the swamp in two directions: to the north west, where the water flows into Lower Bass Lake; and to the south east, where the water flows into Duke Stream [Killey et al., 1998]. Both Lower Bass Lake and Duke Stream flow into Maskinonge Lake.

Up-gradient of WMA-C, the groundwater has low redox potential and low dissolved oxygen content; reflecting its origin as recharge through the bed sediment of Lake 233. The bed sediment of the lake is generally thin, but supports a substantial rate of biological activity. Groundwater beneath WMA-C has higher dissolved oxygen content in comparison to that beneath Lake 233 [Donders et al., 1996]. Groundwater beneath WMA-C flows towards the swamp at a rate of about 150 m $y^{-1}$ [Napier, 2015].

A tentative water balance for Duke Swamp and for groundwater flow from Lake 233 to Duke Swamp beneath WMA-C is provided below. The nomenclature is illustrated in Figure 41.

Meteorological data for Chalk River is given in Table 15. These are monthly averages, based on data collected between 1971 and 2000. They correspond closely to boreal continental climate conditions (subarctic continental conditions according to the Køppen/Trewartha climate classification scheme used in BIOCLIM [2004]).

*Table 15: Monthly average climate data for Chalk River* [k]

| Month | Temperature (ºC) | Rainfall (mm) | Snowfall (cm) | Precipitation (mm) |
|---|---|---|---|---|
| January | -12.1 | 14.2 | 43.7 | 56.7 |
| February | -9.8 | 8.7 | 37.7 | 45.3 |
| March | -3 | 31.4 | 30.7 | 62 |
| April | 5.1 | 51.4 | 9.1 | 60.4 |
| May | 12.6 | 80.2 | 1.4 | 81.6 |
| June | 17.5 | 88.3 | 0 | 88.3 |
| July | 20 | 86.8 | 0 | 86.8 |
| August | 18.7 | 82.1 | 0 | 82.1 |
| September | 13.7 | 84.6 | 0 | 84.6 |
| October | 7.3 | 76.7 | 2.7 | 79.3 |
| November | 0.3 | 48.4 | 24.3 | 72.3 |
| December | -7.9 | 16.6 | 45.8 | 60.9 |

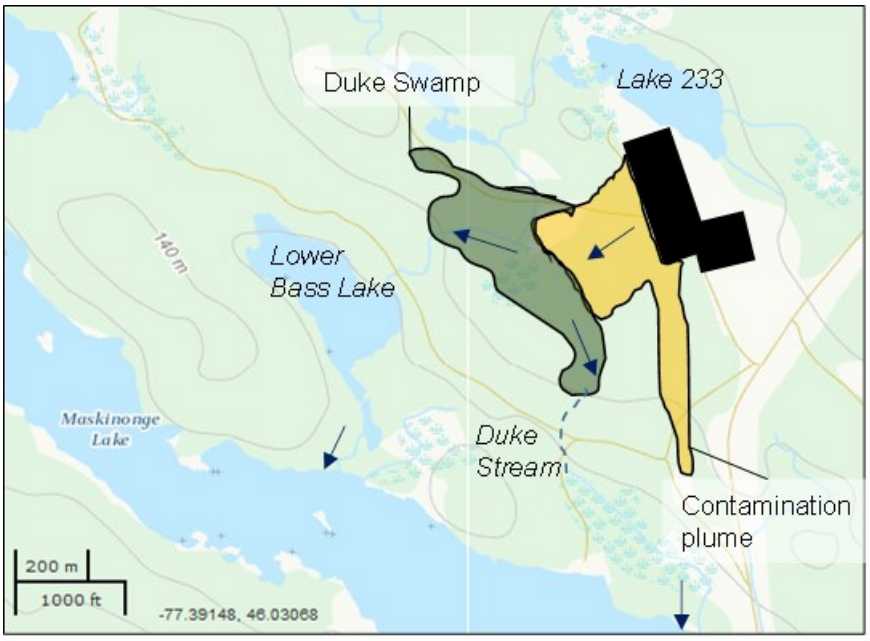


*Figure 40: Indication of groundwater flow into and out of Duke Swamp (drawing on Killey et al. [1998]; underlying map is ©GeoGratis – Canada Base Map)*

[k] Taken from http://www.eldoradocountyweather.com/canada/climate2/Chalk%20River.html

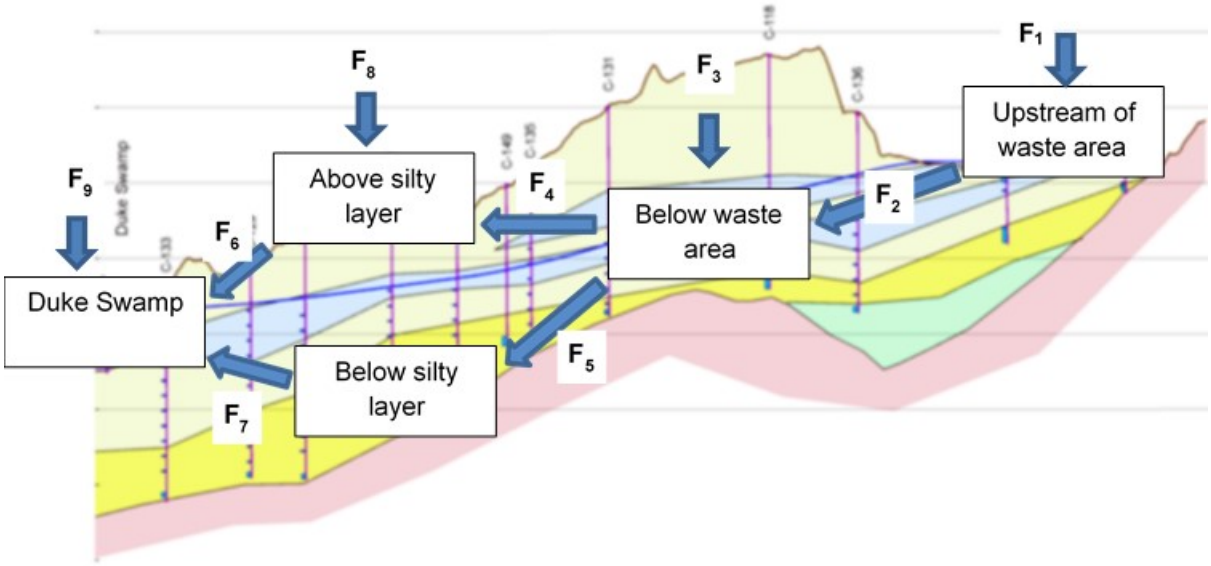


*Figure 41: Water balance for groundwater flow and Duke Swamp*

For these conditions, precipitation (P) typically exceeds potential evapotranspiration (PE) by about 200 mm $y^{-1}$. Thus, if P at the site is taken to be 800 mm $y^{-1}$; PE should be taken as 600 mm $y^{-1}$. Over lake and wetland areas, actual evapotranspiration (AE) is taken to be equal to PE, whereas over other areas AE is taken to be 0.75*PE (i.e. 450 mm $y^{-1}$). Thus, P-AE = 200 mm $y^{-1}$ over lakes and wetlands and 350 mm $y^{-1}$ elsewhere; the latter corresponding well with the 340 mm $y^{-1}$ value given in Killey et al. [1998].

Upstream of the waste area, the area of Lake 233 that is taken to feed groundwater flow beneath WMA-C is taken to be the same area as WMA-C itself (i.e. 350 m x 120 m = 4.2E4 $m^2$; note that this is not the whole of Lake 233, since much of the lake drainage bypasses WMA-C, as shown by the water-table contours of Figure 1 of Killey et al. [1998]); other upslope contributions to groundwater flow beneath WMA-C are taken to arise from a similar area. Thus:

$F_1 = 4.2E4 \times (0.2 + 0.35) = 2.31E4\ m^3\ y^{-1}$

Hence:

$F_2 = 2.31E4\ m^3\ y^{-1}$

By similar arguments:

$F_3 = 350 \times 120 \times 0.35 = 1.47E4\ m^3\ y^{-1}$

Thus:

$F_4 + F_5 = F_2 + F_3 = 3.78E4\ m^3\ y^{-1}$

The partitioning of the total flow between $F_4$ and $F_5$ is unknown, so:

$F_4 = \alpha (F_4 + F_5)$ $\quad$ $F_5 = (1-\alpha) (F_4 + F_5)$

Leakage across the silty layer is excluded, since this is likely to be a minor factor in routing C-14.

Noting that the area above the silty layer is not a lake or wetland and has a downslope length of about 250 m:

$F_8 = 350 \times 250 \times 0.35 = 3.06E4\ m^3\ y^{-1}$

$F_7 = F_5$ and $F_6 = F_4 + F_8$

Thus, the total groundwater flow into Duke Swamp is:

$F_6 + F_7 = F_4 + F_5 + F_8 = 6.84E4\ m^3\ y^{-1}$

Killey et al. [1998] give the streamflow from Duke Swamp as 7.71E4 $m^3\ y^{-1}$, but note that runoff from precipitation falling on the rocky southwestern boundary of Duke Swamp plus direct precipitation onto the swamp contributes 1.04E4 $m^3\ y^{-1}$ to this streamflow. Therefore, groundwater discharge contributes 6.67E4 $m^3\ y^{-1}$ to this streamflow. They also give an estimate of the total groundwater input to Duke Swamp as 10.3E4 $m^3\ y^{-1}$, which includes various contributions other than the downslope flow from WMA-C. Based on these considerations, $F_9$ is estimated by difference to be 1.03E5 – 6.84E4 = 3.46E4 $m^3\ y^{-1}$. It is assumed that some of the overall groundwater inflow into Duke Swamp is lost by subsurface flows and evapotranspiration processes, resulting in a streamflow that is rather less than the sum of the groundwater input plus runoff from precipitation falling on the rocky southwestern boundary of Duke Swamp plus direct precipitation onto the swamp (1.13E5 $m^3\ y^{-1}$).

### 4.3.2 Duke Swamp

The swamp covers an area of about 10 ha and primarily comprises fibrous sphagnum peat, which can extend to a depth of up to 3 m. Vegetation comprises plants such as sphagnum moss, lichen, ferns (bracken, ostrich ferns [Milton et al., 1998]), white spruce, and white cedar [Evenden et al., 1998].

### 4.3.3 Contamination

**WMA-C**

Trial coring was conducted in to WMA-C in 1995 and included analysis of groundwater contamination [Donders et al., 1996]. Five boreholes were sunk into a relatively localised region of WMA-C. Description of the profile through one of the boreholes is given in Figure 42. Dissolved C-14 concentrations from the trial boreholes in WMA-C are given in Table 16.

*Table 16: Dissolved C-14 concentrations in the five trial boreholes into Waste Management Area C c.1995, from Donders et al. [1996]*

| Borehole | Dissolved C-14 Concentration (Bq $L^{-1}$) |
|---|---|
| CT-1 | <45 |
| CT-2 | 67 |
| CT-3 | <45 |
| CT-4 | 112 |
| CT-5 | 720 |

**Area between WMA-C and Duke Swamp**

The raw results from the Napier [2015] study are given in Table 17 and Table 18 for the 2013 and 2014 sample periods, respectively. Point 210 is in Duke Swamp itself. The plant concentration relates to

above-ground bracken (*Pteridium*) collected based on proximity to the groundwater sampling points. Both dissolved organic carbon (DOC) and dissolved inorganic carbon (DIC) concentrations were measured, although the specific activity in water relates to the sum of the activity in DOC and DIC form. Groundwater contamination data are also available from the 1991 study [Killey et al., 1998], with four of the locations coinciding with locations used by Napier [2015]. Multi-level soil gas concentrations were taken at sample location #8 and #369 (see Figure 10 for locations).

Statistical analysis and linear regression applied to the data collected have shown different significant variables between subsets close to the release zone, WMA-C, and the surface emission zone, Duke Swamp. In particular, the data collected indicates the likelihood of two different contamination pathways for the vegetation downstream of WMA-C (Figure 37). Close to the facility, plant C-14 specific activity was best explained through incorporation of C-14 transported in contaminated soil gas emitted by WMA-C. However, close to the swamp, plant C-14 activity was best explained by the distance to the surface of the contaminated groundwater. This suggested a pathway of lateral transport in the aquifer and subsequent upward transport by diffusion through the vadose zone.

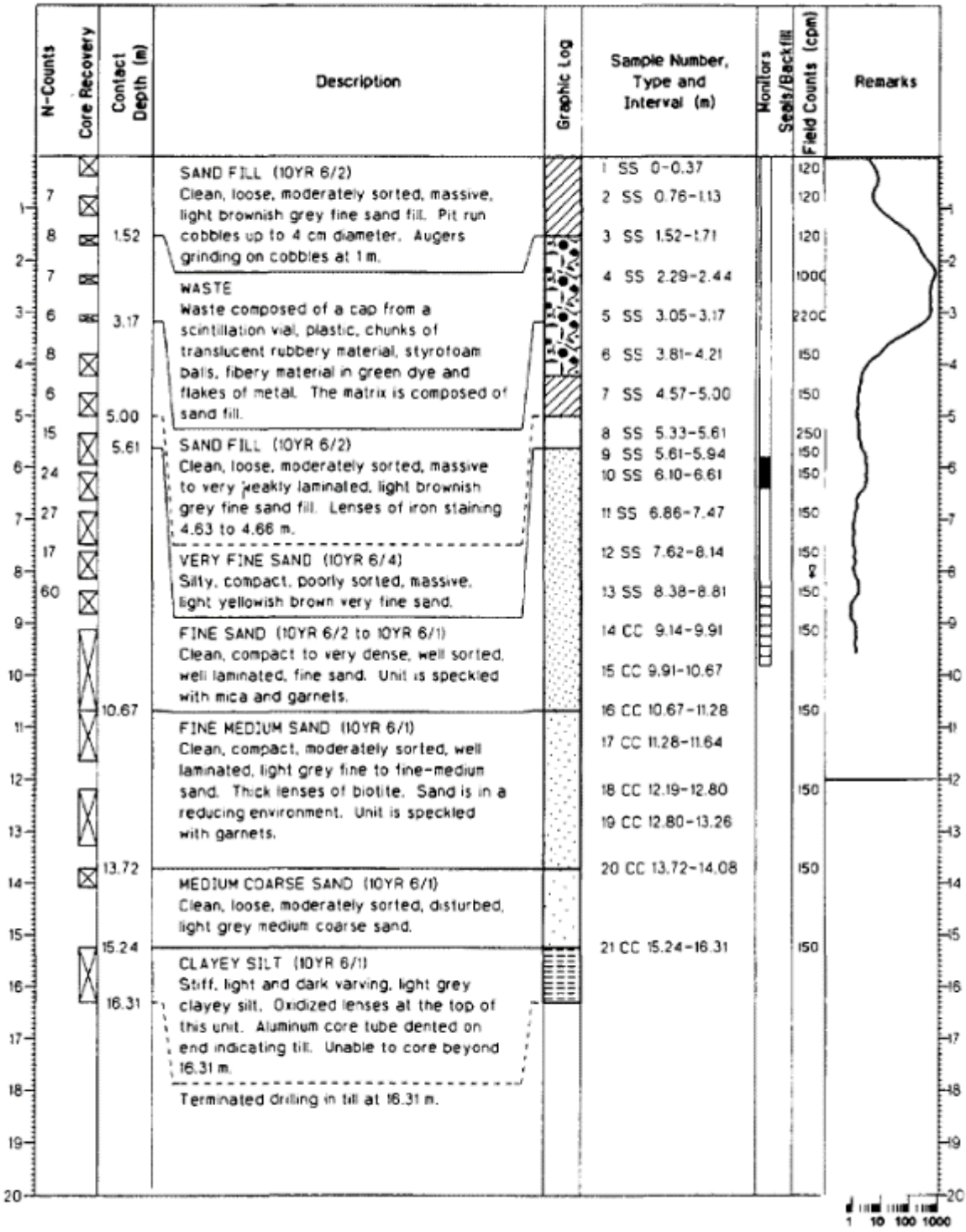


*Figure 42: Borehole log for one of the trial cores into Waste Management Area C, from Donders et al. [1996]*

*Table 17: Raw 2013 data from Napier [2015]. The value of 2.3 Bq $L^{-1}$ in water is the Limit of Detection.*

| Well | Depth (m) | $CO_2$ (ppm) | Plant (Bq $gC^{-1}$) | Water (Bq $L^{-1}$) | Gas (Bq $L^{-1}$) | DOC (mg $L^{-1}$) | DIC (mg $L^{-1}$) |
|---|---|---|---|---|---|---|---|
| 8 | 3.58 | 8327 | 0.161 | < 2.3 | 1.2662 | 0.67 | 16.47 |
| 10 | 1.62 | 9178 | 0.928 | < 2.3 | 0.2668 | 1.67 | 9.1 |
| 11 | 3.46 | 5995 | 0.167 | 759.6 | 0.0292 | 1.53 | 7.73 |
| 12 | 2.01 | 5514 | 0.189 | < 2.3 | 0.153 | 1.76 | 2.21 |
| 13 | 3.45 | 7214 | 0.124 | < 2.3 | 0.0127 | 0.91 | 3.63 |
| 111 | 3.53 | - | 0.364 | < 2.3 | 0.418 | 3.71 | 10.41 |
| 113 | 3.52 | - | 0.919 | < 2.3 | 1.5259 | 2.32 | 12.85 |
| 115 | 3.73 | 8131 | 0.345 | < 2.3 | 0.1483 | 1.68 | 11.56 |
| 210 | 0 | 400 | 3.153 | 77.7 | 0 | 11.46 | 16.87 |
| 211 | 3.23 | 5119 | 0.254 | 1990 | 0.0158 | 1.91 | 8.53 |
| 212 | 2.42 | 4106 | 0.462 | 172.9 | 0.0073 | 12.8 | 14.83 |
| 213 | 1.79 | 9566 | 0.760 | < 2.3 | 0.0239 | 11.3 | 12.06 |
| 214 | 1.77 | 4143 | 0.572 | < 2.3 | 0.0092 | 7.73 | 9.24 |
| 215 | 2.4 | 3711 | 0.463 | < 2.3 | 0.0042 | 6.47 | 12.6 |
| 369 | 3.56 | - | 0.172 | < 2.3 | 0.0503 | 0.55 | 11.92 |

*Table 18: Raw 2014 data from Napier [2015]. The value of 2.3 Bq $L^{-1}$ in water is the Limit of Detection.*

| Well | Depth (m) | $CO_2$ (ppm) | Plant (Bq $gC^{-1}$) | Water (Bq $L^{-1}$) | Gas (Bq $L^{-1}$) | DOC (mg $L^{-1}$) | DIC (mg $L^{-1}$) |
|---|---|---|---|---|---|---|---|
| 8 | 3.58 | 3375 | 0.170 | < 2.3 | 0.3299 | 3.5 | 18.5 |
| 10 | 1.62 | 3476 | 0.709 | < 2.3 | 0.1067 | 4 | 22 |
| 11 | 3.46 | 3003 | 0.148 | 759.6 | 0.0291 | 1.8 | 21.9 |
| 12 | 2.01 | 1403 | 0.167 | < 2.3 | 0.312 | 2.5 | 17.8 |
| 13 | 3.45 | 2212 | 0.116 | < 2.3 | 0.0115 | 3.2 | 3.8 |
| 111 | 3.53 | 4596 | 0.368 | < 2.3 | 0.8345 | 4.4 | 15.2 |
| 113 | 3.52 | 426 | 0.653 | < 2.3 | 1.9706 | 4 | 10.2 |
| 115 | 3.73 | 3595 | 0.373 | < 2.3 | 0.3733 | 3.1 | 11.1 |
| 129 | 2.3 | 2945 | 0.133 | < 2.3 | 0.0373 | 1.5 | 5.8 |
| 130 | 3.55 | 3730 | 0.115 | < 2.3 | 0.0056 | 1.7 | 8.9 |
| 131 | 5.21 | 4321 | 0.132 | < 2.3 | 0.0109 | 18.1 | 17.9 |
| 132 | 4.77 | 2449 | 0.124 | 950 | 0.003 | 3.3 | 17.4 |
| 133 | 1.32 | 2762 | 0.199 | < 2.3 | 0.0219 | 2.3 | 11.5 |
| 134 | 4.06 | 3228 | 0.108 | < 2.3 | 0.0032 | 2.7 | 10.1 |
| 135 | 4.05 | 5648 | 0.112 | 492.2 | 0.018 | 2.3 | 17.8 |
| 210 | 0 | 400 | 1.751 | 77.7 | 0 | 7.8 | 16.7 |
| 211 | 3.23 | 1690 | 0.282 | 1990 | 0.0233 | 4.4 | 28.4 |
| 212 | 2.42 | 1980 | 0.462 | 172.9 | 0.1927 | 12.6 | 15.2 |
| 213 | 1.79 | 1867 | 0.650 | < 2.3 | 0.1189 | 7.6 | 16.6 |
| 214 | 1.77 | 1159 | 0.893 | < 2.3 | 0.016 | 7 | 13.7 |
| 215 | 2.4 | 1795 | 0.063 | < 2.3 | 0.0849 | 9.8 | 13.7 |
| 369 | 3.56 | 3224 | 0.096 | < 2.3 | 0.1115 | 3.1 | 6.4 |

*Table 19: Soil gas activity vertical profiles from multi-level sampling at two locations adjacent to Waste Management Area C [Napier, 2015]*

| Sample | C-14 (Bq $L^{-1}$) |
|---|---|
| 8-A | 0.000185* |
| 8-25 | 0.000792* |
| 8-50 | 0.001039* |
| 8-75 | 0.000319* |
| 8-100 | 0.000525* |
| 8-150 | 0.000597* |
| 8-200 | 0.023714 |
| 8-356 | 0.329867 |
| 8-500 | 2.279455 |

| Sample | C-14 (Bq $L^{-1}$) |
|---|---|
| 369-A | 0.019691 |
| 369-25 | 0.001862 |
| 369-50 | 0.00215 |
| 369-75 | 0.007119 |
| 369-100 | 0.007634 |
| 369-150 | 0.007387 |
| 369-200 | 0.00537 |
| 369-356 | 0.005576 |
| 369-500 | 0.026286 |

Note: The sample numbers have the format NNN-DDD, where the first component is the sample location (see Figure 37) and the second is the sample depth in cm.

* These samples were associated with measured concentrations that were below the reported detection limit of 0.001353 Bq $L^{-1}$ and cannot be regarded as significantly different from zero.

**Duke Swamp**

Yankovich et al. [2014] provide C-14 concentrations in Sphagnum moss and sediment samples taken from Duke Swamp in 2011. The sample locations are shown in Figure 36 and the resulting concentrations are given in Table 20. The study found no significant difference between the moss and sediment concentrations. The moss and sediment were found to have water contents of 85% and 54%, respectively. The sediment samples were taken to a depth of about 5 cm at the same locations as the moss samples. The sediment samples were found to be highly organic in nature and principally consist of decaying moss. A background concentration of approximately 250 Bq $kgC^{-1}$ is reported.

## 4.4 CALCULATION SCENARIO DESCRIPTION

The aim of these calculations was to model the discharge of C-14 from WMA-C via the groundwater pathway over a period of about 30 years. Outputs of interest were: concentrations in groundwater (Bq $L^{-1}$), in soil gas (Bq $L^{-1}$), in Duke Swamp sediment (Bq $kgC^{-1}$) and in vegetation (Bq $kgC^{-1}$). In particular, given the unknown nature of the source term, it was considered pertinent to establish whether the model could replicate the broad patterns seen in the field data. In this regard, the more recent data [Yankovich et al., 2013, 2014; Napier, 2015] were considered for a broad comparison of patterns of concentrations.

In this present study comparisons have only been made between the observed concentrations of C-14 in the groundwater and soil gas, since establishing confidence in the transport pathways is a prerequisite for modelling accumulation in Duke Swamp.

*Table 20: C-14 specific activities (Bq kgC$^{-1}$) in Sphagnum moss and associated sediment from a sampling campaign in 2001 [Yankovich et al., 2014]*

| Location | C-14 specific activity | |
|---|---|---|
| | Moss | Sediment |
| **Group 1** | | |
| DSS-08 | 960 ± 100 | n.a. |
| DSS-11 | 1200 ± 120 | n.a. |
| DSS-12 | 960 ± 140 | n.a. |
| DSS-14 | 2000 ± 84 | 2400 ±180 |
| DSS-15 | 1100 ± 180 | n.a. |
| DSS-16 | 630 ± 120 | n.a. |
| DSS-22 | 380 ± 140 | n.a. |
| DSS-23 | 290 ± 160 | n.a. |
| DSS-25 | 160 ± 140 | n.a. |
| DSS-28 | 8200 ± 200 | 4200 ± 200 |
| DSS-29 | 3500 ± 71 | 1500 ± 82 |
| DSS-30 | 290 ± 41 | 2100 ± 57 |
| DSS-31 | 720 ± 43 | 280 ± 95 |
| DSS-32 | 420 ± 43 | n.a. |
| DSS-36 | 6500 ± 250 | 5600 ± 250 |
| DSS-38 | 1800 ± 140 | n.a. |
| DSS-43 | 3600 ± 310 | 11,000 ± 210 |
| DSS-45 | 1000 ± 36 | 660 ± 150 |
| DSS-46 | 550 ± 79 | n.a. |
| DSS-47 | 370 ± 23 | n.a. |
| DSS-49 | 1800 ± 79 | n.a. |
| DSS-50 | 2300 ± 110 | n.a. |
| DSS-51 | 1900 ± 120 | n.a. |
| **DSS-56** | **2800 ± 190** | **n.a.** |
| DSS-57 | 760 ± 75 | n.a. |

| Location | C-14 specific activity | |
|---|---|---|
| | Moss | Sediment |
| **Group 2** | | |
| DSS-01 | 270 ± 120 | n.a. |
| DSS-02 | 1100 ± 84 | n.a. |
| DSS-04 | 930 ± 110 | n.a. |
| DSS-09 | 1600 ± 110 | n.a. |
| DSS-17 | 980 ± 95 | n.a. |
| DSS-18 | 690 ± 60 | n.a. |
| DSS-27 | 17,000 ± 160 | 38,000 ± 730 |
| DSS-35 | 47,000 ± 330 | n.a. |
| DSS-42 | 15,000 ± 240 | 14,000 ± 130 |
| DSS-48 | 9200 ± 220 | n.a. |
| DSS-55 | 5700 ± 160 | 13,000 ± 250 |
| **DSS-56** | **2800 ± 190** | **n.a.** |
| DSS-60 | 3500 ± 98 | n.a. |
| DSS-61 | 1400 ± 100 | n.a. |
| DSS-64 | 1100 ± 89 | n.a. |
| DSS-65 | 1200 ± 90 | n.a. |
| DSS-69 | 690 ± 69 | n.a. |
| | | |
| **No group** | | |
| DSS-03 | n.d. (450) | n.a. |
| DSS-24 | n.d. (530) | n.a. |
| DSS-37 | n.d. (860) | n.a. |
| DSS-39 | n.d. (760) | n.a. |
| DSS-68 | n.d. (500) | n.a. |

Notes: Taken to be mean ± sigma, where sigma is described as the analytical error. n.d. indicates that detection limit was not exceeded (limit given in brackets).

## 4.5 RESULTS

The Transect Model was run for a 30 year period, assuming a normalised initial inventory of 1 TBq C-14 in WMA-C, released over a 150 year period, which started at the start of the simulation. When reporting results in a spatial manner, the following schematic is given to provide a guide as to the regions (Figure 43). The calculated concentrations of C-14 in the groundwater throughout the transect after 30 years, considering a vadose zone saturation of 0.5 and 0.7 are shown Figure 44a and Figure 44b respectively. For the values of S selected, the higher degree of saturation makes it more difficult for the carbon to reach the surface, and so the majority of the C-14 is transported via advection in groundwater below the water table down to the swamp. As the contamination gets closer to the swamp, the vertical distance

to the surface decreases. Thus, at the higher degree of saturation the concentration of C-14 in groundwater below the water table has less of a decline, and the concentration at the surface of the vadose zone is greater furthest from WMA-C than closer to it.

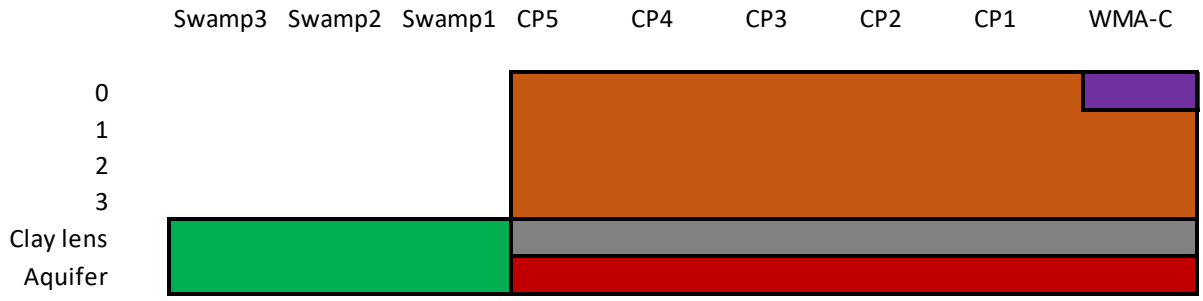


*Figure 43: Schematic of regions of the system in the Transect Model for plotting results*

(a)

| | Swamp3 | Swamp2 | Swamp1 | CP5 | CP4 | CP3 | CP2 | CP1 | WMA |
|---|---|---|---|---|---|---|---|---|---|
| 0 | | | | 5.6E+00 | 6.4E+00 | 7.1E+00 | 7.5E+00 | 7.8E+00 | 3.8E+01 |
| 1 | | | | 1.6E+01 | 2.2E+01 | 2.5E+01 | 2.7E+01 | 2.9E+01 | 1.4E+02 |
| 2 | | | | 2.7E+01 | 4.2E+01 | 4.9E+01 | 5.6E+01 | 6.2E+01 | 1.3E+02 |
| 3 | | | | 4.0E+01 | 7.5E+01 | 9.1E+01 | 1.1E+02 | 1.2E+02 | 1.2E+02 |
| Clay lens | 8.1E-02 | 1.5E-01 | 3.1E-01 | 3.0E+01 | 5.8E+01 | 7.2E+01 | 8.7E+01 | 1.0E+02 | 5.5E+01 |
| Aquifer | 6.3E-01 | 1.4E+00 | 4.0E+00 | 3.4E+01 | 6.0E+01 | 7.5E+01 | 8.9E+01 | 1.0E+02 | 4.8E+01 |

(b)

| | Swamp3 | Swamp2 | Swamp1 | CP5 | CP4 | CP3 | CP2 | CP1 | WMA |
|---|---|---|---|---|---|---|---|---|---|
| 0 | | | | 1.1E+01 | 4.8E+00 | 4.1E+00 | 3.5E+00 | 3.0E+00 | 1.0E+02 |
| 1 | | | | 3.7E+01 | 2.2E+01 | 1.9E+01 | 1.7E+01 | 1.5E+01 | 2.2E+02 |
| 2 | | | | 7.3E+01 | 5.7E+01 | 5.4E+01 | 5.0E+01 | 4.7E+01 | 1.9E+02 |
| 3 | | | | 1.3E+02 | 1.4E+02 | 1.4E+02 | 1.4E+02 | 1.4E+02 | 1.4E+02 |
| Clay lens | 3.3E-01 | 6.2E-01 | 1.3E+00 | 1.3E+02 | 1.6E+02 | 1.7E+02 | 1.7E+02 | 1.7E+02 | 8.3E+01 |
| Aquifer | 1.8E+00 | 4.1E+00 | 1.2E+01 | 1.4E+02 | 1.6E+02 | 1.7E+02 | 1.7E+02 | 1.7E+02 | 7.2E+01 |

*Figure 44: Calculated C-14 concentration in groundwater at 30 years (Bq $L^{-1}$) for differing degrees of saturation: (a) S = 0.5, and (b) S = 0.7.*

The sensitivity of the geometric mean of the calculated groundwater concentration of C-14 in the top two compartments in the third and fifth columns of the vadose zone to the degree of saturation (S) is explored further in Figure 45. These demonstrate further how the increasing degree of saturation assumed forces the C-14 further downstream in the saturated zone before the thinning of the vadose zone allows it to escape to the surface.

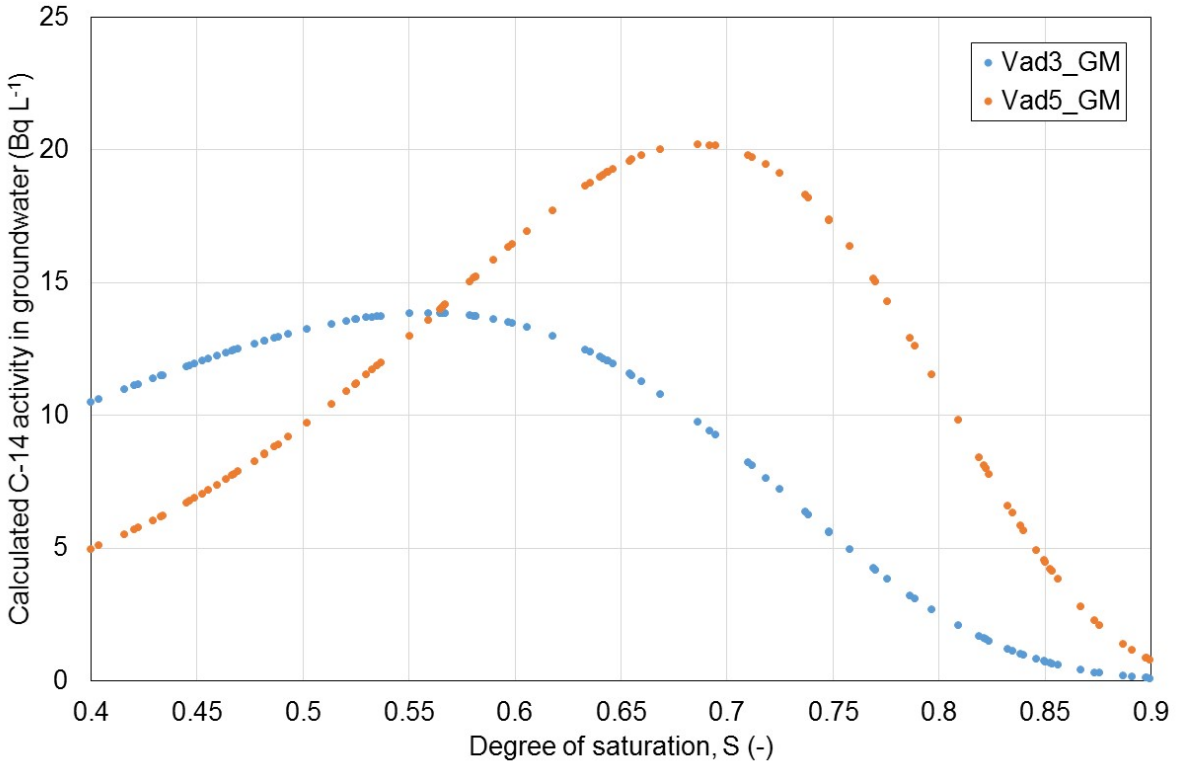


***Figure 45: Sensitivity of the geometric mean of calculated C-14 concentration in groundwater (Bq $L^{-1}$) after 30 years in the third and fifth columns of the Transect Model (top two layers of each column)***

In Table 21 the ratio of average calculated C-14 in the groundwater in the top two layers of the first, third and fifth columns of the Transect Model is compared with the ratio calculated from the data obtained by Napier [2015]. With respect to the observed data, where the observed values were below the limit of detection they have been assumed to equal that limit so that there is a non-zero concentration for column 1 to calculate a ratio with. The field observations indicate a more marked difference than the Transect Model between the C-14 concentration in groundwater adjacent to WMA-C and the C-14 concentration in downslope locations.

***Table 21: Ratio of groundwater concentrations in Transect Model between WMA-C and Duke Swamp***

| **Assumed saturation (S) in model, or field observations (Obs.)** | **Ratio** | | |
|---|---|---|---|
| | **Column 3: Column 1** | **Column 5: Column 1** | **Column 5: Column 3** |
| S = 0.5 | 0.9 | 0.6 | 0.7 |
| S = 0.6 | 1.1 | 1.2 | 1.2 |
| S = 0.7 | 1.3 | 2.6 | 2.1 |
| Obs. | 110.7 | 157.4 | 1.4 |

(a)

| | Swamp3 | Swamp2 | Swamp1 | CP5 | CP4 | CP3 | CP2 | CP1 | WMA |
|---|---|---|---|---|---|---|---|---|---|
| 0 | | | | 7.8E+00 | 9.0E+00 | 9.8E+00 | 1.0E+01 | 1.1E+01 | 0.0E+00 |
| 1 | | | | 2.3E+01 | 3.0E+01 | 3.4E+01 | 3.8E+01 | 4.0E+01 | 2.0E+02 |
| 2 | | | | 3.7E+01 | 5.9E+01 | 6.9E+01 | 7.8E+01 | 8.7E+01 | 1.8E+02 |
| 3 | | | | 5.6E+01 | 1.0E+02 | 1.3E+02 | 1.5E+02 | 1.7E+02 | 1.7E+02 |
| Clay lens | 0.0E+00 | 0.0E+00 | 0.0E+00 | 0.0E+00 | 0.0E+00 | 0.0E+00 | 0.0E+00 | 0.0E+00 | 0.0E+00 |
| Aquifer | 0.0E+00 | 0.0E+00 | 0.0E+00 | 0.0E+00 | 0.0E+00 | 0.0E+00 | 0.0E+00 | 0.0E+00 | 0.0E+00 |

(b)

| | Swamp3 | Swamp2 | Swamp1 | CP5 | CP4 | CP3 | CP2 | CP1 | WMA |
|---|---|---|---|---|---|---|---|---|---|
| 0 | | | | 1.5E+01 | 6.7E+00 | 5.7E+00 | 4.8E+00 | 4.1E+00 | 0.0E+00 |
| 1 | | | | 5.2E+01 | 3.0E+01 | 2.7E+01 | 2.4E+01 | 2.1E+01 | 3.1E+02 |
| 2 | | | | 1.0E+02 | 7.9E+01 | 7.5E+01 | 7.0E+01 | 6.6E+01 | 2.6E+02 |
| 3 | | | | 1.8E+02 | 2.0E+02 | 2.0E+02 | 2.0E+02 | 2.0E+02 | 2.0E+02 |
| Clay lens | 0.0E+00 | 0.0E+00 | 0.0E+00 | 0.0E+00 | 0.0E+00 | 0.0E+00 | 0.0E+00 | 0.0E+00 | 0.0E+00 |
| Aquifer | 0.0E+00 | 0.0E+00 | 0.0E+00 | 0.0E+00 | 0.0E+00 | 0.0E+00 | 0.0E+00 | 0.0E+00 | 0.0E+00 |

***Figure 46: Calculated C-14 concentration in soil gas at 30 years (Bq $L^{-1}$) for differing degrees of saturation: (a) S = 0.5, and (b) S = 0.7.***

The calculated concentrations of C-14 in soil gas (Bq $L^{-1}$) through the transect after 30 years are shown for S equal to 0.5 and 0.7 in Figure 46a and b respectively. The sensitivity of the geometric mean of the calculated soil gas concentration of C-14 in the top two compartments in the third and fifth columns of the vadose zone to the degree of saturation (S) is explored further in Figure 47.

Based on Henry's Law, it would be expected that, expressed on a volumetric basis, the concentration of C-14 as DIC in soil water would be approximately the same, or slightly greater than that of C-14 as $CO_2$ in soil gas, which is what is seen in the model results. This arises because C-14 rapidly exchanges between DIC and soil gas, and because Henry's Law as applied to carbon dioxide implies that concentrations of DIC and $CO_2$ in soil gas are similar on a volumetric basis.

The field data, however, indicate soil gas activities of C-14 much lower than that of the dissolved C-14 activities, which cannot be accounted for simply by consideration of the DOC and DIC ratio in the groundwater (Table 17, Table 18). Napier [2015] describes how soil gas sampling tips were emplaced in the boreholes at a depth of 50% that of the water table depth. The water depth was determined at each point using a conductivity probe. The probe was inserted down the primary borehole at each location. Using a hand held rotary hammer and an extendable drill bit, a two-inch (0.05 m) diameter borehole was drilled into the ground until the desired depth had been reached and a soil-gas sampling tip was put in place after being attached to a length of 1/8" polyvinyl tubing. The full length was measured then fed into the two-inch borehole. The soil from the borehole was backfilled into the hole. The soil gas samples were then collected by using a GeoTech Geopump[l], after twice purging the volume in the sampling tubes. Though it cannot be confirmed, it is possible that the soil gas concentrations of C-14 reported by Napier [2015] are not fully representative of the soil pore space, which is what is calculated in the model. This could have arisen because of the presence of preferential flow pathways through the borehole, e.g. at the interface between the tubing and the repacked soil,

[l] GeopumpTM Persitatltic Pump Series II, Geotech Environmental Equipment Inc., Denver Colorado

through the repacked soil, or at the interface between the repacked and intact soil. Gas extraction by pressure pumping rather than passive diffusive sampling could have exacerbated this effect.

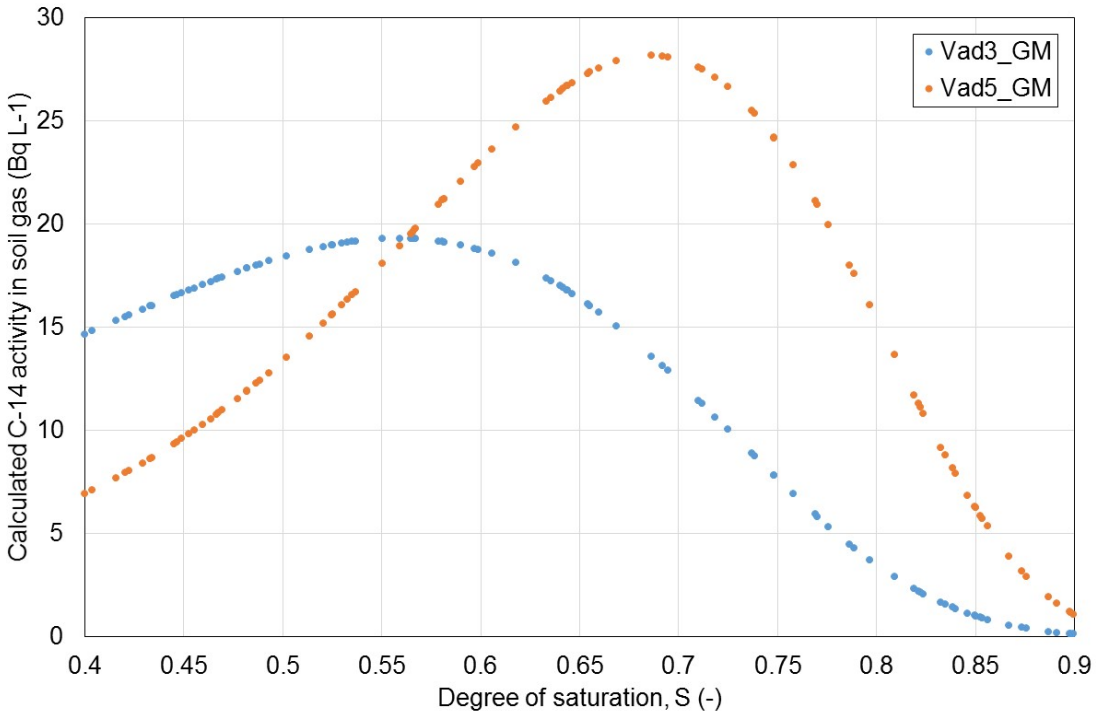


***Figure 47: Sensitivity of the geometric mean of calculated C-14 concentration in soil gas (Bq $L^{-1}$) after 30 years in the third and fifth columns of the Transect Model***

## 4.6 DISCUSSION

In this section, monitoring data associated with the contamination of Duke Swamp with C-14 arising from historic disposals in WMA-C is presented, together with the results of some preliminary modelling. The spatial pattern of observed C-14 concentrations in groundwater between WMA-C and Duke Swamp itself indicate a steeper gradient with respect to the increase in groundwater concentrations away from WMA-C than is seen in the model results (Table 21). The modelled soil gas concentrations of C-14 are similar to those in the groundwater, which agrees with what would be expected based on Henry's Law. The field observations of soil gas, however, are much lower than the field observations of groundwater concentrations. This discrepancy may be explained by the sampling method adopted by Napier [2015].

Comparisons have not yet been made against observed concentrations in Duke Swamp itself. This remains as a potential topic for further consideration, and would require uptake into the swamp vegetation and cycling/retention in soil/sediment organic matter to be included in the model employed above.

The Duke Swamp scenario is a direct analogue for near-surface waste disposal and radionuclide releases. There is merit in further reviewing the available observational data for C-14, and potentially for other radionuclides, to help build confidence in biosphere modelling for these radionuclides under similar conditions/contexts.

# 5 CONCLUSIONS AND DISCUSSION

The study has helped to build understanding and confidence in several aspects of biosphere modelling for C-14.

Specifically, it has shown that, for a well-defined atmospheric source term, the C-14 models used to represent the terrestrial biosphere can replicate observed concentrations of C-14 in pasture (Section 2). In particular, they can capture the short-term fluctuations in C-14 concentrations that might be observed in atmospheric releases. The models for atmospheric uptake to pasture can therefore be considered to be validated in this context.

With respect to the modelling of the migration and oxidation of methane through soil (Section 3), the models, which are typically 1D in nature, tend to overestimate the bulk and isotopically enriched methane in the soil profile in the period following a pulse injection. In the laboratory systems, this could be attributable to the presence of "fast" pathways for soil gas to the surface along the inside of the soil column tubing, which the models do not represent. In the field systems, this could be attributable to lateral diffusion of methane outside of the region being sampled, which the models do not (fully) represent. The models presented in Section 3 typically overestimated the activity in isotopically labelled carbon dioxide generated as a result of the methane oxidation, the one exception being the EDF C-14 model (see Section 3.5.3).

With an unknown source term, the spatial pattern of observed C-14 concentrations in groundwater between a site of historical disposal and a down gradient receptor ecosystem can be seen in the model results, though the gradient of the increase is not replicated (Section 4). The observed concentrations in soil gas are significantly lower than would be expected based on the observed concentrations in groundwater and considering Henry's Law; there is therefore a question mark over the experimental procedure in this respect.

The study time-scales range from hours (in the case of the Nottingham studies), through months (in the La Hague case) to decades (in the Duke Swamp case). Several aspects of C-14 dynamics in the biosphere are relatively rapid, including soil gas transport and conversion of $CH_4$ to $CO_2$, atmospheric dispersion and plant uptake. Understanding of these processes and the way in which they can be adequately modelling, builds confidence in their representation in long-term dose assessments for repositories.

The study has highlighted that there is potential further confidence and understanding to be gained from collaborative model-data comparison studies relating to C-14 in the biosphere. Notably, there is potential to further review observational data relating to the Duke Swamp case, to extend the model employed above to include swamp vegetation and sediments and to employ a wider range of models in the exercise.

In addition to the datasets that have been considered in this current study, the University of Helsinki has been monitoring pollution fall-out in Finnish Scots pine forests since the early 1990s through a series of stations under the "Station for Measuring Ecosystem-Atmosphere Relations" programme (SMEAR). At the SMEAR II station (Figure 48), in addition to a series of high temporal resolution measurements (including numerous meteorological, radiation, soil, flux and aerosol related variables and atmospheric gas concentrations), a series of 116 environmental $^{14}CO_2$ samples were collected between April 2012 and April 2013.

- Atmospheric $^{14}CO_2$ samples were collected at heights of 1, 16, 67 and 125 m between 10 am and 12 pm (and once at night).
- Soil $CO_2$ samples were taken monthly from April to October 2012 in the afternoon (and once at night) at soil heights 0.1, 0.04, -0.02, -0.08, -0.028, -0.48, -0.69 m from the mineral-organic boundary.

The standard SMEAR II measurements permit characterisation of the carbon cycle within the Scots pine boreal forest. The additional C-14 measurements provide potential for building confidence in specialist models for C-14 in forests, soils and/or adapted C-14 soil-plant-atmosphere models for other (e.g. agricultural) systems.

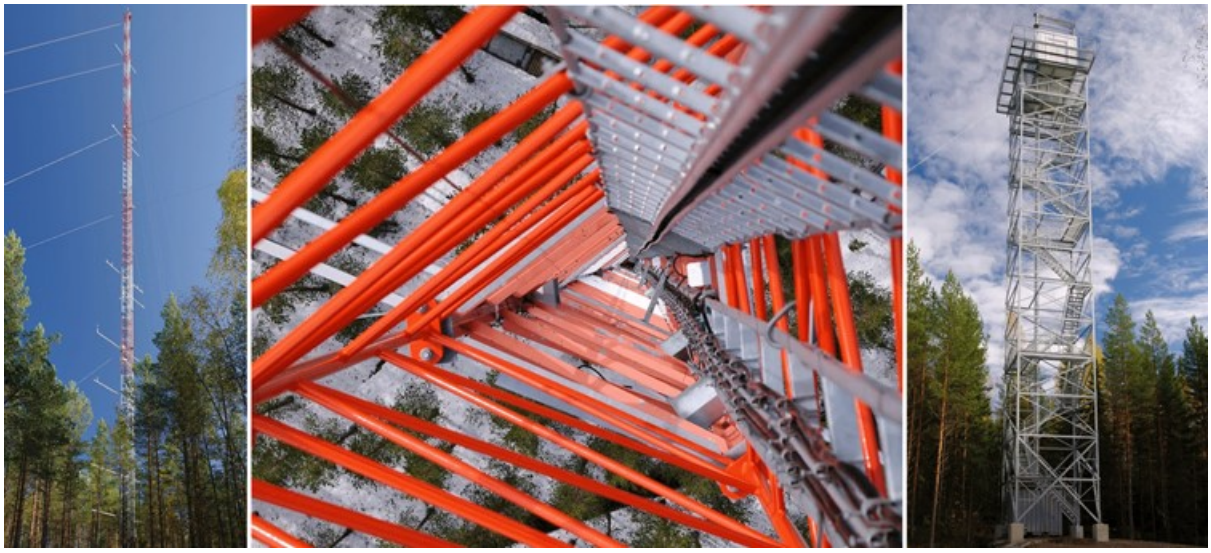

*Figure 48: SMEAR II Mast and Measurement Tower*

# 6 REFERENCES

Akata, N., Abe, K., Kakiuchi, H., Iyogi, T., Shima, N., Hisamatsu, S., 2013. Radiocarbon concentrations in environmental samples collected near the spent nuclear fuel reprocessing plant at Rokkasho, Aomori, Japan, during test operation using spent nuclear fuel. Health Physics, 105, 236–244.

Albrecht, A., 2016. Les équations du modèle de transfert du carbone-14 (14C) dans la biosphère (AquaC_14) et leur intégration dans le code " Modèle Management, MoM "; Note technique. Rapport N°: D.NT.ASTR.10.0052B, Andra, Châtenay-Malabry.

Albrecht A., Miquel S., 2010. Extension of sensitivity and uncertainty analysis for long term dose assessment of high level nuclear waste disposal sites to uncertainties in the human behaviour, Journal of Environmental Radioactivity, Journal of Environmental Radioactivity, 101: 55-67.

Aomori Prefecture, 2008. Bulletin of Aomori Prefectural Nuclear Power Safety Center No. 3. Aomori Prefecture (available at: http://gensiryoku.pref.aomori.lg.jp/center/works/img/120_164a1cd585_65.pdf) (in Japanese).

Aulagnier, C., Le Dizès, S., Maro, D., Hébert, D., Lardy, R., Martin, R., Gonze, M.-A., 2012. Modelling the transfer of $^{14}C$ from the atmosphere to grass: A case study in a grass field near AREVA-NC La Hague. Journal of Environmental Radioactivity, 112: 52-59.

Aulagnier, C., Le Dizès, S., Maro, D., Hébert, D., Lardy, R., Martin, R., 2013. The TOCATTA-χ model for assessing $^{14}C$ transfers to grass: an evaluation for atmospheric operational releases from nuclear facilities. Journal of Environmental Radioactivity, 120: 81-93.

Atkinson B., Meredith W., Snape C., Steven M., Shaw G., 2011. Experimental and Modelling Studies of Carbon-14 Behaviour in the Biosphere: Diffusion and oxidation of isotopically labelled methane ($^{13}CH_4$) in laboratory soil column experiments. NDA Radioactive Waste Management Directorate, report no. AMEC/004041/004, Issue 1.

Atkinson B., Shaw G., Meredith W., Snape C., Steven M., Hoch A., 2012. Uptake of Carbon-14 in the Biosphere: Data from First Field Experiment, and Modelling of Initial Laboratory Experiments (Progress Report for Year 2). NDA Radioactive Waste Management Directorate, report no. Serco/Nott/e.4041/002 Issue 1.

Atkinson, B.S., Meredith, W., Snape, C., Shaw, G., 2014. Uptake of Carbon-14 in the Biosphere: Field and laboratory experiments to determine the fate and behaviour of $^{14}CH_4$ injected into agricultural subsoil. Progress Report for Year 3. AMEC/Nott/004041/005.

Avila, R., Pröhl, G., 2008. Models used in SFR 1 SAR-08 and KBS-3H safety assessments for calculation of $^{14}C$ doses. Svensk Kärnbränslehantering AB (SKB) report R-08-16. Stockholm, Sweden.

Bartelt-Hunt, S.L., Smith, J.A., 2002. Measurement of effective air diffusion coefficients for trichloroethene in undisturbed soil cores. Journal of Contaminant Hydrology, 56, 193–208.

BIOCLIM, 2004. Deliverable D10-12: Development and application of a methodology for taking climate-driven environmental change into account in performance assessments, published by Agence Nationale pour la Gestion des Dechets Radioactifs (Andra), Parc de la Croix Blanche, 1/7 rue Jean Monnet, 92298 Châtenay-Malabry, France, Available from http://www.andra.fr/bioclim/.

BIOPROTA, 2014. Modelling Approaches to C-14 in Soil-Plant Systems and in Aquatic Environments: Report of an International Workshop. BIOPROTA report, Version 4, January 2014. Available from www.bioprota.org

CNSC, 2015. Joint Convention on the Safety of Spent Fuel Management and on the Safety of Radioactive Waste Management. Canada's presentation to the 5th Review Meeting, 13 May 2015, Vienna.

Collatz, G.J., Ball, J.T., Grivet, C., Berry, J.A., 1991. Physiological and environmental regulation of stomatal conductance, photosynthesis and transpiration: a model that includes a laminar boundary layer. Agriculture and Forestry Meteorology, 54, 107–136.

Del Grosso, S.J., Parton, W.J., Mosier, A.R., Ojima, D.S., Potter, C.S., Borken, W., Brumme, R., Butterbach-Bahl, K., Crill, P.M., Dobbie, K., Smith, K.A., 2000. General $CH_4$ oxidation model and comparisons of $CH_4$ oxidation in natural and managed systems. Global Biogeochemical Cycles 14, 999–1019.

Donders, R.E., Killey, R.W.D., Franklin, K.J., Weich, S.J., Strobel, G.S., 1996. Trial Coring in LLRW Trenches at Chalk River, AECL report AECL-11681.

Evenden, W.G., Sheppard, S.C., Killey, R.W.D., 1998. Carbon-14 and tritium in plants of a groundwater-contaminated wetland. Journal of Applied Geochemistry 13, 17-21.

Farquhar, G.D., von Caemmerer, S., Berry, J.A., 1980. A biochemical model of photosynthetic $CO_2$ assimilation in leaves of C3 species. Planta 149, 78–90.

Farquhar, G.D., von Caemmerer, S., 1982. Modeling of photosynthetic responses to environmental conditions. In: Lange, O.L., Nobel, P.S., Osmond, C.B., Ziegler, H. (Eds.), Physiological Plant Ecology II. Encyclopedia of Plant Physiology, New Series, vol. 12B. Springer-Verlag, Heidelberg, pp. 549-587.

Gonze, M.-A., Mourlon, C., Garcia-Sanchez, L., Le Dizès, S., Nicoulaud, V., Métivier, J.-M., Simon-Cornu, M., Gerber P.-P., Vermorel, F., 2011. SYMBIOSE: A Simulation Platform for Performing Radiological Risk Assessments, Proceedings ICRER 2011, 19-24 June, Hamilton (Canada).

Guenot, J., Belot, Y., 1984. Assimilation of $^3H$ in photosynthesizing leaves exposed to HTO. Health Physics, 47, 849–855.

Heyes, D.W., Butcher, E.J., Borwick, J., Milodowski, A.E., Field, L.P., Kemp, S.J., Mounteney, I., Bernal, S.A., Corkhill, C.L., Hyatt, N.C., Provis, J.L., Black, L., 2015. Demonstration of Carbonation of the NRVB, NNL Report NNL (14) 13296 Issue 4.

Hoch A.R., 2014. Uptake of Gaseous Carbon-14 in the Biosphere: Development of an Assessment Model. AMEC/004041/007, Issue 2.

Hoch A.R., Atkinson B., Shaw G., 2014. Uptake of Gaseous Carbon-14 in the Biosphere: Modelling of Field and Laboratory Experiments. AMEC/004041/006, Draft D.

Katata, G., Kajino, M., Hiraki, T., Aikawa, M., Kobayashi, T., Nagai, H., 2011. A method for simple and accurate estimation of fog deposition in a mountain forest using a meteorological model. Journal of Geophysical Research, 116, D20102.

Kightley, D., Nedwell, D., Cooper, M., 1995. Capacity of methane oxidation in landfill cover soils measured in laboratory-scale soil microcosms. Applied and Environmental Microbiology, 61, 592–601.

Killey R.W.D., Rao R.R., Eyvindson S., 1998. Radiocarbon speciation and distribution in an aquifer plume and groundwater discharge area, Chalk River, Ontario. Applied Geochemistry, 13, 3-16.

King-Sharp, K.J., Benz, M.L., Yankovich, T.L., Hartwick, L.A., 2005. Carbon-14 Contaminant Transfer in an Ecosystem Aquatic Pathway: Database and Root Uptake Experiment. AECL Technical Report, 153-121241-ENA-001 (Revision 0).

Komatsu, T., Kawamoto, K., Resurreccion, A., Moldrup, P., 2007. A linear model to predict the soil-gas diffusion coefficient of undisturbed unsaturated volcanic ash soil. The Science and Engineering Reports of Saitama University. 40, 63–66.

Koschorreck, M., Conrad, R., 1993. Oxidation of atmospheric methane in soil: measurements in the field, in soil cores, and in soil samples. Global Biogeochemical Cycles, 7, 109–121.

Le Dizès, S., Maro, D., Hébert, D., Gonze, M.-A., Aulagnier, C., 2012. TOCATTA: a dynamic transfer model of $^{14}C$ from the atmosphere to soil-plant systems. Journal of Environmental Radioactivity, 105: 48-59.

Limer, L., (Ed.) 2017. C-14 Terrestrial Model-Data Comparisons: Report of an International Workshop. A report prepared within the BIOPROTA international cooperation programme. Available from www.bioprota.org

Limer, L., Smith, K., Albrecht, A., Marang, L., Norris, S., Smith, G.M., Thorne, M.C., Xu, S., 2011. C-14 Long-term dose assessment: Data review, scenario development, and model comparison; Final report. A report prepared within the BIOPROTA international cooperation programme. Available from www.bioprota.org

Limer, L.M.C, Albrecht, A., Smith, K., Marang, L., Norris, S., Smith, G.M., Thorne, M.C., Xu, S., 2012. C-14 Long-Term Dose Assessment in a Terrestrial Agricultural Ecosystem: FEP Analysis, Scenario Development, and Model Comparison. A report prepared within the BIOPROTA international cooperation programme and published by the Swedish Radiation Safety Authority: 2012:47.

Limer, L., Klos, R., Shaw, G., Walke, R., 2013a. Terrestrial Biosphere Modelling of $^{14}C$ Research. Swedish Radiation Safety Authority Report 2013:20.

Limer L., Klos, R., Walke, R., Shaw, G., Nordén, M., Xu, S., 2013b. Soil-plant-atmosphere modeling in the context of releases of $^{14}C$ as a consequence of nuclear activities. Radiocarbon 55(2-3): 804-813.

Limer, L., Klos, R., 2014. Biosphere modelling of $^{14}C$: aquatic and terrestrial ecosystems. A report prepared for the Swedish Radiation Safety Authority.

Limer L., Les Dizès-Maurel S., Klos R., Maro D., Nordén M., 2015. Impacts of $^{14}C$ discharges from a nuclear fuel reprocessing plant on surrounding vegetation: Comparison between grass field measurements and TOCATTA-$\chi$ and SSPAM$^{14}C$ model computations. Journal of Environmental Radioactivity, 147: 115-124.

Maro, D., Masson, M., Fiévet, B., Bailly du Bois, P., Connan O., Boust, D., Germain, P., 2008. Analyse critique des données disponibles de carbone 14 et de tritium dans le nord cotentin et en manche. IRSN. Report DEI/SECRE n°08-006.

Milton, G.M., King, K.J., Sutton, J., Enright, S., 1998. Tracer studies of carbon source utilization in a wetland on the Canadian Shield. Journal of Applied Geochemistry 13, 23-30.

Mobbs S, Shaw G, Norris S, Marang L, Sumerling T, Albrecht A, Xu S, Thorne M, Limer L, Smith K, Smith G, 2013. Developments in modeling of C-14 in the biosphere for solid radioactive waste disposal. Radiocarbon, 55 (2-3), 814-825.

Mourlon, C., Gonze, M.-A., Métivier, J.-M., Olive, G., Parache, V., Vermorel, F., Cadet, M., 2011. A Landscape-level Dose Assessment of a French NPP Using the SYMBIOSE Platform Proceedings ICRER 2011, 19-24 June, Hamilton (Canada).

Nagai, H., 2002. Validation and sensitivity analysis of a new atmosphere-soil-vegetation model. Journal of Applied Meteorology, 41, 160–176.

Nagai, H., 2005. Incorporation of $CO_2$ exchange processes into a multiplayer atmosphere-soil-vegetation model. Journal of Applied Meteorology, 44, 1574–1592.

Napier, J.B., 2015. Analysis of Carbon-14 Transport from a Contaminated Groundwater Source. PhD Thesis, Radiation Health Physics, Oregon State University.

Norris S, Albrecht A, Limer L, Cummings R, Marang L, Smith G, Smith K, Thorne M., Xu S., 2011. A Comparison of Models for Assessing the Radiological Impact of 14C released to Soils in Gaseous Form following the Geological Disposal of Solid Radioactive Wastes. International Conference of Radioecology and Radioactivity, Hamilton, Canada, June 19-24.

Ota, M., Iida, T., Yamazawa, H., Nagara, S., Ishimori, Y., Sato, K., Tokizawa, T., 2007. Suppression of radon exhalation from soil by covering with clay-mixed soil. Journal of Nuclear Science and Technology, 44, 791–800.

Ota, M., Nagai, H., Koarashi, J., 2012. A land surface $^{14}C$ transfer model and numerical experiments on belowground $^{14}C$ accumulation and its impact on vegetation $^{14}C$ level. Journal of Environmental Radioactivity, 107, 13–22.

Ota, M., Nagai, H., Koarashi, J., 2013. Root and dissolved organic carbon controls on subsurface soil carbon dynamics: A model approach. Journal of Geophysical Research: Biogeosciences, 118, 1646–1659.

Ota, M., Nagai, H., Koarashi, J., 2016a. Modeling dynamics of $^{137}Cs$ in forest surface environments: Application to a contaminated forest site near Fukushima and assessment of potential impacts of soil organic matter interactions. Science of the Total Environment, 551–552, 590–604.

Ota, M., Katata, G., Nagai, H., Terada, H., 2016b, Impacts of C-uptake by plants on the spatial distribution of 14C accumulated in vegetation around a nuclear facility—Application of a sophisticated land surface 14C model to the Rokkasho reprocessing plant, Japan. Journal of Environmental Radioactivity 162–163, 189–204.

Penfold J P and Watkins B (1998). Transfer of C-14 in the Biosphere Bibliography and Modelling. Rapport QuantiSci n° C NT OQUA 98-001.

Penman, H.L., 1940. Gas and vapor movements in the soil: 1. the diffusion of vapors through porous solids. The Journal of Agricultural Science, 30, 437–462.

Pruess, K., 1987. TOUGH User's Guide, Nuclear Regulatory Commission Report NUREG/CR–4645 (also Lawrence Berkeley Laboratory Report LBL-20700).

Pruess, K., 1991. TOUGH2 – A General Purpose Numerical Simulator for Multiphase Fluid and Heat Flow, Lawrence Berkeley Laboratory Report LBL-29400.

Pruess, K., Oldenburg, C., Moridis, G., 1999. TOUGH2 User's Guide – Version 2.0, Lawrence Berkeley National Laboratory Report LBNL-43134.

Ridgwell, A., Marshall, S.J., Gregson, K., 1999. Consumption of atmospheric methane by soils: A process-based model. Global Biogeochemical Cycles, 13, 59–70.

Saetre P., Nordén S., Keesmann S., Ekström P.-A., 2013. The biosphere model for radionuclide transport and dose assessment in SR-PSU. SKB R-13-46, Svensk Kärnbränslehantering AB.

Sheppard, S.C., Amiro, B.D., Sheppard, M.I., Stephenson, M., Zach, R., Bird, G.A., 1994. Carbon 14 in the biosphere: modelling and supporting research for the Canadian nuclear fuel waste management program. Waste Management, 14, 445-456.

Sheppard S., Thorne, M.C., 2005. Model Review and Comparison for C-14 Dose Assessment. BIOPROTA Theme 2: Task 3. Available from www.bioprota.org

Smith K. (Ed.), 2015. Long-term Dose Assessment for Carbon-14: Report of an International Workshop. A BIOPROTA Report, Version 2.0, August 2015.

Smith K., Smith G. (Eds), 2014. C-14: Data, Ecosystems and Dose Assessment: Report of an International Workshop, Aix-en-Provence, 1 – 3 April 2014. A report prepared within the BIOPROTA international cooperation programme. Available from www.bioprota.org

Tucker S., Shaw G., 1997. Quality Assured Modelling Data for 14CO2 Fixation by Crops. IC.CARE/MAFF/REP/C-14/4.0, Imperial College report to the Ministry of Agriculture, Fisheries and Foods, London, UK.

van Hecke W., 2001. Intégration du modèle C14 développé par Quantisci au code de calcul Aquabios et comparaison avec le modèle utilisé précédemment. Report Andra N° C NT ABSE 00-032/A, Châtenay-Malabry.

Walke R., Thorne M., Watson C., Limer L., 2016. The PRISM Foodchain Modelling Software: Version 3.5 Technical Report. Quintessa Limited report to the Food Standards Agency QRS-3004I-1, Version 1.0.

Webb, S.W., 2013. T2Plants Version 1.1: Modification of TOUGH2 for Near-surface Transport of Gases, Including Atmospheric Boundary Conditions and the Effects of Plants, AMEC Report AMEC/004041/003, Issue 1.

Whalen, S.C., Reeburgh, W.S., 1990. Consumption of atmospheric methane by tundra soils. Nature, 346, 160–162.

Whalen, S.C., Reeburgh, W.S., Sandbeck, K.A., 1990. Rapid methane oxidation in a landfill cover soil. Applied Environmental Microbiology, 56, 3405–3411.

Whalen, S.C., Reeburgh, W.S., Barber, V.A., 1992. Oxidation of methane in boreal forest soils: a comparison of seven measures. Biogeochemistry, 16, 181–211.

Yamazawa, H., 2001. A one-dimensional dynamical soil-atmosphere tritiated water transport model. Environmental Modelling and Software. 16, 739–751.

Yankovich, T.L., King-Sharp, K.J., Benz, M.L., Carr, J., Killey, R.W.D., Beresford, N.A., Wood, M.D., 2013. Do site-specific radiocarbon measurements reflect localized distributions of $^{14}C$ in biota inhabiting a wetland with point contamination sources. Journal of Environmental Radioactivity, 126, 352-366.

Yankovich, T.L., King-Sharp, K.J., Carr, J., Killey, R.W.D., Beresford, N.A., Wood, M.D., 2014. Spatial analysis of Carbon-14 dynamics in a wetland ecosystem (Duke Swamp, Chalk River Laboratories, Canada). Journal of Environmental Radioactivity, 137, 173-180.

# APPENDIX A. FURTHER DETAILS OF THE MODELS USED

This appendix contains additional details about the models used in this study, beyond the overview summaries provided in the main report.

## A.1 FANC MODEL USED FOR THE LA HAGUE SCENARIO

The mean uptake of C-14 from the atmosphere to the Stored Energy compartment, $D$, Bq $s^{-1}$, is given by:

$$D = v_d^{CO2}\ C\ A \quad (1)$$

$$v_d^{CO2} = \frac{k\ G\ F_{GC}}{C_C} \quad (2)$$

where $v_d^{CO2}$ is the 'deposition velocity' for $CO_2$ to the stored energy compartment (m $s^{-1}$), $C$ is the concentration of C-14 in the atmosphere as $^{14}CO_2$ (Bq $m^{-3}$), $A$ is a unit area ($m^2$), $k$ is reciprocal of the plant assimilation factor (unitless), $G$ is the total biomass growth rate (kg dry weight $m^{-2}$ $day^{-1}$), $F_{GC}$ is the fraction of the plant dry matter that is carbon (unitless) and $C_C$ is the concentration of carbon in the atmosphere (kgC $m^{-3}$).

The loss rate from the Stored Energy due to respiration is given by:

$$\lambda_{Resp} = \frac{(\mathrm{k}-1)\ G\ F_{FG}}{M_{ES}} \quad (3)$$

where $M_{ES}$ is the mass of carbon in the Stored Energy compartment (kgC $m^{-2}$).

The transfer to Structural Biomass is given by:

$$\lambda_{SB} = \frac{G\ A\ F_{GC}}{M_{ES}}. \quad (4)$$

The loss rate due to removal of pasture is calculated from the measured amount of pasture removed.

## A.2 EDF C-14 MODEL USED FOR THE NOTTINGHAM FE2 SCENARIO

### 1.1.2 Soil sub-model

In this exercise, the number of soil layers was fixed to N = 10. The mass balance equations of $^{14}CO_2$ and $^{14}CH$ over soil layers considers the vertical gaseous and liquid transport and the reaction and loss processes. They are expressed as:

$$\frac{\partial A_{14CO2\_soil}}{\partial t} = D_{soil\_ef\_14CO2}\frac{\partial^2 A_{14CO2\_soil}}{\partial h_{soil}{}^2} - V_{adv\_14CO2}\frac{\partial A_{14CO2\_soil}}{\partial h_{soil}} - Uptake_{root\_14CO2} + A_{14CH4\_soil} \times K_{oxi} \quad (5)$$

$$\frac{\partial A_{14CH4\_soil}}{\partial t} = D_{soil\_ef\_14CH4}\frac{\partial^2 A_{14CH4\_soil}}{\partial h_{soil}{}^2} - V_{adv\_14CH4}\frac{\partial A_{14CH4_{soil}}}{\partial h_{soil}} - Uptake_{root\_14CH4} - A_{14CH4\_soil} \times K_{oxi} \quad (6)$$

where

$A_{14CO2\_soil}$ is the activity of $^{14}CO_2$ in total soil (Bq), $t$ is time (h), $D_{soil\_ef\_14CO2}$ and $D_{soil\_ef\_14CH4}$ are the effective diffusion coefficients in soil for $^{14}CO_2$ and $^{14}CH_4$, respectively ($m^2\ h^{-1}$), $h_{soil}$ is the thickness of the soil layer (m), $V_{adv\_14CO2}$ and $V_{adv\_14CH4}$ are the advection velocities for $^{14}CO_2$ and $^{14}CH_4$, respectively ($m\ h^{-1}$), $Uptake_{root\_14CO2}$ and $Uptake_{root\_14CH4}$ are the root uptakes in the transpiration stream, respectively for $^{14}CO_2$ and $^{14}CH_4$ (Bq $h^{-1}$), $A_{14CH4\_soil}$ is the activity of $^{14}CH_4$ in soil (Bq), and $K_{oxi}$ is the first-order oxidation rate constant ($h^{-1}$).

The model assumes that there is no activity of $^{14}C$ below the bottom soil layer (the bottom of rhizosphere), and hence that the transport by diffusion does not take place between the bottom soil layer and the layers below it.

The effective diffusion coefficient in soil for $CO_2$ is determined by the gas-phase diffusion coefficient and the aqueous-phase diffusion coefficient:

$$D_{soil\_ef\_14CO2} = \frac{D_{soil\_ef\_gas\_CO2}}{\theta_{a\_soil} \times Retard_{air\_CO2}} + \frac{D_{soil\_ef\_w\_CO2}}{\theta_{w\_soil} \times Retard_{w\_CO2}} \quad (7)$$

where $D_{soil\_ef\_gas\_CO2}$ is the gas-phase effective diffusion coefficient in soil for $CO_2$ ($m^2\ h^{-1}$), $\theta_{a\_soil}$ is the volumetric air content in soil (calculated as $\theta_{a\_soil} = \varphi_{soil} - \theta_{w\_soil}$, where $\varphi_{soil}$is the porosity in soil) (-), $Retard_{air\_CO2}$ is the retardation factor for $CO_2$ in air (-), $D_{soil\_ef\_w\_CO2}$ is the aqueous-phase effective diffusion coefficient in soil for $CO_2$ ($m^2\ h^{-1}$), $\theta_{w\_soil}$ is the volumetric water content in soil (-), and $Retard_{w\_CO2}$ is the retardation factor for $CO_2$ in water (-). $D_{soil\_ef\_14CH4}$ is calculated in a same way.

The gas-phase and aqueous-phase effective diffusion coefficients are given considering tortuosity factors in corresponding phases [Jury et al., 1983]:

$$D_{soil\_ef\_gas\_CO2} = D_{air\_CO2} \times \frac{{\theta_{a\_soil}}^{10/3}}{{\varphi_{soil}}^2} \quad (8)$$

$$D_{soil\_ef\_w\_CO2} = D_{w\_CO2} \times \frac{{\theta_{w\_soil}}^{10/3}}{{\varphi_{soil}}^2} \quad (9)$$

where $D_{air\_CO2}$ is the molecular diffusion coefficient of $CO_2$ in air ($m^2\ h^{-1}$), and $D_{w\_CO2}$ is the molecular diffusion coefficient of $CO_2$ in water ($m^2\ h^{-1}$).

The advection velocity for $^{14}CO_2$ (and $^{14}CH_4$) is calculated by the percolation rate obtained from the water balance in each soil layer.

$$V_{adv\_14CO2} = \frac{Percolation}{Retard_{w\_CO2}} \quad (10)$$

The root uptake of $^{14}CO_2$ (and $^{14}CH_4$) dissolved in soil pore water by transpiration stream is calculated as:

$$Uptake_{root\_14CO2} = \frac{A_{14CO2\_soil}}{(Kd_{soil\_w\_CO2} \times \rho_{soil\_dry} + K_{AW\_CO2} \times \theta_{a\_soil} + \theta_{w\_soil})} \times \frac{Transpiration \times RRD}{h_{soil}} \quad (11)$$

where the first term in the right side of the equation represents the activity of $^{14}CO_2$ dissolved in soil pore water. $Kd_{soil\_w\_CO2}$ is the soil-water partition coefficient for $CO_2$ ($m^{-3}\ kg_{dw}^{-1}$), $\rho_{soil\_dry}$ is the dry

density of soil ($kg_{dw}^{-1}$ $m^{-3}$), $K_{AW\_CO2}$ is the air-water partition coefficient for $CO_2$ (-), $Transpiration$ is the plant transpiration flow ($m^3$ $m^{-2}$ $h^{-1}$), $RRD$ is the relative root density (-). It should be noted that $Kd_{soil\_w\_CO2}$ here is used as an empirical soil-specific relationship encompassing precipitation as well as exchange processes, according to Sheppard et al. [2006].

According to Sau et al [2004], the plant transpiration can be estimated from the actual evapotranspiration as a function of the LAI (leaf area index) and an extinction factor:

$$Transpiration = ET_a \times [1 - exp(-\alpha_{extinction} \times LAI)] \quad (12)$$

where $ET_a$ is the Actual evapotranspiration (m $h^{-1}$), $\alpha_{extinction}$ is the extinction factor for partitioning of evapotranspiration to plant transpiration (-), and $LAI$ is the time-dependent leaf area index (-).

The model assumes that the oxidation process follows first-order kinetics and thus the process is represented by a first-order rate constant $K_{oxi}$ ($h^{-1}$).

In addition to the processes included in equations (1) and (2), the mass balance equation for the top soil layer takes into account a loss by the diffusion process at soil-air interface. The net diffusion flux of $^{14}CO_2$ from soil to air is calculated using the single film model:

$$N_{diff\_soil\_air\_14CO2} = D_{air\_CO2} \times \left(\frac{AC_{14CO2\_soil\_1\_air}}{\delta air} - \frac{AC_{14CO2\_canopy\_air}}{\delta air}\right) \times A_{crop} \quad (13)$$

where $N_{diff\_soil\_air\_14CO2}$ is the net diffusion flux of $^{14}CO_2$ from soil to canopy air (Bq $h^{-1}$), $D_{air\_CO2}$ is the molecular diffusion coefficient of $CO_2$ in air ($m^2$ $h^{-1}$), $AC_{14CO2\_canopy\_air}$ is the activity concentration of $^{14}CO_2$ in the canopy air (Bq $m^{-3}$), $AC_{14CO2\_soil\_1\_air}$ is the activity concentration of $^{14}CO_2$ in soil air at the top soil layer (Bq $m^{-3}$), $\delta air$ is the effective thickness of the stagnant air film above the ground surface (m), $A_{crop}$ is the cropped surface area (the soil-air interface area) ($m^2$). The net diffusion flux for $^{14}CH_4$ is calculated in an identical manner to that for $^{14}CO_2$.

### 1.1.3 Root sub-model

The root compartment receives the total amounts of $^{14}CO_2$ (and $^{14}CH_4$) transferred from all the soil N layers and carries them out to the shoot compartment by the xylem outflow.

$$\frac{dA_{14CO2\_root}}{dt} = \sum Uptake_{root\_14CO2} - Flow_{xylem\_14CO2} \quad (14)$$

where $A_{14CO2\_root}$ is the activity of $^{14}CO_2$ in root (Bq), $\sum Uptake_{root\_14CO2}$ is the total amount of $^{14}CO_2$ transferred from all the soil layers (Bq $h^{-1}$), $Flow_{xylem\_14CO2}$ is the xylem outflow from root to above-ground plant (Bq $h^{-1}$). The same mass balance equation is used for $^{14}CH_4$.

The model assumes that a portion of $^{14}CO_2$ (and $^{14}CH_4$) in the transpiration flow is partitioned to the lipid of root and to the gaseous phase of root. The outflow of $^{14}CO_2$ from root to above-ground plant is then calculated using the partition coefficient of $CO_2$ between root and water in transpiration flow:

$$Flow_{xylem\_14CO2} = A_{14CO2\_root} \times \frac{\sum Transpiration}{0.001 \times K_{RW\_CO2} \times m_{root}} \quad (15)$$

where $\sum Transpiration$ is the total transpiration flow from all the soil layers ($m^3$ $m^{-2}$ $h^{-1}$), $K_{RW\_CO2}$ is the partition coefficient of $CO_2$ between root and water in transpiration flow (L $kg_{fw}^{-1}$), and $m_{root}$ is the mass of root per unit area of soil ($kg_{fw}$ $m^{-2}$).

### 1.1.4 Shoot sub-model

The shoot compartment receives $^{14}CO_2$ and $^{14}CH_4$ transported by the xylem outflow and interacts with the canopy air compartment by the gas exchange of $^{14}CO_2$.

$$\frac{dA_{14C\_shoot}}{dt} = Flow_{xylem\_14CO2} + Flow_{xylem\_14CH4} + G_{ex\_air\_shoot\_14CO2} - G_{ex\_shoot\_air\_14CO2} \quad (16)$$

where $A_{14C\_shoot}$ is the activity of $^{14}C$ (the sum of $^{4}CO_2$ and $^{14}CH_4$) in shoot (Bq), $G_{ex\_air\_shoot\_14CO2}$ and $G_{ex\_shoot\_air\_14CO2}$ are respectively the amounts of $^{14}CO_2$ transferred by gas exchange from canopy air to shoot and from shoot to canopy air (Bq $h^{-1}$).

The gas exchange process occurring between shoot and canopy air is expressed by:

$$G_{ex\_air\_shoot\_14CO2} = AC_{14CO2\_canopy\_air} \times A_{crop} \times \frac{2.0 \times LAI}{Re_T} \quad (17)$$

$$G_{ex\_shoot\_air\_14CO2} = \frac{A_{14C\_shoot}}{K_{LA} \times m_{leaf}} \times \frac{2 \times LAI}{Re_T} \quad (18)$$

where $AC_{14CO2\_canopy\_air}$ is the active concentration of $^{14}CO_2$ in canopy air (Bq $m^{-3}$), $A_{crop}$ is the cropped surface area ($m^2$), $Re_T$ is the total resistance of leaf which is calculated as the sum of aerodynamic and stomatal resistances (h $m^{-1}$), $A_{14C\_shoot}$ is the activity of $^{14}C$ in shoot (Bq), $K_{LA}$ is the partition coefficient between leaf and air for $CO_2$ ($m^3$ $kgfw^{-1}$), and $m_{leaf}$ is the time-dependent mass of leaf per unit area of soil ($kg_{fw}$ $m^{-2}$).

The active concentration of $^{14}CO_2$ in canopy air is calculated as:

$$AC_{14CO2\_canopy\_air} = \frac{A_{14CO2\_canopy\_air}}{h_{canopy} \times A_{crop}} \times CD \quad (19)$$

where $A_{14CO2\_canopy\_air}$ is the activity of $^{14}CO_2$ in canopy air (Bq), $h_{canopy}$ is the time-dependent height of top canopy (m), and $CD$ is the canopy dilution factor that considers mixing with external air (-).

### 1.1.5 Canopy air sub-model

The canopy air compartment interacts with the shoot compartment by the gas exchange process (only for $^{14}CO_2$) and receives the net diffusion flux from soil to air.

$$\frac{dA_{14CO2\_canopy\_air}}{dt} = G_{ex\_shoot\_air\_14CO2} - G_{ex\_air\_shoot\_14CO2} + N_{diff\_soil\_air\_14CO2} \quad (20)$$

$$\frac{dA_{14CH4\_canopy\_air}}{dt} = N_{diff\_soil\_air\_14CH4} \quad (21)$$

where $A_{14CH4\_canopy\_air}$ is the activity of $^{14}CH_4$ in canopy air (Bq), and $N_{diff\_soil\_air\_14CH4}$ is the net diffusion flux of $^{14}CH_4$ from soil to air.

### 1.1.6 Water balance model

The water balance in the model is calculated using the tipping bucket approach where soil layers are considered as buckets that can be filled up to a field capacity and then water overflows to the lower layer when the water content exceeds the field capacity. Figure 49 shows a schematic representation of the tipping bucket approach.

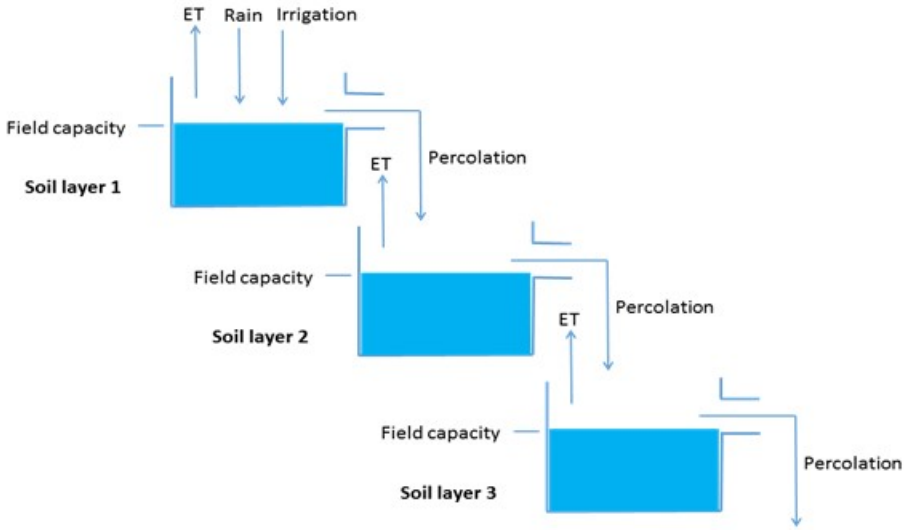


***Figure 49: Schematic representation of the tipping buckets approach***

The water balance equation at the top soil layer is given as follows:

$$\frac{d\theta_{w\_soil\_1}}{dt} = \frac{Rain + Irrigation - ET_{a\_1} \times RRD_1 - Percolation_1}{h_{soil\_1}} \quad (22)$$

where $\theta_{w\_soil\_1}$ is the volumetric water content in the top soil layer (-), $Rain$ is the precipitation (m $h^{-1}$), $Irrigation$ is the water input by irrigation (m $h^{-1}$), $ET_{a\_1}$ is the actual evapotranspiration at the top soil layer (m $h^{-1}$), $RRD_1$ is the relative root density at the top soil layer (-), $Percolation_1$ is the percolation at the top soil layer (m $h^{-1}$), and $h_{soil\_1}$ is the thickness of the top soil layer (m). At the lower layers, the water balance is calculated by:

$$\frac{d\theta_{w\_soil\_i}}{dt} = \frac{Percolation_{i-1} - ET_{a\_i} \times RRD_i - Percolation_i}{h_{soil\_i}} \quad (23)$$

where where $\theta_{w\_soil\_i}$ is the volumetric water content in the soil layer i (-), $Percolation_{i-1}$ is the percolation from the upper soil layer i - 1, $ET_{a\_i}$ is the actual evapotranspiration at the soil layer i (m $h^{-1}$), $RRD_i$ is the relative root density at the soil layer i (-), $Percolation_i$ is the percolation at the soil layer i (m $h^{-1}$), and $h_{soil\_i}$ is the thickness of the soil layer i (m).

The percolation is calculated as follows:

$$If\ \theta_{w\_soil\_i} > \theta_{fc};\ Percolation = \frac{(\theta_{w\_soil\_i} - \theta_{fc})}{\Delta t} \times h_{soil\_i}$$
$$Else;\ Percolation = 0 \quad (24)$$

where $\theta_{fc}$ is the volumetric water content at field capacity (-) and $\Delta t$ is the time interval (fixed at 1 h).

The evapotranspiration is obtained from the following empirical equations:

$$If\ K_s > 0;\ \ ET_a = 0.001 \times ET_p \times K_s \times K_c$$
$$Else;\ \ ET_a = 0 \qquad (25)$$

where $ET_p$ is the potential evapotranspiration (mm $h^{-1}$), $K_s$ is the water stress coefficient that is calculated from the balance between $\theta_{w\_soil\_i}$ and the water content at wilting point ($\theta_{wp}$) (-), and $K_c$ is the crop coefficient that depends on crop type and growing season (-).

The potential evapotranspiration is estimated using the Turc method [Turc, 1961]:

$$If\ Rh > 50;\ ET_p = 0.0133 \times \left(\frac{T_{air}}{T_{air} + 15}\right) \times (R_s \times 23.89 + 50.0)$$
$$Else;\ ET_p = 0.0133 \times \left(\frac{T_{air}}{T_{air}+15}\right) \times (R_s \times 23.89 + 50.0) \times \left(1.0 + \frac{(50.0 - Rh)}{70.0}\right) \qquad (26)$$

where $Rh$ is the relative humidity (%) and $T_{air}$ is the temperature in air (°C), and $R_s$ is the solar radiation (MJ $m^{-2}$ $h^{-1}$).

## A.3 JAEA SOLVEG II MODEL USED FOR THE NOTTINGHAM FE2 SCENARIO

In the present study, transport of $^{14}CH_4$ in the atmosphere-soil system was modelled and incorporated to the calculation of $^{14}CO_2$ transport model of SOLVEG-II (Fig. 1). In the $^{14}CH_4$ model, turbulent diffusion of $^{14}CH_4$ was considered for the atmospheric $^{14}CH_4$ transport:

$$\frac{\partial \chi_a}{\partial t} = \frac{\partial}{\partial z} K \frac{\partial \chi_a}{\partial z} \qquad (27)$$

where $\chi_a$ (Bq $m^{-3}$) is the concentration of $^{14}CH_4$ in the atmosphere, $t$ (s) is the time, $z$ (m) is the coordinate (height) above the ground, and $K$ ($m^2$ $s^{-1}$) is the turbulent diffusivity that is calculated by a turbulence closure model of SOLVEG-II [Nagai, 2002, 2005]. The upper boundary condition of the $^{14}CH_4$ transport of Eq. (27) is given by the input of $^{14}CH_4$ concentration to the top atmospheric layer. The bottom boundary condition is achieved by the atmosphere-soil exchange of $^{14}CH_4$ at the ground surface.

In modelling the $^{14}CH_4$ transport in the soil, we considered molecular diffusion of $^{14}CH_4$ in the soil air and oxidation of $^{14}CH_4$ by methanotrophic bacteria:

$$\frac{\partial(\eta_{sat} - \eta_{sw})\chi_s}{\partial t} = \frac{\partial}{\partial z}(\eta_{sat} - \eta_{sw}) D_{eff} \frac{\partial \chi_s}{\partial z} - e_o \qquad (28)$$

where $\eta_{sat}$ ($m^3$ $m^{-3}$) is the porosity of the soil, $\eta_{sw}$ ($m^3$ $m^{-3}$) is the volumetric water content in the soil, $\chi_s$ (Bq $m^{-3}$) is the concentration of $^{14}CH_4$ in the soil air, $z$ (m) is the depth in the soil, $D_{eff}$ ($m^2$ $s^{-1}$) is the effective diffusivity of $^{14}CH_4$ in the soil, and $e_o$ (Bq $m^{-3}$ $s^{-1}$) is the oxidation rate of $^{14}CH_4$. In the SOLVEG-II model, the porosity is parameterized by texture of the soil (Table 22) and the water content in each soil layer is calculated by the soil water model [Yamazawa, 2001; Nagai, 2005].

The effective diffusivity was calculated by the Penman's model [Penman, 1940]:

$$D_{eff} = D_{air}(\eta_{sat} - \eta_{sw})/1.5 \qquad (29)$$

where $D_{air}$ = 2.1 × $10^{-5}$ $m^2$ $s^{-1}$ is the molecular diffusivity of $CH_4$ in the air at normal temperature and pressure [Ridgwell et al., 1999; Walter and Heimann, 2000] and the factor '($\eta_{sat} - \eta_{sw}$)/1.5' represents the tortuosity of the air-filled space in soil.

For the oxidation of $^{14}CH_4$, studies have shown that methane oxidation by soil follows a first-order reaction [King and Adamsen, 1992; Adamsen and King, 1993; Ridgwell et al., 1999; Walter and Heimann, 2000; Ito and Inatomi, 2012]. Therefore, the oxidation of $^{14}CH_4$ in the soil was modelled, as:

$$e_o = (\eta_{sat} - \eta_{sw})\chi_s \Lambda \quad (30)$$

where Λ ($s^{-1}$) is the rate of the methane oxidation in the soil. Methane oxidation is biologically mediated process and so depends on the environmental factors such as water content and temperature of the soil [Conrad 1996; Le Mer and Roger, 2001]. In the present model, the rate of the methane oxidation throughout a soil profile was related to rate of the methane oxidation at the soil surface, scaled by the dependencies on the soil temperature, soil water content and depth of the soil profile itself [Ridgwell et al., 1999; Del Grosso et al., 2000]:

$$\Lambda = \Lambda_{ref} f_{st}(T_s) f_{sw}(\eta_{sw}) F_z(z) \quad (31)$$

where $\Lambda_{ref}$ ($s^{-1}$) is the reference rate of methane oxidation defined for a moderately-wet surface soil at temperature of 25°C, and the factors $f_{st}$ and $f_{sw}$ represent the dependencies of the methane oxidation on temperature and water content of the soil, respectively, and $F_z$ represents the vertical profile of the methane oxidation.

The reference rate of oxidation was set to: $\Lambda_{ref}$ = 8.3 × $10^{-4}$ $s^{-1}$, a value obtained from an experiment that used a surface landfilled soil (depths of 3 – 12 cm) in California under a condition with soil water content of ~10% by weight and soil temperature of 25°C (Whalen et al., 1990). This reference rate corresponded to a time-scale of methane oxidation at: $1/\Lambda_{ref}$ = ~0.3 h, which is within the reported range of the time-scales of methane oxidation by upland soils: from 0.1 to 5.0 h, and greater [Whalen and Reeburgh, 1990; King and Adamsen, 1992; Adamsen and King, 1993; Ridgwell et al., 1999; Walter and Heimann, 2000].

For the temperature dependency, controlled laboratory experiments have shown that the rate of methane oxidation by soils increases with rising the soil temperature from ~0°C to ~30°C, and decreases with increasing the soil temperature higher than ~30°C [Whalen et al., 1990; King and Adamsen, 1992; Whalen and Reeburgh, 1990; Ridgwell et al., 1999; Scheutz and Kjeldsen, 2004]. Temperature dependency of methane oxidation below the temperature of ~30°C is probably attributable to enhanced activity of methanotrophic bacteria at a higher temperature [Conrad, 1996]. Low methane oxidation at higher temperatures (> 30°C) is thought to be caused by heat stresses or resulting death of methanotrophic bacteria. Below 0°C, methane oxidation by soils ceases or becomes extremely low, probably due to regulated transport of $CH_4$ gas to the oxidation site (microorganisms) by shielding of frozen water [King and Adamsen, 1992; Koschorreck and Conrad, 1993]. To express such temperature dependency of methane oxidation, an empirical formulation proposed by Ridgwell et al. [1999] was used (Figure 50a):

$$f_{st}(T_s) = \begin{cases} \exp\left\{0.0693(T_s - T_{25}) - 8.56\times10^{-7}(T_s{}^4 - T_{25}{}^4)\right\}, \text{ for } T_s \geq 0°C \\ 0, \text{ for } T_s < 0°C \end{cases} \quad (32)$$

where $T_s$ (°C) is the soil temperature that is calculated by the soil heat model of SOLVEG-II [Yamazawa, 2001; Nagai, 2005], and $T_{25}$ = 25°C is the soil temperature at the reference condition (see the definition of $\Lambda_{ref}$ in Eq. (5)).

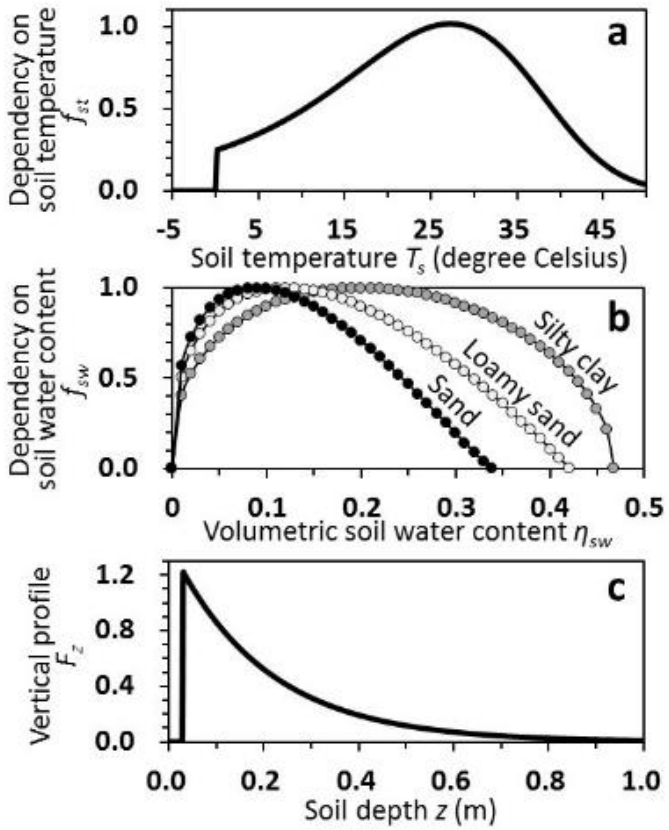


***Figure 50: Dependencies of the rate of methane oxidation on (a) temperature and (b) water content in soil, and (c) vertical profile of the methane oxidation in the soil. Formulation of $f_{st}$, $f_{sw}$ and $F_z$ are provided by Eq. (6), (7), and (9), respectively. In the panel (b), $f_{sw}$ are shown for textures of sand, loamy sand and silty clay. The parameters used in the calculation of $f_{sw}$ are listed in Table 15.***

As for the moisture response of methane oxidation, experiments have shown that methane oxidation exhibits optimum values under moderately wet conditions [Whalen et al., 1990; Adamsen and King, 1993; Scheutz and Kjeldsen, 2004]: e.g. soil water content of 40 – 50% of field capacity [Whalen and Reeburgh, 1996]. Fully dried soils reveal almost no oxidation of methane, which is thought to be caused by drought stresses on the methanotrophic bacteria [Scheutz and Kjeldsen, 2004]. At water-logged, or near saturated conditions, methane oxidation by soils also become quite low, being ~5% of the value observed at the optimum (moderately wet) condition [Whalen et al., 1990; Adamsen and King, 1993], probably due to the regulated transport of $CH_4$ from the soil air to the microorganisms by increased thicknesses of films of soil water [Koschorreck and Conrad, 1993; Del Grosso et al., 2000].

Based on these observations, it was assumed that the methane oxidation does not occur in fully-dry or saturated soil (Fig. 2b) and modelled the moisture dependency of methane oxidation by modifying an existing formula of Del Grosso et al. [2000]:

$$f_{sw}(\eta_{sw}) = \left(\frac{\eta_{sw}}{\eta_{opt}}\right)^{0.4} \left(\frac{\eta_{sw} - \eta_{sat}}{\eta_{opt} - \eta_{sat}}\right)^{\frac{0.4(\eta_{sat} - \eta_{opt})}{\eta_{opt}}} \quad (33)$$

where $\eta_{opt}$ ($m^3\ m^{-3}$) is the optimum water content of the methane oxidation that is related to the field capacity $\eta_{capa}$ ($m^3\ m^{-3}$) of the soil [Del Grosso et al., 2000], as:

$$\eta_{opt} = 0.67\eta_{capa} - 0.07 \quad (34)$$

In the SOLVEG-II model, the field capacity is parameterized by the texture, and thus the optimum water content has a value specific to the texture (Table 22). Value of $f_{sw}$ calculated for the three texture types are presented in Figure 50b.

As for the below-ground distribution of methane oxidation, studies in the literature have shown that methane oxidation is mainly located in the subsurface horizon (i.e., not the surface horizon) in most upland soils [Born et al., 1990; Whalen et al., 1990, 1992; Adamsen and King, 1993; Koschorreck and Conrad, 1993; Schnell and King, 1994; Kightley et al., 1995; Reeburgh et al., 1997; Shoemaker and Schrag, 2010]. Laboratory experiments that used vertically-sectioned soil cores sampled at a subarctic temperate forest showed that the maximum of the methane oxidation occurred in the soil at the depth of 6 – 7 cm and the overlying surface 5 cm horizon revealed little or no methane oxidation [Adamsen and King, 1993]. Low or no methane oxidation in the surface horizon would be attributable to water stresses on the methanotrophic bacteria due to repeated dry-wet cycles in this region [Whalen et al., 1992; Conrad, 1996] or perhaps high contents of ammonium and nitrate deposited from the atmosphere which strongly inhibits the activity of methanotrophic bacteria [Adamsen and King, 1993; Schnell and King, 1994; Conrad, 1996]. In the subsurface horizon, methane oxidation decreases with depth [Born et al., 1990; Adamsen and King, 1993; Koschorreck and Conrad, 1993; Schnell and King, 1994]. Lower methane oxidation in the deeper parts in the subsoil is thought to be due to smaller populations of methanotrophic bacteria, because of the limited growth of such populations under low substrate (methane) conditions; i.e., the atmospheric methane does not penetrate to the deeper parts of the soil [Koschorreck and Conrad, 1993; Conrad, 1996].

Based on these observations, it was assumed that the methane oxidation occurs in the subsurface horizon and the rate of methane oxidation in the subsurface horizon decreases with increasing soil depth (Figure 50c), according to the equation:

$$F_z(z) = \begin{cases} 0, \text{ at } z < z_{nul} \\ \exp\{-(z - z_{ref})/z_{oxi}\}, \text{ at } z \geq z_{nul} \end{cases} \quad (35)$$

where $z_{nul}$ (m) is the thickness of the surface horizon where methane oxidation does not occur, $z_{oxi}$ (m) is the depth-scale of the methane oxidation in the subsurface horizon, and $z_{ref}$ = 7 cm is the reference depth defined for the reference rate of the oxidation (see Eq. (5)). The thickness of the non-oxidative surface layer was set to: $z_{nul}$ = 3 cm, from measured vertical profiles of methane oxidation in some forest soils [Whalen et al., 1990; Adamsen and King, 1993; Koschorreck and Conrad, 1993]. The depth-scale of the methane oxidation in the subsoil was set to: $z_{oxi}$ = 20 cm, based on below-ground distributions of methane oxidation found in German forests ($z_{oxi}$ = 9 – 15 cm; Born et al., 1990) and Alaskan forests ($z_{oxi}$ = 23 – 39 cm; Whalen et al., 1992).

The top boundary condition of the modelled below-ground transport of $^{14}CH_4$ (Eq. (28)) was set by the rate of $^{14}CH_4$ exchange at the ground surface (Eq. (27)). The bottom boundary condition was specified for each scenario of $^{14}CH_4$ release in the soil. The oxidization of $^{14}CH_4$ (the term $e_o$) calculated using

the model was used as a volume source of $^{14}CO_2$ at each soil layer in the calculation of soil $^{14}CO_2$ transport by SOLVEG-II (Figure 9), i.e. 100% conversion efficiency was assumed.

*Table 22: Porosity, field capacity and optimum water content of methane oxidation parameterized by texture.*

| Texture[a] | Porosity $\eta_{sat}$[b] | Field capacity $\eta_{capa}$[b] | Optimum water content $\eta_{opt}$[c] |
|---|---|---|---|
| Sand | 0.339 | 0.236 | 0.088 |
| Loamy sand | 0.421 | 0.283 | 0.120 |
| Sandy loam | 0.434 | 0.312 | 0.139 |
| Sandy clay loam | 0.404 | 0.314 | 0.140 |
| Loam | 0.439 | 0.329 | 0.150 |
| Sandy clay | 0.406 | 0.338 | 0.156 |
| Silt loam | 0.476 | 0.360 | 0.171 |
| Silt | 0.476 | 0.360 | 0.171 |
| Clay loam | 0.465 | 0.382 | 0.186 |
| Silty clay loam | 0.464 | 0.387 | 0.189 |
| Silty clay | 0.468 | 0.404 | 0.201 |
| Clay | 0.468 | 0.412 | 0.206 |

Notes:

[a] Classification by the U.S. Department of Agriculture.

[b] Default parameterizations by SOLVEG-II [Yamazawa, 2001; Nagai, 2005].

[c] See Eq. (7) for the definition. Values were calculated from the field capacity using Eq. (8).

## A.4 RWM T2PLANTS MODEL USED FOR THE NOTTINGHAM LE3 AND FE2 SCENARIOS

One of the key processes represented in this model is molecular diffusion, which is generally the dominant process for gaseous transport through a partially-saturated soil, and which is described using Fick's law. When applying Fick's law, the diffusion coefficient for a gaseous species in free air, $d$ ($m^2\ s^{-1}$), is multiplied by a property of the soil called the tortuosity, $\tau$ (-), to get the diffusion coefficient in the soil gas, $D$ ($m^2\ s^{-1}$):

$$D = \tau \times d \tag{36}$$

Correlations have been developed that relate the tortuosity to other properties of a soil, e.g. its porosity φ (-) and water content $w$ (-). In particular, a recent review has proposed the following correlation:

$$\tau = \frac{1}{\varphi}\left(\varphi - w\right)^{2+C_m\varphi} \tag{37}$$

where $C_m$ (-) is a fitting parameter called the "media complexity factor". An analysis of 280 intact soils led to the recommendation that the media complexity factor should be $C_m$ = 2.1 for such systems. Therefore, if a soil has porosity φ = 0.4 and water content w = ½ φ, then its tortuosity is predicted to be 0.026.

Detailed modelling was performed to simulate diffusion of methane and carbon dioxide through the soil, and then the outputs from the numerical models were compared against the experimental observations. Calibrating the model's media complexity factor to fit the data gave $C_m$ = 1.73, which implies a tortuosity of 0.033. It is this value which is used in the model-data comparisons presented in the main report.

## A.5 TECHNICAL SUPPORT TEAM NOTTINGHAM MODEL

In modelling the Nottingham scenarios, the TST used the reciprocal theorem to relate pulse-injection results to those that would be obtained if the pulse injection was to be replaced by a continuous constant flux (which is the situation of interest for assessment purposes). In 1-D, the response to a unit pulse input at $x = 0$ and at $t = 0$ (x being distance and $t$ being time) is defined as $R(x,t)$. Assuming that the response of the system is linear, i.e. scales in proportion to the input, the response, $H(x,t)$ for any time-dependent input, $q(u)$ starting at $t = 0$ is given by the convolution:

$$H(x,t) = \int_0^t q(u)R(x,t-u)du \quad (38)$$

If we define $q(u)$ to be the Dirac Delta function, $\delta(u)$, which is only non-zero at $u = 0$ and has an integral of unity, we immediately recover:

$$H(x,t) = R(x,t) \quad (39)$$

However, for continuous uniform input, we have $q(u) = q$, where $q$ is constant on the interval $[0,t]$. This yields:

$$H(x,t) = q\int_0^t R(x,t-u)du = q\int_0^t R(x,v)dv \quad (40)$$

Thus, the response for continuous uniform input is simply the integral of the response to a pulse input for any model for which the response is proportional to the input.

Now, we know by observation that the response of the soil system to a pulse input in the Nottingham experiments is all over on a timescale of a few days, whereas timescales of relevance in assessments are typically years or longer, with C-14 fluxes entering the soil system constant over these longer timescales. Therefore, $t$ tends to infinity in the above expression.

Physically, we expect the system to come into an equilibrium state after a large period of continuous uniform input. Thus, $H(x,t) \rightarrow H(x)$. Note that this is a second assumption that does not hold for all physical systems. For example, a thermally isolated system with a constant heat input will continue to rise in temperature indefinitely.

In the Nottingham dataset context, it is interesting to examine the implications of the above for a specific model of the system. Consider first a column experiment, so that the lateral extent is constant with depth, and neglect lateral variations in concentration. Assume that transport of methane is governed by the advection-dispersion equation with losses arising by depth-independent metabolism of the methane to carbon dioxide. Thus, the concentration of methane per unit length $x$[m], $C(x,t)$, is governed by:

$$dC(x,t)/dt = -vdC(x,t)/dx + \frac{d}{dx}\left(D\frac{dC(x,t)}{dx}\right) - kC(x,t) \quad (41)$$

[m] i.e. The volumetric concentration multiplied by the cross-sectional area and the gas-filled porosity.

For continuous uniform input, the system is expected to achieve equilibrium, so d$C(x,t)$/d$t$ = 0. Thus:

$$-v\mathrm{d}C(x)/\mathrm{d}x + \frac{d}{dx}\left(D\frac{dC(x)}{dx}\right) - kC(x) = 0 \quad (42)$$

Assuming that $v$ and $D$ are independent of $x$, a solution of this equation, for an infinitely long column, is:

$$C(x) = A\exp(-\lambda x) \quad (43)$$

Where $A$ is an arbitrary value and the above expression becomes:

$$\lambda^2 D + \lambda v - k = 0 \quad (44)$$

As $\lambda$ is expected to be non-negative, the appropriate solution is:

$$\lambda = \{-v + (v^2 + 4Dk)^{0.5}\}/2D \quad (45)$$

Note that for $k$ = 0 (no depletion), $\lambda$ = 0 and the concentration becomes independent of height in the column, as would physically be expected.

The methane flux up the column at equilibrium, $F(x)$ comprises two components, i.e. the advective flux and the dispersive flux. Thus:

$$F(x) = vC(x) - D\mathrm{d}C(x)/\mathrm{d}x = A(v + \lambda D)\exp(-\lambda x) \quad (46)$$

However, at x = 0, the flux must be that entering the column, i.e. $F_0$. Thus:

$$F(x) = F_0 \exp(-\lambda x) \quad (47)$$

Thus:

$$A = F_0/(v + \lambda D) \quad (48)$$

Hence:

$$C(x) = A\exp(-\lambda x) \qquad \lambda = \{-v + (v^2 + 4Dk)^{0.5}\}/2D \qquad A = F_0/(v + \lambda D) \quad (49)$$

Note that $v$ is the velocity of advective flow, i.e. $v = Q/\phi S$, where Q is the total volumetric flow rate, $\phi$ is the gas-filled porosity and $S$ is the cross-sectional area. Thus, the concentration normalisation factor $A$ for a non-depleting system is $F_0/v = F_0\phi S/Q$. However, if the flux $F_0$ is due to a volumetric concentration $C_0$ in the gas entering the system and it enters at velocity $v$, then $F_0 = QC_0$ and the normalisation factor $A$ becomes $C_0\phi S$, i.e. the concentration per unit length on entry.

## A.6 CONVERSION OF C-13 FIELD MEASUREMENTS TO C-14 FOR EDF AND JAEA MODEL-DATA COMPARISONS

In the field experiment of the present study, measurement of $CH_4$ concentration in soil air was performed for bulk of the $CH_4$ concentration, $\chi_{bulk}$ (ppm), which includes both forms of $^{12}CH_4$ and $^{13}CH_4$, as:

$$\chi_{bulk} = \chi_{12} + \chi_{13} \quad (50)$$

where $\chi_{12}$ (ppm) and $\chi_{13}$ (ppm) are the concentration of $^{12}CH_4$ and $^{13}CH_4$ in the sampled soil-air, respectively. Measurement of isotope ratio of $^{13}C/^{12}C$ in the same soil-air sample is expressed by "$\delta^{13}C$", which is defined as:

$$\delta^{13}C = \frac{R_{sam}}{R_{stn}} - 1 \quad (51)$$

where $R_{stn}$ = 0.011237 is the reference ratio of $^{13}C/^{12}C$ for the standard sample of Vienna PeeDee Belemnite [Preuss et al., 2013], and $R_{sam}$ represents the $^{13}C/^{12}C$ ratio in the sampled-air which is expressed, as:

$$R_{sam} = \frac{\chi_{13}}{\chi_{12}} \quad (52)$$

With Eqs (50), (51) and (52), the concentration of $^{13}CH_4$ in the sampled-air ($\chi_{13}$ (ppm)) can be determined from the measurements of $\chi_{bulk}$ and $\delta^{13}C$, by:

$$\chi_{13} = \chi_{bulk} \frac{R_{stn}(1+\delta^{13}C)}{1+R_{stn}(1+\delta^{13}C)} \quad (53)$$

Measurement results of $^{13}CH_4$ concentration ($\chi_{13}$) in the soil in the unit of "ppm" were converted to the corresponding activity concentration of $^{14}CH_4$ in the unit of "Bq m$^{-3}$", as follows. First, the concentration $\chi_{13}$ (ppm) was converted to molar unit $\chi_{13,mol}$ (mol m$^{-3}$), by:

$$\chi_{13,mol} = \frac{P}{R^* T} \frac{\chi_{13}}{10^6} \quad (54)$$

where $P$ (Pa) is the air pressure (set to 101300 Pa), $R^*$ (8.31 J mol$^{-1}$ K$^{-1}$) is the universal gas constant and $T$ (K) is the temperature. In Eq. (54), the air pressure was assumed to be 101300 Pa, and the field measurements of the soil temperature were used for $T$ at each soil depth. With the obtained $\chi_{13,mol}$, the activity concentration $\chi_{Bq}$ (Bq m$^{-3}$) was calculated by:

$$\chi_{Bq} = N_A \lambda \chi_{13,mol} \quad (55)$$

where $N_A$ (mol$^{-1}$) is the Avogadro constant (6.02 × 10$^{23}$ mol$^{-1}$) and $\lambda$ is the decay constant of $^{14}C$ (3.84 × 10$^{-12}$ s$^{-1}$).

## A.7 TECHNICAL SUPPORT TEAM DUKE SWAMP TRANSECT MODEL

Figure 51 illustrates the processes in a single column of the Transect Model, shown in Figure 38 of the main report. The modelling of those transport processes is described below.

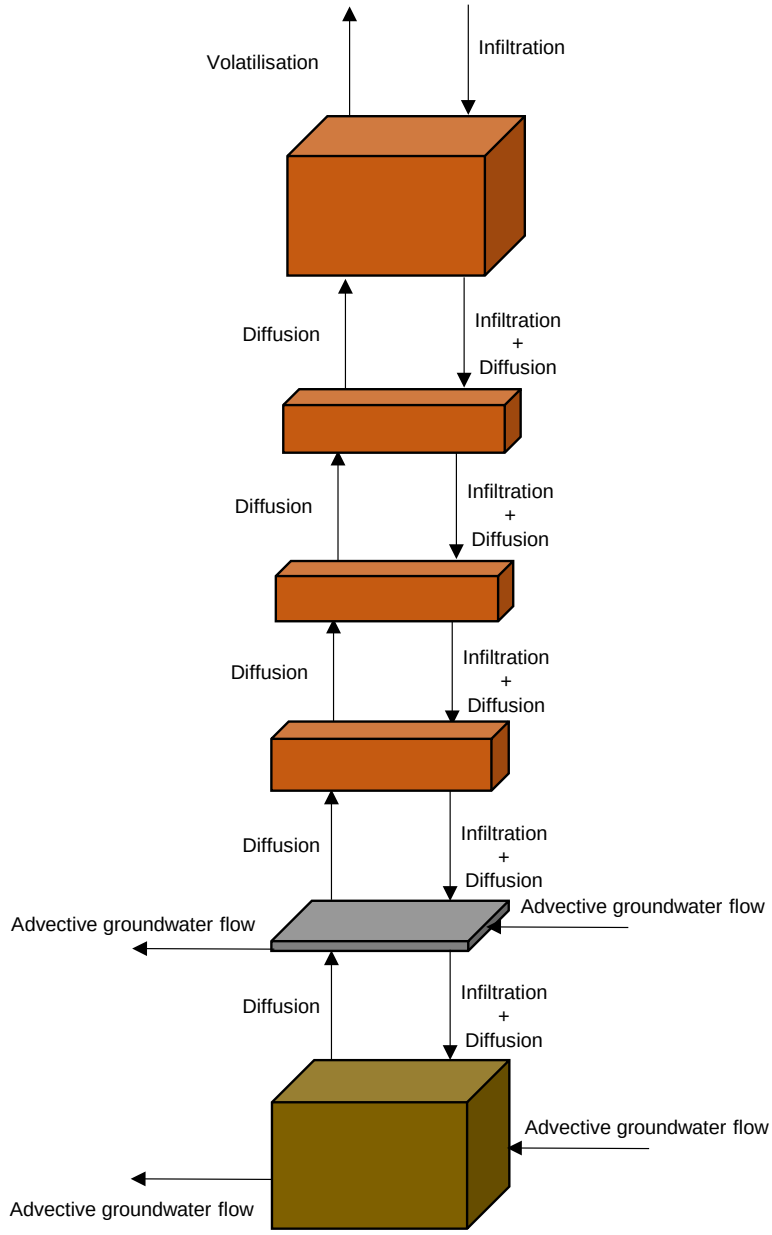


*Figure 51: Single column, j, in the Transect Model*

### TRANSPORT PROCESSES

#### 1.1.7 Lateral advection

Below the water table, it is assumed that all the C-14 is either in solution or rapidly exchangeable with solution, i.e. that it is all in a dissolved form. C-14 is taken to be laterally advectively transported, with lateral diffusion not explicitly modelled. Noting that it is difficult to argue for a significant degree of

sorption, except for some rather specific chemical forms, sorption of C-14 is neglected. Whilst this is a limitation of the model, it is thought to be a realistic assumption.

Thus, the transfer rate out of a compartment in either the aquifer or silty-clay lens layer is defined as:

$$\text{lambda\_Advection}_{\text{Region\_j}} = \frac{V_{\text{groundwater}}}{R_{\text{Re}gion\_j} \cdot \theta_{e,\text{Re}gion\_j} \cdot L_{\text{Re}gion\_j}} \quad (56)$$

### 1.1.8 Diffusive Vertical Migration

The diffusive fluxes arise from both the soil gas and soil water pools. Whilst the flux is in the gas phase, the exchange between the water and gas phases is so rapid that the loss in the gas phase (which would tend to decrease the concentration in the soil atmosphere) is immediately compensated by outgassing from the water phase, so that the Henry's Law equilibrium between the water and gas phases is restored

**Below the water table:** For a horizontal groundwater velocity $u$ (m $s^{-1}$), the upward dispersion coefficient, $D$ ($m^2$ $s^{-1}$) is defined as $\alpha u$, where $\alpha$ (m) is the characteristic dispersion length. This dispersion length is not well constrained. However, in this study it is assumed that the transverse dispersion is less than longitudinal dispersion and that the longitudinal dispersion length should be no larger than the length of the grid element. Thus:

$$\alpha = f_1 f_2 L \quad (57)$$

where $L$ (m) is the horizontal length of the grid element, $f_2$ (0.1 to 1.0) is the longitudinal dispersion expressed as a fraction of $L$, and $f_1$ (~0.1) is the transverse dispersion expressed as a fraction of the longitudinal dispersion.

**Above the water table:** In the vadose zone, only vertical dispersion is considered, as it can be argued that horizontal transport can be neglected. Vertical dispersion is modelled by:

$$D = E\tau D_0 \quad (58)$$

where $D_0$ ($m^2$ $s^{-1}$) is the diffusion coefficient for carbon dioxide in free air, $\tau$ is the tortuosity factor obtained from the Millington and Quirk model [1961], and $E$ (1 to 10) is an enhancement factor to allow for the effects of atmospheric pumping.

The tortuosity factor is defined as:

$$\tau = \{\varphi(1 - S)\}^{[1 + \varsigma\varphi]}\{1 - S\} \quad (59)$$

where $\varsigma$ (-) is the model complexity factor (typically 0.5), $\varphi$ is the porosity of the soil and $S$ is the degree of saturation.

This gives us a complete set of $D$ values ($m^2$ $s^{-1}$) for upward and downward migration. Let the activity in any compartment be A (Bq). As this is a transect, we take it to be of unit width (W m), length L (m) and height H (m). Therefore, the concentration in the compartment is A/WLH (Bq $m^{-3}$).

Consider two adjacent overlying compartments 1 and 2. These are taken to be co-extensive, i.e. $W_1 = W_2$ and $L_1 = L_2$. Define the effective diffusion coefficient between the two compartments, $De = (D_1 * D_2)^{0.5}$ and the effective length over which that diffusion operates as $H_e = (H_1 + H_2)/2$. Thus, the diffusive flux, F (Bq $s^{-1}$), between the two compartments is given by:

$$F = WLD_e(C_1\text{-}C_2)/H_e = D_eA_1/H_1H_e - D_eA_2/H_2H_e \quad (60)$$

This gives the diffusive rate coefficients from compartment 1 to compartment 2 and from compartment 2 to compartment 1 as $D_e/H_1H_e$ and $D_e/H_2H_e$, respectively.

A special case arises for the surface compartment (here denoted 1), as the atmosphere is taken to have zero concentration. In this case, $D_e = D_1$ and $H_e = H_1/2$, with the concentration gradient defined from the centre of the compartment to the surface.

### 1.1.9 Infiltration

Infiltration of soil water is assumed to occur in the unsaturated vadose zone, so the infiltrating water can flow through a subset of the pores (and possibly mainly macropores) bypassing the soil atmosphere. There is one small caveat on this. The infiltrating water can exchange C-14 with the soil atmosphere, but this effect will essentially be compensated by the continuous equilibration that is implied between the soil water and the soil gas in the diffusion context. The infiltration rate is assumed to be $I$ m $s^{-1}$.

## PARTITIONING OF C-14 BETWEEN AQUEOUS AND GASEOUS FORMS

Assuming the simple inorganic forms means that the carbon can readily be partitioned between dissolved and gaseous form using Henry's Law.

Thus, if $\varphi$ is the total porosity and $S$ is the degree of saturation, the gas-filled porosity per unit volume will be $\varphi(1 - S)$ and the water-filled porosity will be $\varphi S$. For a partial pressure of $P$, the content in the gas phase per litre of soil or sediment will be $P\varphi(1 - S)$ /22.4 moles, since 1 mole of gas at Standard Temperature and Pressure (STP) occupies 22.4 litres. The content of the solution phase will be 0.032 $\varphi SP$ moles. Thus, the fraction in the gas phase will be $0.0446 (1 - S)/\{0.0446 (1 - S) + 0.032S\}$. Thus, at $S$ = 0.5, about 60% of the soil or sediment $CO_2$ will be in the gas phase and $^{14}C$ entering soil in solution incorporated in $CO_2$ will be partitioned similarly.

Carbon dioxide present in the gas-filled pore space of unsaturated soils or sediments will rapidly exchange with the above-ground atmosphere. Thus, $^{14}CO_2$ entering the unsaturated zone in solution, will rapidly equilibrate between the solution and gas phases and will be lost from that mixed 'pool' across the soil surface by gas exchange processes (mainly diffusion, but with a small advective component due to the pumping effect of atmospheric pressure variations).

The $^{14}C$ in solution in unsaturated soils and sediments after its entry to those soils and sediments as $^{14}CO_2$, will mainly remain as $^{14}CO_2$. However, small fractions will also be present as carbonate, bicarbonate and carbonic acid (see above). The proportions of each will depend upon the chemical composition of the soil or sediment water.

The specific activity will be the same in the soil water and soil gas (Bq $kgC^{-1}$). The volumetric activities in the soil water and soil gas are then obtained by scaling that specific activity by the masses of dissolved and gas phase carbon per unit volume of water or soil gas, respectively.

## A.8 REFERENCES FOR THE APPENDIX

Adamsen, A.P.S., King, G.M., 1993. Methane consumption in temperate and subarctic forest soils: rates, vertical zonation, and responses to water and nitrogen. Applied and Environmental Microbiology, 59, 485–490.

Born, M., Dörr, H., Levin, I., 1990. Methane consumption in aerated soils of the temperate zone. Tellus, 42B, 2–8.

Conrad, R., 1996. Soil microorganisms as controllers of atmospheric trace gases ($H_2$, CO, $CH_4$, COS, $N_2O$, and NO). Microbiol. Rev. 60, 609–640.

Del Grosso, S.J., Parton, W.J., Mosier, A.R., Ojima, D.S., Potter, C.S., Borken, W., Brumme, R., Butterbach-Bahl, K., Crill, P.M., Dobbie, K., Smith, K.A., 2000. General $CH_4$ oxidation model and comparisons of $CH_4$ oxidation in natural and managed systems. Global Biogeochemical Cycles, 14, 999–1019.

Ito, A., Inatomi, M., 2012. Use of a process-based model for assessing the methane budgets of terrestrial ecosystems and evaluation of uncertainty. Biogeosciences, 9, 759–773.

Jury, W.A., Spencer, W.F., Farmer, W.J., 1983. Behaviour assessment model for trace organic in soil: I. Model description. Journal of Environmental Quality, 12(4): 558-564.

Kightley, D., Nedwell, D., Cooper, M., 1995. Capacity of methane oxidation in landfill cover soils measured in laboratory-scale soil microcosms. Applied and Environmental Microbiology, 61, 592–601.

King, G.M., Adamsen, A.P.S., 1992. Effects of temperature on methane consumption in a forest soil and in pure cultures of the methanotroph *Methylomonas rubra*. Applied and Environmental Microbiology, 58, 2758–2763.

Koschorreck, M., Conrad, R., 1993. Oxidation of atmospheric methane in soil: measurements in the field, in soil cores, and in soil samples. Global Biogeochemical Cycles, 7, 109–121.

Le Mer, J., Roger, P., 2001. Production, oxidation, emission and consumption of methane by soils: A review. European Journal of Soil Biology, 37, 25–50.

Millington, R.J., Quirk, J.P., 1961. Transport in porous media [in soil science], Transactions, 7th International Congress of Soil Science, 7(1), 97–106.

Nagai, H., 2002. Validation and sensitivity analysis of a new atmosphere-soil-vegetation model. Journal of Applied Meteorology, 41, 160–176.

Nagai, H., 2005. Incorporation of CO2 exchange processes into a multiplayer atmosphere-soil-vegetation model. Journal of Applied Meteorology, 44, 1574–1592.

Penman, H.L., 1940. Gas and vapor movements in the soil: 1. the diffusion of vapors through porous solids. The Journal of Agricultural Science, 30, 437–462.

Preuss, I., Knoblauch, C., Gebert, J., Pfeiffer, E.-M., 2013. Improved quantification of microbial $CH_4$ oxidation efficiency in arctic wetland soils using carbon isotope fractionation. Biogeosciences, 10, 2539-2552.

Reeburgh, W.S., Hirsch, A.I., Sansone, F.J., Popp, B.N., Rust, T.M., 1997. Carbon kinetic isotope effect accompanying microbial oxidation of methane in boreal forest soils. Geochimica et Cosmochimica Acta. 61, 4761–4767.

Ridgwell, A., Marshall, S.J., Gregson, K., 1999. Consumption of atmospheric methane by soils: A process-based model. Global Biogeochemical Cycles, 13, 59–70.

Sau, F., Boote, K.J., Bostick, W.M., Jones, J.W., Minguez, M.I., 2004. Testing and Improving Evapotranspiration and Soil Water Balance of the DSSAT Crop Models. Agronomy Journal, 96: 1243-1257.

Scheutz, C., Kjeldsen, P., 2004. Environmental factors influencing attenuation of methane and hydrochlorofluorocarbons in landfill cover soils. Journal of Environmental Quality, 33, 72–79.

Schnell, S., King, G.M., 1994. Mechanistic analysis of ammonium inhibition of atmospheric methane consumption in forest soils. Applied and Environmental Microbiology, 60, 3514–3521.

Sheppard, S.C., Ciffroy, P., Siclet, F., Damois, C., Sheppard, M.I., Stephenson, M., 2006. Conceptual approaches for the development of dynamic specific activity models of $^{14}C$ transfer from surface water to humans. Journal of Environmental Radioactivity, 87: 32-51.

Shoemaker, J.K., Schrag, D.P., 2010. Subsurface characterization of methane production and oxidation from a New Hampshire wetland. Geobiology, 8, 234–243.

Turc, L., 1961. Water requirements assessment of irrigation, potential evapotranspiration: Simplified and updated climatic formula. Annales Agronomiques,12, 13-49.

Walter, B.P., Heimann, M., 2000. A process-based, climate-sensitive model to derive methane emissions from natural wetlands: Application to five wetland sites, sensitivity to model parameters, and climate. Global Biogeochemical Cycles, 14, 745–765.

Whalen, S.C., Reeburgh, W.S., 1990. Consumption of atmospheric methane by tundra soils. Nature, 346, 160–162.

Whalen, S.C., Reeburgh, W.S., Sandbeck, K.A., 1990. Rapid methane oxidation in a landfill cover soil. Applied and Environmental Microbiology, 56, 3405–3411.

Whalen, S.C., Reeburgh, W.S., Barber, V.A., 1992. Oxidation of methane in boreal forest soils: a comparison of seven measures. Biogeosciences, 16, 181–211.

Yamazawa, H., 2001. A one-dimensional dynamical soil-atmosphere tritiated water transport model. Environmental Modelling and Software, 16, 739–751.